DENDRITIC CELL MIGRATION AND TRACTION FORCE GENERATION IN ENGINEERED MICROENVIRONMENTS

Brendon Guenther Ricart

A Dissertation

in

Chemical and Biomolecular Engineering

Presented to the Faculties of the University of Pennsylvania in Partial Fulfillment of the Requirements for the Degree of Doctor of Philosophy

2010

_____
Professor Daniel A. Hammer
Supervisor of Dissertation

_____
Professor Raymond J. Gorte
Graduate Group Chairperson

Dissertation Committee:
Professor Christopher A. Hunter, Pathobiology
Professor John C. Crocker, C.B.E.
Assistant Professor Casim A. Sarkar, C.B.E.
Assistant Professor Matthew J. Lazzara, C.B.E.

DENDRITIC CELL MIGRATION AND TRACTION FORCE GENERATION IN ENGINEERED MICROENVIRONMENTS

Acknowledgements

At the end of my formal education, I don't know how to begin thanking the people who have brought me here. I will start with the two people who have known me longest. Thank you to my parents, Glenn Ricart and Patricia Guenther. From playing math games with me as a preschooler to trying to understand my thesis, you have never waivered in your support of my education.

To the most important person in my life, Erin Ricart. You have been unyielding in your continuous love and support throughout this process. I appreciate the sacrifices you have made more than you know and I hope you view this thesis as your achievement as well. Marrying you overshadows any accomplishment contained in this text.

I am grateful to my advisor, Daniel Hammer. The student-advisor relationship is crucial, and I could not have been paired with a more compassionate yet demanding mentor. You have always supported me, and the trust we have built has contributed greatly to my success. To my thesis committee: Dr. John Crocker, Dr. Chrisopher Hunter, Dr. Matthew Lazarra and Dr. Casim Sarkar. Our conversations lifted me out of ruts, put new tools in my hands, and opened my mind to new perspectives.

To the members of the Hammer Lab, you have made this experience pleasantly bearable. My mentors, Risat Jannat and Natalie Christian, laid the groundwork for my thesis and

guided me through the most trying period of my research. Each and every member of the Hammer Lab has enriched my experience in their own way. Thank you Randi, Aaron, Dalia, Jered, Josh, Kelly, Kevin, Laurel, Lauren, Lee, Neha, Nimil, Olga, Pam, and Steven. I would also like to thank my collaborators, Beena John, Michael Yang, Dooyoung Lee, Fiona Clarke and Debbie Klos Dehring. I could not have finished this work without you.

I have had the blessing of forming some amazing friendships at Penn. Bob Meyer, Michael Beste, Calixte Monaste, Greg Robbins, Parag Shah and Ashley Vissing, you all know how special our bond has been over the last three years. To my other good friends, Alex, Andrew, Ben, Dan, Jeremy, Joel, Manash, Matt, Raynaldo and Tom, I look forward to a time when our paths cross again.

Finally, I would like to thank the food trucks and cafés on Penn's campus. Frida's, El Rosa, Magic Carpet, Kim's Chinese, King's Wok, Fresh Fruit, MexiPhilly, The Pari Café, The Chem Café, Taco Bell and Potbelly's, your delicious and budget-friendly meals truly enhanced my graduate school experience.

ABSTRACT

DENDRITIC CELL MIGRATION AND TRACTION FORCE GENERATION IN ENGINEERED MICROENVIRONMENTS

Brendon Guenther Ricart

Professor Daniel A. Hammer, Advisor

Dendritic cells (DCs) are potent initiators of the adaptive immune response. Their trafficking from sites of inflammation to lymphoid tissue is essential to their function. Exactly how dendritic cells integrate multiple chemotactic cues to organize an accurate migratory path is not fully understood. We first characterize DC random motility (chemokinesis) on extracellular matrix proteins in the presence of chemokines. Then, using a microfluidic device, we present both single and competing chemokine gradients to murine bone-marrow derived DCs in a controlled, time-invariant microenvironment. We show that in counter gradients, CCL19 is 10 to 100 fold more potent than other chemokines CCL21 or CXCL12. Interestingly, when the chemoattractive potencies of opposing gradients are matched, cells "home" to a central region in which the signals from multiple chemokines are balanced. These results provide fundamental insight into the processes that DCs use to migrate toward and position themselves within secondary lymphoid organs. We extended this work to a combination of the microfluidic gradient generator and micropost array detectors to develop a novel method for probing traction forces during chemotaxis. We find DC migration is driven by short-lived traction

stresses at the leading edge or filopodia. We illustrate that spatiotemporal pattern of traction stresses can be used to predict changes in the direction of DC motion. Additionally, we determine the characteristic duration of local dendritic cell traction forces and correlate this duration with force. Overall, DCs show a mode of migration distinct from both mesenchymal cells and other leukocytes, characterized by rapid turnover of traction forces in leading filopodia. In this thesis, we extend the current understanding of DC motility to include signal integration and traction forces.

Table of Contents

List of Figures

List of Tables

Chapter 1: Introduction

What is important in life? What makes us happy? These are the persistent questions we have asked ourselves since the beginning of our existence. If you were to ask the *Kohelet*, a sage of the Old Testament, you may get a bleak answer.

> "'Meaningless! Meaningless!' says the Teacher. 'Utterly meaningless! Everything is meaningless.'" —Ecclesiastes 1:2 (NIV)

George Vaillant, director of a longitudinal study of 268 Harvard students that began in the 1930's, has a more attractive outlook. Asked to answer the question "What is happiness?" he sums up the study's findings this way:

> "Happiness is love. Full stop." —George Vaillant, The Atlantic, Interview, 2009.

Indeed, presenting these transcendent questions to 20 of your closest friends is likely to yield 20 different answers. As varied as opinions may be on the human condition, there is one thing, at least, we may all agree upon. Herophilus, no less than a co-inventor of the Scientific Method (1), tells us:

> "When health is absent, wisdom cannot reveal itself, art cannot manifest, strength cannot fight, wealth becomes useless, and intelligence cannot be applied."
> —Herophilus, per Sextus Empiricus (2)

Thus regardless of the true answer to life's persistent questions, this author feels that health is essential to achieve and enjoy it.

Motivation

Directed cell migration plays a central role in maintaining health, from just prior to conception until death. This migration process choreographs the morphogenesis of nascent tissues in the embryo during development. Failure of cells to migrate, or inaccurate navigation of cells to inappropriate loci, can precipitate life threatening conditions such as congenital brain defects, dysplasia, and congenital heart disease. In adults, cell migration remains central for homeostatic processes such as mounting an innate or adaptive immune response and the repair of wounded tissues. On the other hand, cell motility contributes to disease states including vascular disease, chronic inflammatory diseases, and tumor metastasis. Understanding the mechanisms underlying cell migration will also be important for emerging areas of interdisciplinary research such as creation of artificial tissues, controlling tumor metastasis, and development of new therapeutic strategies for modulating the immune response.

Fetal development is directed by several proteins involved in cell migration. Defects in these proteins can be manifest in the first stages of embryogenesis and can lead to the failure of the blastocyst to implant in the uterine wall, resulting in early loss of pregnancy. At later stages in development, defects in cell migration can result in malformed embryos with disorganized tissues because their component cells have failed to migrate to the correct location. Non-fatal developmental abnormalities caused by

improper cell migration can lead to a number of congenital abnormalities in brain development, including epilepsy, focal neurological deficits and mental retardation.

Unfortunately, cell migration also contributes to tumor metastasis. Cancerous cells can migrate as individuals or as small groups away from the initial tumor site. For tumors to become metastatic, some cells must acquire an invasive phenotype characterized by weakening of cell-cell interactions and increased cell motility. These cells then undergo intravasation to either lymphatics where they travel to lymph nodes, or to the blood from which they can extravasate the vasculature to distal organs where they may establish a secondary tumor site.

Cell migration is particularly important for immune cell function and the inflammatory response. As a prerequisite for migration, white blood cells (leukocytes) undergo polarization with the formation of distinct leading and trailing edges. Intracellular polarization allows cells to convert actomyosin forces into net cell-body displacement. Leukocyte chemoattractants, especially chemokines, provide directional cues for leukocyte motility, directing cells to sites of infection or to lymphoid tissue to exchange information. A complex system of signal transduction molecules, including G-protein coupled receptors, integrins, second messengers and members of the Rho family of small GTPases regulate the adhesion, contraction and protrusion underlying leukocyte polarization and migration. The elucidation of the signals and mechanisms that orchestrate this complex reorganization will lead to a better understanding of critical issues in immunology and the treatment of disease.

The motility of dendritic cells, in particular, within the mammalian immune system facilitates the surveillance and targeted cellular responses that contribute to host defense. Compartmental segregation of lymphoid tissue, however, requires precise trafficking of dendritic cells and their precursors between the circulation, tissues, and lymph nodes. Within lymph nodes, dendritic cells have been identified as an essential element of the immune system, acting as an initiator and modulator of the host response due to their potential to express high levels of the co-stimulatory molecules that direct and fine-tune T-cell activation. Dendritic cells play the intermediary between local sites of infection and lymphoid tissue where they orchestrate the immune response. Thus, the migration toward and within secondary lymphoid organs following infection is essential to the function of dendritic cells and will be a major focus of this thesis.

Organization of the Thesis

This thesis is comprised of seven chapters; Chapters 1 and 7 are an introduction and conclusion, respectively. Chapter 2 is a comprehensive background, describing both previous work and topics of study central to this work. Chapter 2 provides an overview of dendritic cells, their role in the immune system, chemokines and their downstream signals, and a summary of assays for measuring chemotaxis and traction forces. The background should provide sufficient detail for the reader to understand the context of the research described here.

Chapter 3 begins the experimental section of the thesis, starting with quantification of common motility metrics. We place dendritic cells on the two most commonly studied extracellular matrix proteins and quantify their adhesion. This elucidates understanding of previous reports on these substrates. We also quantify their motility in uniform fields of chemokine, specifically studying the response to increasing concentrations of chemokine.

In Chapter 4, we examine dendritic cell chemotaxis. Previous studies have shown that DCs migrate toward specific chemokines, but we are the first to capture detailed information about cell trajectories in stable, controlled gradients. This is achieved via a microfluidic gradient generator and videomicroscopy which allows quantitative investigation of migration in response to varying chemoattractant gradients. This tool allowed us to answer several fundamental questions about chemokine signal integration. We showed that DCs respond almost identically to single gradients of chemokine, but show a hierarchical preference for some chemokines over others when presented with overlapping, counter-gradients. This helps elucidate how DCs find their ultimate position within secondary lymphoid organs, where they interact with T and B cells. We delve further to probe the underlying signaling pathways involved with migration, and determine that some common migration pathways are dispensable for DC migration, while others regulate either navigation or cell speed, but not both.

Chapter 5 represents the application of our microfluidic gradient technology to a specific need. In this chapter, we study the role of HS1 in dendritic cells. This protein is not

well-studied, but believed to be involved in cell migration. We carefully characterized the HS1 knockout phenotype, especially its role in dendritic cell migration. This chapter places greater emphasis on immature dendritic cells, which form podosomes to facilitate their migration. By the application of our microfluidic gradient generator and direct observation of migration, we were able to observe subtle effects of HS1 deficiency. This lead to the conclusion that HS1 helps stabilize filopodia extended in the correct direction of migration.

In the final data chapter, Chapter 6, we extend our knowledge of DC chemotaxis in engineered gradients to studies of traction forces. We compare the magnitude of DC stresses to other cells such as neutrophils and mesenchymal cells. We also make statements about the orientation of traction stresses underneath a motile DC and place them in context with other motile cells. Based on our findings, we are able to make predictions about the direction of migration from a single traction map. Additionally, we were able to determine the characteristic duration of local dendritic cell traction forces, and correlate the duration with traction force. This represents the first measurement of traction forces in dendritic cells.

Specific Aims

Aim 1: Chemokinesis

In this aim, we will measure basic migration parameters for dendritic cells and hypothesize that migration will go through a maximum as a function of the chemokine

concentration in the extracellular environment and the surface ligands available for integrin binding.

Aim 2: Chemotaxis

In this aim, we seek to quantify chemotactic parameters for DCs in gradients of CCL19, CCL21, and CXCL12 as well as characterize their behavior in counter gradients. We hypothesize that there may be a hierarchy of preferred chemokine signals. Additionally, we will probe intracellular pathways to determine their role in DC migration. Finally, in this aim we will examine the effects of HS1 protein deficiency in DC chemotaxis.

Aim 3: Traction Forces

In this aim, we will extend the use of microfluidic gradient technology to the study of DC migration on substrates suitable for traction force measurements to enable simultaneous monitoring of migration and force in individual cells. We hypothesize that traction forces will have a characteristic distribution under a motile cell, that force generation may be altered or interrupted by conflicting gradients or chemical inhibitors, and that the integration of traction forces may be used to predict the direction of motion.

References

1. Staden HV (1989) *Herophilus: the art of medicine in early Alexandria* (Cambridge University Press, New York, NY).
2. Prioreschi P (1996) *A history of medicine* (Horatius press, Omaha) 2nd Ed.

Chapter 2: Background and Techniques for Studying Dendritic Cell Migration

Overview of Dendritic Cells

Discovery of Dendritic Cells

Although the Dendritic Cell (DC) was formally named in 1973, earlier research had described a cell that emigrated from the peripheral tissues to secondary lymphoid organs via the lymphatic system. In this early article by Smith *et al.*, "veiled macrophages" were observed in the draining lymph of sheep (1). This study, performed by cannulating the lymphatic vessels of adult sheep, showed that draining lymph is composed of approximately 80% lymphocytes and 20% 'veiled', mononuclear, phagocytic cells resembling macrophages (1). They were called 'veiled' for their numerous cytoplasmic extensions, which ultimately gave DCs their name. Later studies were able to link 'veiled' cells in draining lymph to DCs in other tissues, unifying them as a single cell type (2-4).

Dendritic cells were named in 1973 by Steinman and Cohn (5). Their seminal paper described an immune cell identified by unique "stellate" morphological characteristics which was found in the spleen and peripheral lymph nodes. They used the term "dendritic" to describe the myriad filopodial protrusions extending from the cell body. In further studies by the same authors, they showed that DCs express high levels of major histocompatibility complex (MHC) molecules, which are known to be the primary mechanism of antigen presentation (6). This role as possible antigen presenting cells was

confirmed in 1978 by the use of a mixed lymphocyte reaction assay with T lymphocytes; an experiment used to determine the DCs' ability to present antigen using MHC and the capacity to activate T cells which recognize the specific antigen being presented. In this *in vitro* experiment, DCs outperformed other splenic cells by two to three orders of magnitude, setting DCs apart as the most potent antigen presenting cell characterized to date (7).

Reaching further back, the earliest known report of a dendritic cell was made in 1868 by a German medical student, Paul Langerhans (8). He found cells in the epidermis with a 'dendritic' appearance. Since neurons were the only known 'dendritic' cell type, he mistook these cells for part of the nervous system. The identification of Langerhans cells as DCs, however, would not be made until a century after their discovery. We now know that Langerhans are one of many dendritic-cell subtypes, often differentiated by the tissues in which they reside, and by their surface markers. For example, in the epidermis of mucosal tissues, C-type lectins can be used to differentiate Langerhans cells from other DC subtypes (9); Non-Langerhans DCs in the subepithelium express DC-SIGN (10), whereas Langerhans cells are generally distinguished by their expression of Langerin.

Initial studies on DCs were difficult due to their relatively low abundance both in the blood (11) and in secondary lymphoid organs (5). Indeed, their reported frequency in both cases was less than 1% of all nucleated cells. A major advance in DC research was the development of a new technique for culturing large numbers of cells *in vitro* by Inaba *et al*. in 1992 (12). They used granulocyte-macrophage colony stimulating factor (GM-

CSF) to differentiate DCs from a myeloid lineage precursor. This technique facilitated an explosion in DC research, which has now reached saturation with over 2,000 journal articles each year containing the term "dendritic cell" in the title (see Figure 2.1).

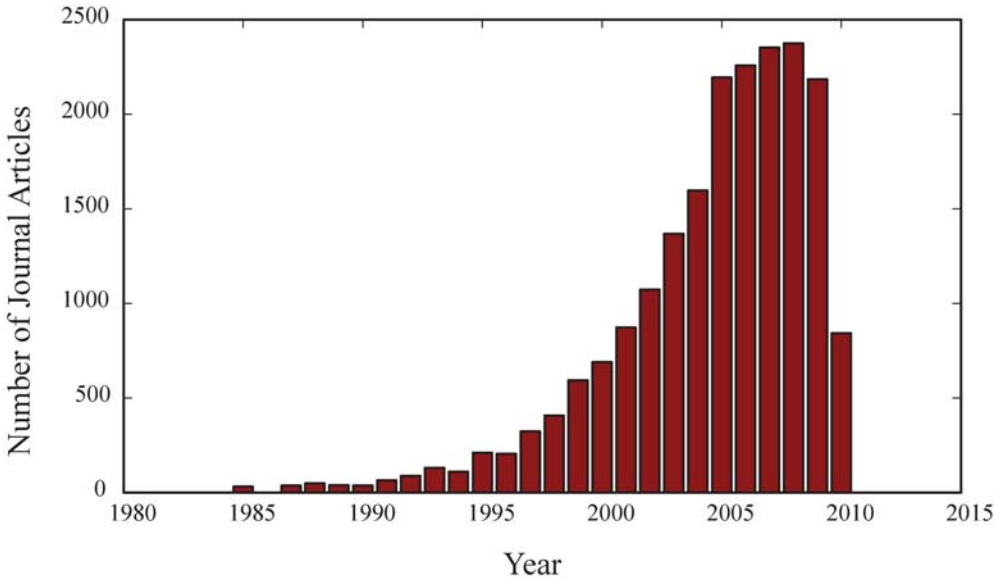

Figure 2.1. The number of peer-reviewed journal articles with "dendritic cell" in the title, as of June 14th, 2010. Source: ISI Web of Knowledge.

Subtypes of Dendritic Cells

As noted, DCs can be generally classified by the tissues within which they reside. Since DCs act as sentinels of the immune system, they are posted at the main points of pathogen entry. This includes the skin, gut and airway. As previously identified, Langerhans cells (Langerin$^+$, CD11b$^+$CD207$^+$) are responsible for monitoring the skin. Within the gut, conventional DCs are predominantly of the CD11c$^+$CD11b$^+$CD8α$^-$, CD11c$^+$CD11b$^-$CD8α$^+$ and CD11c$^+$CD11b$^-$CD8α$^-$ subtypes (13), with unique functional properties associated with each.

An additional distinction within dendritic cells is the myeloid, or conventional (sometimes referred to as cDCs, but here referred to only as DCs), and plasmacytoid (pDC) subtypes. They are differentiated based on phenotype, different progenitor cells (14), and their expression of toll-like receptors (TLRs) (15). While both DC subsets express TLR1 through TLR6, only pDCs express TLR7 and TLR9, allowing the immune system to uniquely respond to pathogen associated molecular patterns (PAMPs) recognized through those receptors (15). In their phenotype, pDCs are relatively small and spherical, resembling plasma cells, while conventional DCs are characterized by their many membrane protrusions, as discussed above. While myeloid DCs come from a myeloid lineage, pDCs come from a lymphoid progenitor (14). Despite their differences, both subtypes are potent initiators of the immune response.

The present work will focus on bone marrow derived DCs (BMDCs), which are generated via the myeloid lineage. $CD34^+$ stem cells are found in the bone marrow, and through the use of granulocyte-macrophage colony stimulating factor (GM-CSF), the myeloid lineage is stimulated while other leukocyte lineages are outcompeted. Macrophages are also of myeloid decent and are generated in large numbers by the use of GM-CSF, but they are easily separated from dendritic cells because of their strong adherence to substrates, whereas dendritic cells are only loosely adherent cells. BMDCs are heavily researched because they are easy to harvest and culture, but there may be further distinctions between BMDCs and DCs collected from the spleen, lymph nodes, or peripheral tissue. A direct comparison of DC subtypes or generation methods has not

been carried out. In general, it seems that plasmacytoid DCs are primarily involved in promoting the innate immune system (16) and are more difficult to prepare than myeloid DCs. Adaptive immunity is more useful in most potential DC applications—such as anti-cancer treatment or DC-based vaccines—so relatively few studies have been performed with plasmacytoid DCs. We now define DC subsets according to their cell surface marker expression. Murine DCs are essentially identified by their expression of CD11c, MHC Class II, CD4, CD8α, CD11b, and CD205. A summary of DC subtypes, their expression of surface markers, and where they are found within the mouse are summarized in Table 2.1 (17).

DC Subsets	Conventional					*Plasmacytoid
	Spleen and Lymph nodes			Lymph nodes		IPCs
	$CD4^{-}$ $CD8\alpha^{high}$	$CD4^{-}CD8\alpha^{-}$	$CD4^{+}CD8\alpha$	$CD4^{-}$ $CD8\alpha^{low}$	$CD4^{-}CD8\alpha^{-}$	
Lineage	Lymphoid	Myeloid	Myeloid	Myeloid	Myeloid	Lymphoid/ Myeoild
Phenotype						
CD8α	+++	-	-	var.	-	var.
CD4	-	-	++	-	-	var.
CD11b	-	var.	++	++	++	-
CD11c	+++	var.	+++	+++	+++	++
CD205	+++	-	-	+++	+	+
33D1	-	-	++	-	-	-
B220	-	-	-	-	-	++
Gr-1	-	-	-	-	-	++
128G	-	-	-	-	-	+++
440c	-	-	-	-	-	+++
mPDCA-1	-	-	-	-	-	+++
CD40	+	+,-	+	+++	++	-
CD80	+	+,-	+	+++	++	-
CD86	+	+,-	+	+++	++	-
MHCII	+++	+++	+++	+++	+++	++
Langerin	-	-	-	+++	-	-
Anatomical site	T-cell area	Marginal zone	Marginal zone	Skin-draining	All lymph nodes	All areas

-, negative; +, low; ++, intermediate; +++, high; var., heterogenous.

*Plasmacytoid DCs can be CD4-CD8α+, CD4+CD8α-, CD4-CD8α-, CD4+CD8α+subsets, and they are found mostly in the periarteriolar lymphoid sheaths, but scattered plasmacytoid DCs are present in the marginal zone and red pulp.

Table 2.1. Heterogeneity of murine DCs. Adapted from reference (17).

Role of Dendritic Cells in the Immune System

Dendritic cells act as sentinels in the immune system, positioned throughout the body, constantly sampling for foreign antigen. They remain relatively sessile in the tissue as immature cells, as soldiers waiting for orders. Dendritic cell maturation is the differentiation step taken by an immature DC after encountering a "danger signal". This danger signal is typically generated by local cells under distress, and can include interferons, uric acid (18), bradykinin (19), heat-shock proteins, nucleotides, reactive oxygen intermediates, and even extracellular-matrix breakdown products (20). The DC may also sense danger signals directly from a pathogen, such as lipopolysaccaride (LPS) from bacteria or pathogen-associated molecular patterns (PAMPs) which are bound by toll-like receptors (TLRs) on the DC. When DCs are exposed to these danger signals, antigen uptake is downregulated, while MHC expression, costimulatory molecules (CD86, CD80, CD83) are upregulated (21).

DCs will also regulate their expression of chemokine receptors depending on maturation state. Monocyte DC precursors circulate through the blood and transmigrate into peripheral tissue both constitutively and in response to inflammatory signals (22). Immature DCs in peripheral tissue then continue to express a variety of chemokine receptors which act to confer responsiveness to inflammatory chemokines and direct migration of DCs toward inflammatory stimuli and peripheral tissues in general. Specifically, immature DCs can express chemokine receptors CCR1 through CCR6 as well as CXCR3 and CXCR4 to navigate through the body (23). However, upon exposure

to danger signals such as inflammatory cytokines and foreign antigens, DCs down-regulate most chemokine receptors, with the notable exception of CXCR4, while upregulating the inflammatory receptor CCR7 (23-26). A clear role for CXCR4 has not been defined, but CCR7 is the receptor that directs DC migration to SLOs where high levels of CCR7 ligands CCL19 and CCL21 are constitutively expressed (27). Overall, maturation state dictates the chemokine receptor expression profile.

The remarkable organization of the mammalian immune system facilitates the efficient surveillance and targeted cellular response that contribute to host defense. Compartmental segregation of lymphoid tissues does, however, rely on the precise trafficking of immune cells between the circulation, tissues, and SLOs to achieve this efficiency. To achieve this level of tissue specificity, DCs developmentally regulate their expression of chemokine receptors. As stated above, they are fairly sessile as immature cells, but when matured they become highly motile and migrate to SLOs. The migration toward and within SLOs is essential to the function of dendritic cells and will be a major focus of research in this thesis.

Once DCs reach the SLO, they become maestros, orchestrating the adaptive immune response (21). DCs are widely accepted to be the most potent and versatile antigen presenting cells (APCs) in the immune system, due to their superior capacity for acquiring and processing antigens for presentation to T cells and their potential to express high levels of the co-stimulatory molecules that direct and fine-tune T-cell activation (22). Their migration and function is highlighted in Figure 2.2.

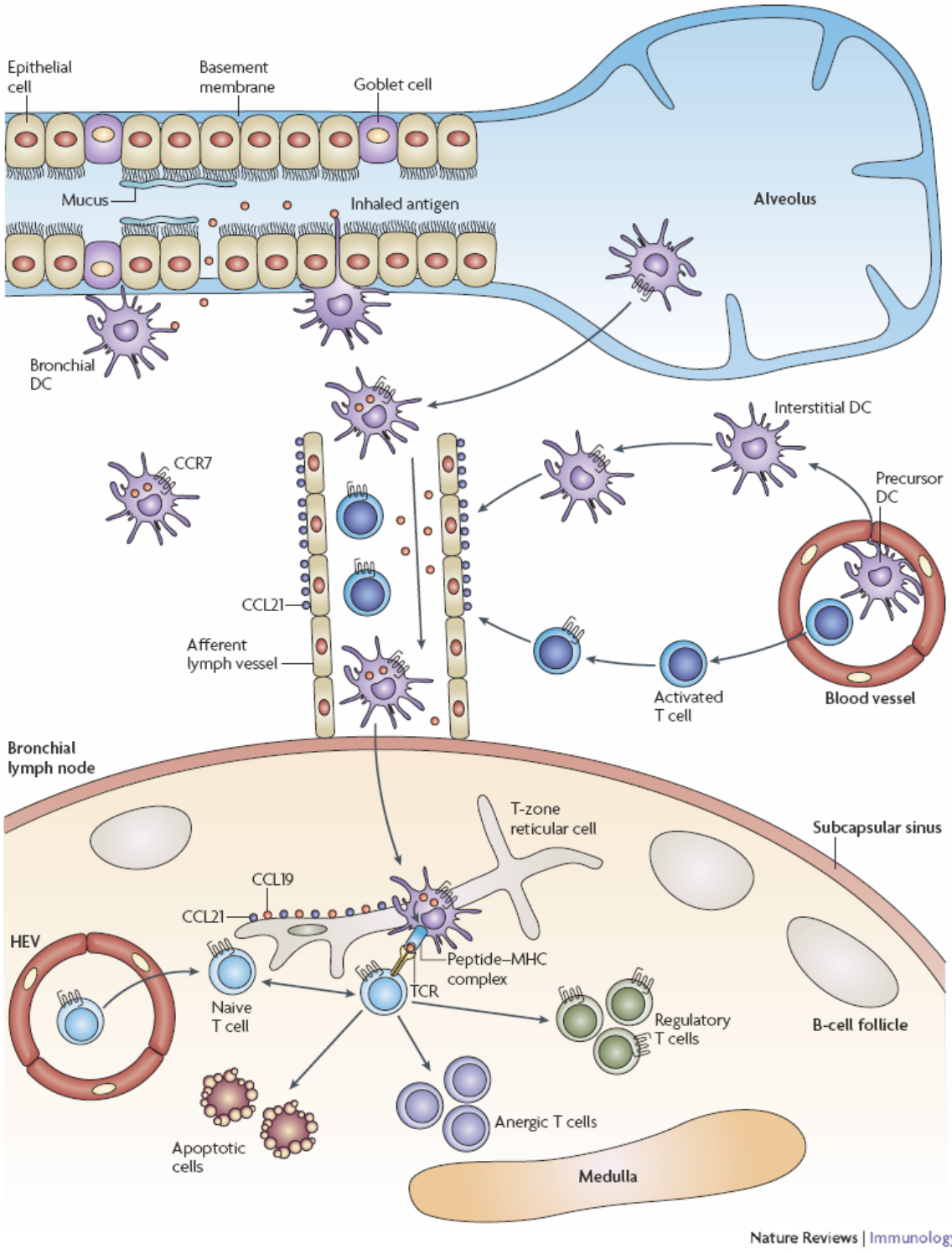

Figure 2.2. Overview of DC migration from tissue to lymph nodes. Adapted from (28).

All APCs use Class II MHC molecules as a platform for antigen presentation. As opposed to Class I MHC, which is expressed by nearly every cell in the body and is used to present self-antigens to natural killer (NK) cells, Class II MHC is only expressed by professional APCs. Previously endocytosed antigens are degraded in late endosome/early lysosomes within the APC. Separately, vesicles bud from the endoplasmic reticulum (ER) loaded with pre-formed MHC Class II molecules, whose conformation is preserved by Class II-associated invariant chain peptide (CLIP) which sits in the binding pocket. When the late endosomes fuse with MHC Class II loaded vesicles, unfolded or fragmented proteins from the endosome displace CLIP in the MHC Class II binding pocket (29). The complete, loaded, MHC Class II complex is then transported to the cell membrane where it is displayed on the cell surface. The MHC Class II complex is the primary means of communication between DCs and lymphocytes.

In SLOs, DCs prime T and B lymphocytes using the "immune synapse". The immune synapse is comprised of MHC Class II on the APC binding to the T cell receptor (TCR) on the T lymphocyte (30). Additionally, several co-stimulatory molecules are involved in stabilizing the immune synapse and sending secondary messages from the APC to the lymphocyte. Notably, CD3 is required from the T cell to stabilize the interaction (30). Either CD4 or CD8 is also required from the T cell and binds to the MHC complex (31). Once a successful immunological synapse has been formed, downstream signaling in the T cell through Ras and MAPK leads to gene expression and often proliferation (32). If

no secondary signal is received from the APC, the T cell is "tolerized" and undergoes apoptosis (33). If a secondary signal such as CD86 is presented by the APC (such molecules are upregulated upon maturation), the T cell will be activated and proliferate. Finally, the DC sends extra information through "Signal 3." This is interleukin 12 (IL-12) and interferon-alpha or IL-4 secreted from the DC (34). IL-12 and interferon-alpha generally promote an antibody-based Th1-type adaptive response. Conversely, IL-4 stimulates a $CD8^+$ T cell-based Th2-type response. Thus DCs are able to direct the type of adaptive immune response the host will pursue.

Chemokine Signaling: Critical Cues

Lymphocytes express a variety of chemokine receptors (CCRs) that allow them to navigate throughout the body. The unique combination of CCRs expressed on a cell is thought to provide direction toward, and retention within a specific organ. As previously noted, mature dendritic cells upregulate CCR7 which receives signals from CCL21 and CCL19 which are expressed on the afferent lymphatics and in the lymph node, directing mDCs to the site of T cell activation.

Chemokines themselves are small (approximately 8–14 kDa), generally basic, and structurally related cytokines that direct cell migration for a variety of leukocytes via their cognate binding interactions with G-protein coupled receptors (GPCRs) (35-36). All chemotactic cytokines belong to the chemokine superfamily, but they can be subdivided into 4 distinct groups (CXC, CX3C, CC, and C) according to the positioning

of the first 2 closely paired and highly conserved cysteines of the amino acid sequence which give the chemokine its tertiary structure (37). Currently, over 40 chemokines are known in the human genome, most having homologs in mice. They main cell types directed by chemokines are neutrophils, dendritic cells, monocytes, and lymphocytes, all of which have a role in host defense mechanisms. In addition to providing directional cues for chemotaxis, it has been suggested that chemokines play fundamental roles in the development, homeostasis, and function of the immune system (35-36, 38). Further, chemokines are used outside of the immune system in a variety of cell types, including cells of the central nervous system (39) or endothelial cells, where they can produce either angiogenic or angiostatic effects (40). However, we will focus on the chemokines relevant for inducing chemotaxis in leukocytes, especially CCL19, CCL21 and CXCL12.

Chemokine receptors are a family of 7-transmembrane G-protein coupled receptors found predominantly on leukocytes (37, 41). To date, 19 chemokine receptors have been identified in humans, with homologs in mice (37-38). CCRs are generally composed of approximately 350 amino acids, and have conserved structural motifs. The N-terminus generally has a short section of acidic residues, which is oriented into the extracellular space where it acts to bind specific chemokines. The seven helical transmembrane domains orient into a barrel shape butted by three intracellular and three extracellular hydrophilic loops, and an intracellular C-terminus containing hydroxyl groups (serine and threonine) which provide sites for phosphorylation which in turn regulate receptor signaling (41). G-proteins couple to the C-terminal end, which is the only known mechanism for receptor signaling following ligand binding. Although chemokine

receptors bear significant homology in their primary sequences, they typically bind only a small number of ligands, often only one. The chemokine receptor is named for the subtype of chemokine it binds, and is numbered according to an agreed-upon standard (35). A summary of chemokines and their receptors are shown in Figure 2.3. Our focus is on CCR7 and CXCR4, which are relevant for mature dendritic cell chemotaxis.

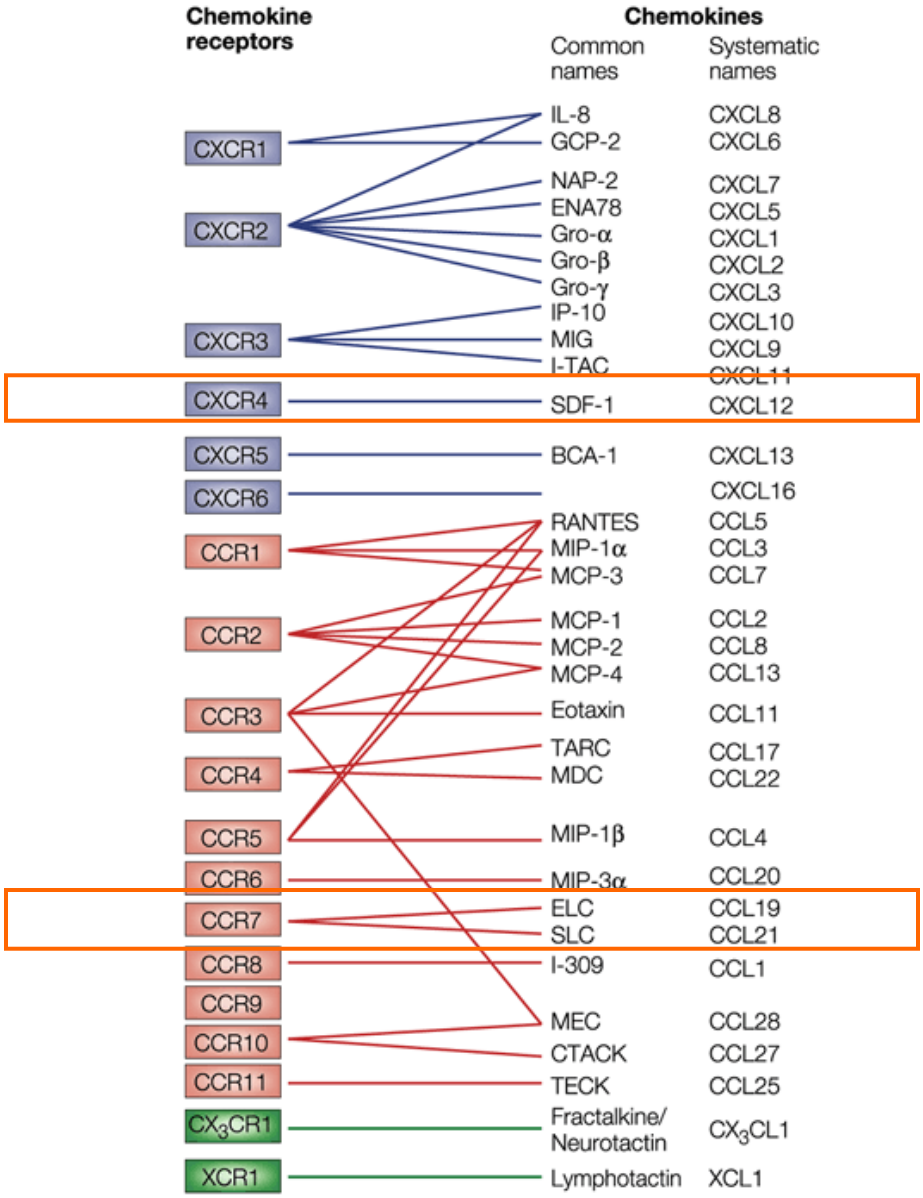

Figure 2.3. Chemokines and the receptors they bind. Adapted from (38).

Chemokines and Dendritic Cells

CCR7 is a typical member of the 7-transmembrane domain G-protein coupled receptor (GPCR) family. Its two known ligands CCL19 and CCL21 exhibit similar affinities for receptor binding (~7nM) (42). Signaling is thought to proceed by activation of a G-protein of the $G_{\alpha i}$ subfamily, which may or may not be precoupled to the receptor. CCR7 binds the α-subunit of the G-protein and releases the βγ-subunit, potentially activating both for downstream signaling. It has not been established which of CCR7's effects are downstream of the α and βγ subunits, though preliminary evidence points to PI3K activity downstream of the βγ subunit (43). Following activation, GPCRs become desensitized and ultimately downregulated through a chain of reactions occurring near the cytoplasmic carboxyl terminus. This process of adaptation begins with receptor phosphorylation by GRKs. In one of the few studies of CCR7 phosphorylation, CCL19 was shown to induce significantly more phosphorylation than CCL21 in a human T cell lymphoma cell line (44-45). Once the GPCR is phosphorylated, arrestins are recruited and bind the carboxyl terminus. Binding of arrestins then induces clathrin-mediated endocytosis. CCL19 has been shown to induce a lower steady-state level of CCR7 surface expression by higher rates of endocytosis in a human T cell lymphoma cell line (45). Finally, CCL19 is able to desensitize a T cell's responsiveness to CCL21, but not vice versa (42). *In vivo*, this may allow cells to respond first to CCL21 expressed on afferent lymphatic vessels, then subsequently to CCL19 within the lymph node to find the T-cell rich paracortex. Cumulatively, significant evidence suggests that although CCL19

and CCL21 have similar affinities for CCR7, their downstream regulation has the potential to activate distinct physiological responses.

Deletion of CCR7 or its ligands CCL19 and CCL21 (in the *plt* mouse) does not fully impair DC migration to lymph nodes, implying that the process is complex and that additional chemokine-receptor pairs are likely to be involved. One such candidate is the chemokine CXCL12, recently shown to be present in murine dermal lymphatics by fluorescent immunohistochemistry, and its cognate receptor CXCR4, shown to be expressed in cutaneous MHC class II+ DCs (46). The relative contributions of CCR7/CCL21 and CXCR4/CXCL12 to dendritic cell migration have not been well-studied, but are a focus of this thesis. In one study, the effects of the two chemokines were not additive (47). Hence, these chemokine–receptor pairs may function independently of one another.

Measuring Chemotaxis: Quantifying Cellular Navigation

Chemotaxis is the directed motion of cells toward a soluble chemical signal. Related are haptotaxis and durotaxis, which describe directed migration toward a surface-bound stimulus or a stiffer surface, respectively. These types of directed motion are important for maintaining organ structure (27, 36, 48), wound repair (40), neuronal function (39), bacterial navigation (49) and leukocyte navigation (50-52). To understand these behaviors in greater detail, it has become necessary to develop precise assays to measure chemotaxis.

Observation of chemotaxis is facilitated by the direct observation of cells, first made possible by the application of light microscopy to biological questions lead by Antoine van Leeuwenhoek in the early 1700's. The term chemotaxis was was first used by Pfeffer, *et al* in 1884 (53) to describe the behavior of cells moving in response to chemical mediators. Direct observation of the chemotaxis in leukocytes was made soon after in 1888 by Leber, *et al* in excised rabbit ocular tissues (54). It was not until the 1960's, however, that any quantitative technique was developed to measure chemotaxis.

Boyden Chamber Technique

The introduction of the membrane filter chamber method in 1962 by Australian biologist Stephen Boyden greatly facilitated the study of cellular chemotaxis (55). Using this setup, cells were introduced into an upper chamber and soluble chemotactic substances were added to a lower chamber, separated by a membrane. This technique allowed quantization of the cells that had transmigrated the membrane barrier, making results more reproducible and easier to compare across different conditions. The Boyden chamber, with subsequent improvements culminating in what is now known as a "transwell assay", has since become a popular choice for studies of leukocyte chemotaxis *in vitro* (56-57).

Although it is commonly used, the Boyden chamber/transwell assay has several limitations that hinder its use as a quantitative technique. The setup involves dispensing

cells onto a non-physiological, porous membrane. This membrane may be a good mimic of basement membranes, but it is generally far too stiff to simulate tissue. The chemokine is generally placed in a lower chamber, and allowed to diffuse through the membrane over time. This creates a time-dependent diffusion problem presenting an ever-changing gradient to the cells. No analysis of gradient perception is possible, and the kinetics of convection/diffusion may change based on subtle differences in the experimentalist's technique. Although results are more reliable than passive observations, they are notoriously variable, and sometimes produce spectacular results which cannot be repeated, such as in Paoletti *et al* (51). Although rigorous mathematical analysis can be applied to extract advanced metrics (58), the vast majority of researchers do not go to such lengths, and simply report the number of transmigrated cells after an arbitrary amount of time.

Under Agarose Technique

Another widely used technique for measuring chemotaxis is the "under agarose assay." It was originally developed in 1975 as an alternative to the Boyden chamber assay (59). According to the original authors, the under-agarose assay

> "has application to both polymorphonuclear leukocytes and monocytes, permits measurement of both chemotaxis and spontaneous migration, requires fewer cells per test, and is rapid, simple, reproducible, and inexpensive to set up." (59)

This method involves curing a gel of agarose in a thin layer over a glass or plastic surface. Holes are punched in the gel, then cells are added to one well, while a

chemoattractant is added to another. Using this technique, direct visualization of the migrating cells is possible. Additionally, multiple competing signals can be presented to the cells (60). This technique is a substantial upgrade over transwell assays, but still suffers from the fundamental lack of gradient control. The chemoattractant must diffuse under the gel, meaning the concentration profile is a function of time and space.

Zigmond/Dunn Chamber Technique

In 1977, a further advance in the assays to study leukocyte chemotaxis was made by Sally Zigmond *et al* (61). This technique is quite similar to the under-agarose technique, but since it allows diffusion over a small bridge between two large reservoirs, the gradient is significantly more stable over time. The cells are observed as they move across the bridge toward the chemoattractant-containing reservoir. Using this direct-visualization technique,

> "Observational studies can determine whether a given alteration in the chemotactic response is due to variations in (a) the percentage of cells responding, (b) the accuracy of the orientation, (c) the frequency or magnitude of turns, or (d) selective changes in the rate of movement by cells in a certain orientation relative to the direction of the gradient." (61)

A highly similar setup was later devised by Graham Dunn and colleagues (62), which used a center reservoir for cells encircled by a ring-shaped bridge separating the cells from a large outer reservoir containing chemoattractant. It was proposed as an alternative

to the Zigmond chamber and optimized for slower moving cells such as fibroblasts. It also avoids edge-effects that can be present in a Zigmond chamber, but at the expense of not being able to replenish the center reservoir during an experiment.

Ultimately, both techniques were an improvement over the Boyden/transwell assay because they allowed direct observation of moving cells and significantly better control of the chemical gradient. These were critical steps forward in gaining engineering control over the experimental system. The main drawback presented by these techniques are that only a small number of cells can be observed in an experiment, and importantly, the gradient changes as a function of time. During startup, the gradient changes rapidly as a diffusion front crosses the bridge. The gradient is then pseudo-stable and approximately linear, with the endpoints changing as the chemoattractant slowly bleeds into the opposing reservoir. After long observation periods, the gradient will ultimately flatten as the chemoattractant becomes equally distributed between the reservoirs. Thus despite the advances of the Zigmond/Dunn chambers, limitations remain.

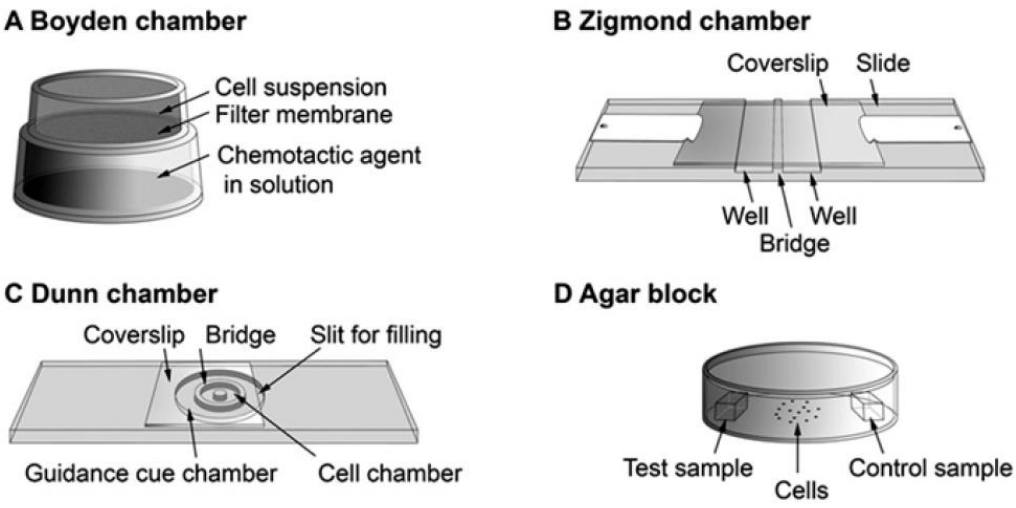

Figure 2.4. Survey of available chemotaxis assays. Adapted from (63).

Microfluidic Devices

Recently, microfluidic devices (MFDs) have been applied to the study of leukocyte chemotaxis (64-71). The implementation of this technique varies widely, but generally involves mixing two microfluidic streams—one containing chemokine and one empty—to create a gradient. The gradient flows over cells that are adhered to a substrate. Thus this technique offers all the advantages of direct observation, with the improvement of a time-invariant gradient. The hydrodynamic flow can be a confounding factor of cell behavior, but the flow rate is generally minimized to reduce shear on the cells and limit impact on their migration. Another key advantage of microfluidic gradient generators is the possibility of presenting multiple, overlapping gradients to the cells, which can aid in detecting a signaling hierarchy.

Despite being developed only 10 years ago, MFDs have already been used to study a variety of cell types in a vast array of configurations. The most popularly studied cell type is neutrophils (64, 66-67, 69, 71-72), but slower moving cells such as endothelial cells (73) and cancer cells (74) have also been examined. Importantly, Francis Lin was the first to extend the use of MFDs to the study of lymphocytes in 2006 (65). Some basic studies using dendritic cells have also been recently reported by Haessler *et al* (71). In their study, they combine the agarose and MFD techniques to show that dendritic cell chemotaxis is possible to a microfluidic gradient of CCL19. On the whole, these studies show the value of microfluidics for presenting stable, time-invariant gradients of chemokine to motile cells.

The Rise of Microfluidic Devices

The evolution of microfluidic devices began with the application of photolithography, literally "optical stone writing", to silicon substrates in the 1950's (75). This process allowed patterns of arbitrary complexity to be etched into very flat surfaces. Indeed, photolithography was originally developed for use in the semiconductor industry, where patterning ever-smaller features was the driving force behind Moore's Law (76), which describes the ever-increasing speed of transistor-based processors as feature sizes decrease. Building upon photolithography, the invention of soft lithography by George Whitesides in the late 1990's (77) was the next step toward microfluidic devices.
Soft lithography uses photomasks, polymer-based stamps and molds in various combinations to fabricate or replicate patterns. The term "soft" is derived from soft lithography's use of elastomeric materials, especially polydimethylsiloxane (PDMS). The

soft lithography platform is generally used to create features on the micron scale, but can be scaled down to the nanometer scale (78-79).

PDMS: A crucial material

Polydimethylsiloxane (PDMS) is the material that makes current bio-microengineering applications possible. PDMS is one of a family of organic silicon polymers that together are referred to as silicones. Of the silicones, PDMS is by far the most widely used in biological applications, due to a number of factors. It's rheological properties make it suitable for casting into complex 3D structures, and cured to permanently maintain its shape. For its physical properties, PDMS is ideal for microscopy because it is optically clear, and it is stiff enough to withstand high pressures seen in microfluidic devices. The shear modulus of PDMS varies with the ratio of prepolymer to crosslinker, and it can vary from approximately ~100 kPa to ~10 MPa (80). For its chemical properties, PDMS is not fully bio-compatible, but it is considered to be inert, non-toxic and non-flammable. After polymerization/cross-linking, the surface of solid PDMS presents a hydrophobic surface (80). The predominant -Si surface chemistry makes it difficult for polar solvents like water to wet the PDMS surface, and makes the surface attractive for binding hydrophobic compounds such as proteins. Plasma cleaning and ozone treatment can be used to oxidize the surface, creating silanol (Si-OH) groups at the surface. After oxidation, the PDMS surface is hydrophilic, making it easy to wet channels with water and the oxidized surface resists hydrophobic protein adsorption. More often, however, the surface is simply blocked with serum proteins or bovine serum albumin (BSA) because oxidized surfaces are only stable for approximately 30 minutes. Even solid

PDMS is able to undergo hydrophobic recovery of the surface, regardless of the surrounding medium (water, air, vacuum). While other applications for PDMS include shampoos, caulking, heat-resistant tiling, and lubricating oils, the physical and chemical properties of PDMS make it ideal for studying reductionist biological systems on a small scale.

Soft Lithography

The soft lithography process is comprised of two parts. First, the fabrication of a pattern onto a substrate creating a 'master', and second, the use of that pattern to produce features negatively defined by the pattern's relief structure in an elastomeric substrate. The two steps are generally quite distinct, though in some cases the stamp created from the master can be used to generate a replica of the original master. The master can be produced using any number of techniques that produce a well-defined structure on a surface. Several elastomeric replicates can be fabricated from a single master. Typically, the pattern on the master is created by the previously mentioned photolithography. In this process, a thin layer of photoresist is deposited on a hyper-flat silicon substrate by spin-coating. The pattern is then created in the photoresist by shining collimated light through a high-resolution photomask. The photomask is typically a pattern printed onto a transparency, and feature size is limited only by printer resolution. Two types of photoresist are used: negative photoresists cure upon exposure to light, while positive photoresists are pre-cured, then degrade upon exposure to light. Due to the development of optimized materials and chemistries, this fabrication technique has remarkably high fidelity (81). Once the master has been created, the creation of a negative replicate in

PDMS is relatively simple. PDMS pre-polymer is poured over the master, the system is degassed to remove any bubbles, and the PDMS is then cured at 25-150°C to crosslink the polymer.

Recent Advances in Microfluidic Devices

With the advent of facile methods for rapidly fabricating and testing prototypes of microfluidic devices has come an avalanche of innovative applications for this flexible platform. Some of the most basic gradient generators used a simple Y-junction, and depended upon diffusion to establish a non-linear gradient (65). Other more advanced gradient generators use a "Christmas-tree" splitting and recombining of streams to create stepped gradients and serpentine channels to fully mix streams, smoothing the gradients (82). These chambers can also be manipulated to give non-linear profiles by using asymmetric flow (83), or serial dilutions schemes (84). Since not all biological gradients are linear, these approaches are valuable. Taken to an extreme, exponential shaped gradients have been formed to simulate a constant ratio of $\Delta C / \overline{C}$. Another interesting extension of the microfluidic platform has been rapid gradient switching to show how cells make turns (66). This is especially important for neutrophils, which are following a moving target—bacteria—but less important for DCs, which follow relatively time- and space-invariant gradients to reach stable structures.

Previous work using microfluidic devices to study leukocytes other than neutrophils is sparse. Neutrophils are well-studied because they are readily obtained from human peripheral blood, and are reliably motile across a wide variety of substrate ligands and

stiffnesses. As mentioned above, the first application of microfluidics to T cells was completed by Francis Lin in 2006 (65). Although DC migration has been shown in confined microchannels (85), it did not use a gradient generator to present a chemotactic signal. Thus the use of microfluidic gradient generators in leukocyte research (especially DC research), is an open area of investigation.

Cell Polarity and Motility

To properly respond to an external gradient, a cell must polarize its cellular response (43). This polarization is generally considered in terms of two distinct regions: the "front" and the "rear". The front leading edge, or pseudopod, is characterized by f-actin rich protrusions, either lamellipodia or filopodia. Lamellipodia are broad, flat coherent protrusions, whereas filopodia are long, thin finger-like projections from the cell membrane. The rear trailing edge, or uropod, is generally characterized by the retraction of old adhesions from the substratum. The two edges of a cell are also thought to be governed by distinct signaling molecules and pathways. Molecules typically found near the leading edge of a migrating cell are PI3K (86), Rac, CDC42 (87) and most molecules associated with actin polymerization such as ARP 2/3 and ENA/VASP (52). At the other end, molecules associated with the trailing edge are PTEN, Rho signaling molecules such as ROCK, and the crucially important myosin IIb (88). Although several relevant molecules have been identified and their spatial structure determined, there is still much debate about the precise combination of molecules and signaling pathways that govern the migration seen in various cell types, not least dendritic cells (89).

Amoeboid Cell Motility

Although many molecules and pathways associated with motility are conserved across a wide variety of species and cell types, an important distinction should be made between amoeboid and lamellipodial cell migration. Amoeboid motility may be considered a primitive mode of cell migration, as even prokaryotes are able to display this relatively fast locomotion. Amoeboid cells do not use the long-lasting, highly stable focal adhesions used in the lamellipodial model; rather, they manipulate their body shape to effect cell displacement. These cells are capable of squeezing through tight junctions such as gaps in barrier membranes and transwell plate assays. In contrast, the lamellipodial model prefers to remodel the extracellular matrix through proteolysis using matrix metalloproteases (MMPs).

Neutrophils are classical exhibitors of amoeboid migration, but are surpassed by the slime-mold *Dictyostelium discoideum* (52, 90-91) and fish keratocytes (92-93) as the most intensively studied amoeboid cell models. Although recent research has begun to focus on DCs as models for amoeboid cell migration (94-95), the field is still in its nascent stages and many open questions remain.

Cell Polarization

Though much progress has been made, the question of how a cell establishes and maintains the polarity necessary for directed migration remains unsolved. One leading theory is the mutual inhibition hypothesis (43). In this scheme, there are two distinct

signaling pathways that are both triggered by GPCRs. Since they mutually inhibit one another, small fluctuations are easily amplified into stable signals at the front and rear. A schematic of this theory is shown in Figure 2.5.

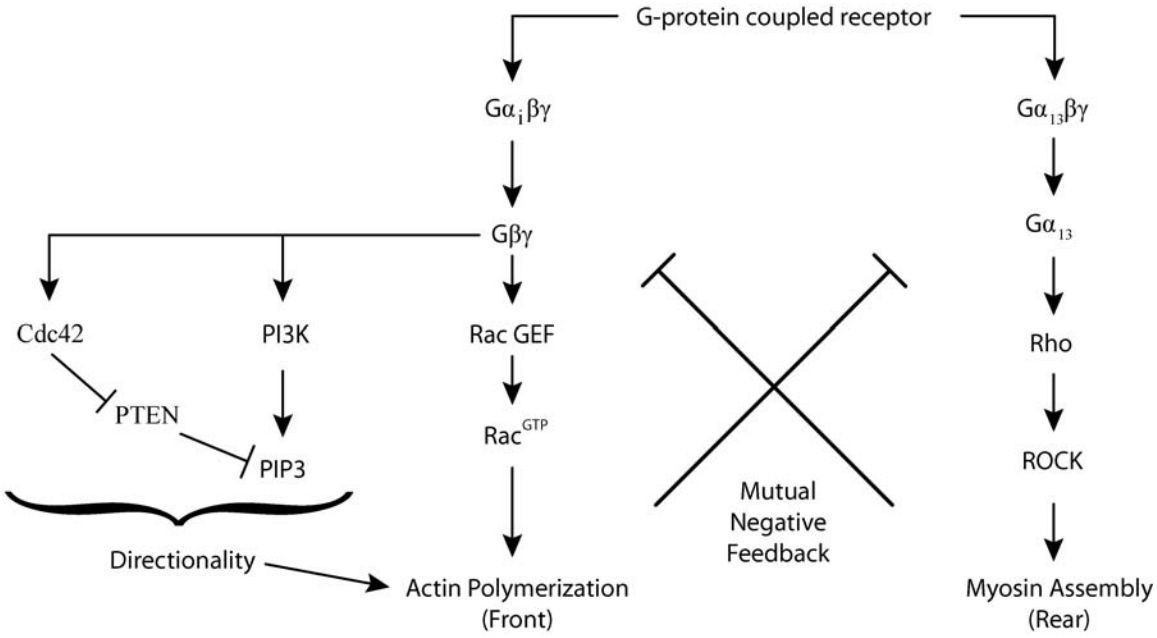

Figure 2.5. Mutual inhibition pathways establish cell polarity and provide directionality for chemotaxis. Adapted from (43).

Under the mutual inhibition theory, signaling in the front of the cell is initiated by $G\alpha_i$ proteins. The $\beta\gamma$ subunit separates from $G\alpha_i$ and signals through at least three downstream pathways: Cdc42, PI3K and Rac. Thus these proteins are typically found at the leading edge. For DCs, Cdc42 has been shown to be particularly important for directional navigation toward chemokines (87). In neutrophils, PI3K is an important molecule for organizing the leading edge (96-97). In monocytes and some T cells, however, it was shown to be dispensable for directed migration (98). In dendritic cells, it

was shown to be necessary for chemotaxis to LBT4 (99). Rac is an important activator of actin assembly, often found at the leading edge of migrating cells (100).

Signaling at the rear of the cell is thought to be directed by $G\alpha_{13}$ proteins. They activate the small GTPase RhoA, which is commonly localized to the uropod or trailing edge (101-102). Rho and Rac work in concert to maintain the mutual inhibition at the front and rear. Rho then activates Rho-associated protein kinase (ROCK), which in turn phosphorylates the light chain of myosin II, inducing contractility (103). Another important molecule for maintaining polarity is PTEN, which is localized to the rear of the cell. PTEN is inhibited by Cdc42, and it inhibits PIP3, so it is a critical fulcrum of the front-rear mutual inhibition (90). Loss of PTEN is associated with endothelial-mesenchymal transitions (EMT) and subsequent cancer metastasis (104).

Traction Forces: Measuring Cellular Footsteps

Measuring traction forces is a non-trivial endeavor. Several techniques have been developed over the last 30 years to enable to measurement of forces exerted by the cell on its surroundings. Starting with silicone films, moving to elastic polymer networks, and even a bed of needles, there are several ways to approach the problem, each with unique advantages and drawbacks.

Silicone Films

One of the first observations of cells producing force was made using fibroblasts on a thin film. The observations were published in 1959 by biologist Paul Weiss using fibroblasts on thin films of plasma clots (105). Weiss developed a methodology for studying the fibroblasts and during cell culture he observed the formation of thin lines and wrinkles underneath and emanating from the fibroblasts. Interestingly, Weiss believed that the presence of the wrinkles was a result of dehydration and shrinkage of the protein networks within the clot film, and not actually produced by the cells themselves. The wrinkles extended in a radial fashion from both individual cells and groups of cells. Further, Weiss observed that cells would reorient themselves with along the axis of the wrinkles, providing the first observations of what is now a well-studied phenomenon: contact guidance (106).

It was not until a few decades later that a new—also incorrect—explanation was proposed for the wrinkles in cell substrata. In 1980, Harris *et al*. began using a new type of substratum: silicone films (106). Harris, like Weiss, observed wrinkles in a film beneath a cell, but Harris hypothesized that the wrinkles were due to the presence of a cell's rearward-directed traction force. This was the first use of thin films of silicone in the field of cell mechanics and it represented a major step forward in the detection of cellular traction forces.

Using silicone films to detect traction forces represented a breakthrough, because it allowed direct observation of cellular forces. Although the results were qualitative, they

were able to provide information about the location of forces underneath the cell and give a rough idea of their magnitude. This allowed for the observation that wrinkles started just behind the leading edge and were less prominent in the lamellipodia itself.

The response of cells to substrates of different stiffnesses has become a relevant area of research for stem cell differentiation (107-108) and leukocyte migration (64, 109). Using silicone substrates, the substrate stiffness could be modulated by differential curing of the substrate; notably by varying exposure to heat and using different silicone polymers.

Despite making some early and important contributions to the field, silicone films present a number of limitations that ultimately led to the use of other substrates for measuring traction forces. Most importantly, the use of silicone substrates gives only qualitative results. Some authors attempted to correlate cell wrinkling patterns with those obtained my mechanically applying a known force (110), but the results remain correlative. They did, however, make the first estimates of fibroblast force, stating that chick heart fibroblasts exert shear forces of approximately 0.001 dynes/m. Another disadvantage was the difficulty in reproducibly making substrates of the same stiffness. Due to these important disadvantages, the use of silicone gels to study traction forces seems to have run its course. Ultimately, polyacrylamide gels would prove themselves superior for studying cellular response to stiffness due to the limitations listed above and the advantages of gels listed below.

Polyacrylamide Gels with Fluorescent Beads

Motivated by the difficulty of controlling the stiffness of silicone films, Pelham and Wang pioneered the use of functionalized polyacrylamide (PA) gels to study traction forces (111). These PA gels were thin films, but did not wrinkle like silicone films. To prevent wrinkling of the gels, the PA is covalently attached to a glass coverslip using glutaraldehyde. This was a major advance in traction force studies, and the use of PA gels remains popular. Non-wrinkling PA gels also have a major advantage in that they are elastic. Elasticity greatly simplifies force measurements, because measured strains are linearly related to imposed stresses. As Pelham and Wang were the first to demonstrate, the stiffness of the PA gel can be easily modulated by varying the amount of pre-polymer (acrylamide) and crosslinker (bis-acrylamide) used in the uncured solution. Both the absolute amount of pre-polymer and crosslinker and their relative ratio are critical for determining gel stiffness, and the possible combinations lead to a range of gel stiffnesses from 400 to over 70,000 Pa (112).

Polyacrylamide itself is inert to cells, and considered non-adhesive to proteins and cells. Thus another moiety must be added to the gel surface to provide a foothold for the cells. Typically this is a protein found in the extracellular matrix (ECM) such as fibronectin, collagen, or a peptide mimicking such proteins (113). The ECM protein is covalently linked to the surface—either via a photo-activated crosslinker (64) or via a protein-adhesive group copolymerized into the gel (114)—providing a solid linkage from the gel to the adhesion ligand.

To make quantitative measurements of strain, the PA gel is embedded with nanometer-scale fluorescent beads. The beads are able to report gel displacements. Bead displacements can then be used to infer cell traction forces. Micah Dembo collaborated with Pelham and Wang to develop a complex computational method for mapping bead displacements to traction forces (115). Despite the linear response of PA gels to imposed forces, this reverse mapping is extremely complex. Dembo breaks the problem down into several small, overlapping strain fields acting on a single plane. His theory defines the displacement field of the elastic substrate as an integral over the traction field. Since an arbitrary number of displacement fields can produce the same traction field, the equation does not have an analytic solution and must be solved numerically using statistical methods. This method can resolve traction forces with an arbitrary mesh size, so forces can be visualized at fine spatial resolution within a cell. Other laboratories have developed similar mathematical techniques for determining traction forces from bead displacements; their work is reviewed in reference (116). The technique developed by Dembo and coworkers is now referred to as traction force microscopy (TFM).

TFM has been used to study a variety of cell types, starting with fibroblasts (115) and ranging to endothelial cells (113) and neutrophils (117). The traction forces produced by endothelial cells are quite strong, on the order of fibroblasts (118) and their orientation profile resembles that of fibroblasts. Specifically, mesenchymal cells seem to exert their traction forces at the leading edge, with the newest focal adhesions generating the greatest force (119). In contrast, Smith and colleagues were the first to use TFM to analyze neutrophils, and found that their forces are concentrated at the rear of a migrating

cell (117), similar to their amoeboid cousins, fish keratocytes (110). The magnitude of neutrophil forces was found to be significantly lower than mesenchymal cells, at approximately 70 nN/cell (117).

Until recently, TFM was limited to measuring traction forces in two dimensions. Recent advances have allowed the measurement of traction forces in the third dimension. This problem was first tackled by the Chien lab, providing calculations for forces that cells may exert in three dimensions even on two dimensional substrates (120). This was quickly followed by experimental data showing that indeed, cells do exert upward forces in the uropod as cells retract old adhesions, and can sometimes produce downward forces in the lamellipod (121). Finally, a fully three dimensional traction force technique is being developed in Christopher Chen's laboratory at the University of Pennsylvania, where cells are embedded in a three dimensional environment. This represents the future of traction force microscopy.

Micromachined Cantilevers

The methods for measuring traction force discussed above all use substrates that provide a continuous surface for cell migration. In addition to these surface continuum methods, there are techniques that define patterned surfaces to which cells can adhere. An initial study in this discrete surface approach was presented by Galbraith and Sheetz using micromachined cantilevers (122). The force on each cantilever can be calculated as a cell migrates across a densely packed field, yielding highly specific information about the

local force. Deflections are recorded using standard microscopy techniques, and are easily converted to forces using the known stiffness of a cantilever. Since the cantilevers are independent of one another, measurements of single focal adhesions are possible. In this system, the cantilevers are restricted to motion in one-dimension, so three dimensional calculations are not possible. Additionally, machining of the cantilever array is technically challenging.

Microfabricated Post Array Detectors

Capitalizing on the advantages of micromachined cantilevers, an improved discrete method was developed by Chen and colleagues (123). In their experimental system, ECM proteins are stamped onto the tips of microposts fabricated in PDMS. The simplified production technique based on soft lithography allows rapid production of several substrates. As with micromachined cantilevers, micropost deflections are easily correlated to forces by a linear relationship. Initially, spring constants of microposts were determined by recording the deflection of calibrated glass pipettes which had been manipulated to deflect individual microposts by predetermined distances. With this simple but reproducible fabrication technique, once a post pattern has been calibrated, it can be replicated with high fidelity. To functionalize the tips of the microposts, the PDMS is exposed to oxygen plasma to break the silicone chains at the surface, activating them to bind hydrophilic proteins (80). Then a separate, flat PDMS stamp with ECM protein is brought into contact with the microposts, transferring the ECM to the micropost tips. The mPAD system is quite flexible because the height and diameter of the microposts can be varied to give different effective stiffnesses. A range from 1.5 kPa to

over 1000 kPa can be generated simply by changing micropost height (124). Another advantage of the high-fidelity manufacturing technique is that the unstressed state of the posts can be reliably estimated from the grid pattern, so a "null" image is not required to calculate displacements.

Micropost array detectors are quite useful for force measurement, but like any technique, they have drawbacks. The most important is the discrete nature of the substrate. It is difficult to compare the results from a micropost array with those on a continuous substrate, but both are difficult to compare to a true three-dimensional *in vivo* environment. Another issue is the limitation of adhesion sizes to micropost tips. By using deep reactive ion etching process, however, smaller resolutions can be realized in the silicon templates used to fabricate the microposts (125). Microposts 1 micron in diameter and 3 microns center-to-center spacing can now be produced. By increasing the number of posts underneath each cell, the spatial resolution of forces was improved, but the sensitivity was decreased since the force applied per post was smaller. Overall, mPADs are accurate assays of cellular force whose analysis is straightforward and results are reliable.

References

1. Smith JB, McIntosh GH, & Morris B (1970) The traffic of cells through tissues: a study of peripheral lymph in sheep. (Translated from eng) *J Anat* 107(Pt 1):87-100 (in eng).
2. Kelly RH, Balfour BM, Armstrong JA, & Griffith S (1978) Functional anatomy of lymph nodes. II. Peripheral lymph-borne mononuclear cells. *The Anatomical Record* 190(1):5-21.

3. Drexhage HA, Mullink H, Groot J, Clarke J, & Balfour BM (1979) A study of cells present in peripheral lymph of pigs with special reference to a type of cell resembling the langerhans cell. *Cell and Tissue Research* 202(3):407-430.

4. Pugh C, MacPherson G, & Steer H (1983) Characterization of nonlymphoid cells derived from rat peripheral lymph. *The Journal of Experimental Medicine* 157(6):1758-1779.

5. Steinman RM & Cohn ZA (1973) IDENTIFICATION OF A NOVEL CELL TYPE IN PERIPHERAL LYMPHOID ORGANS OF MICE. *The Journal of Experimental Medicine* 137(5):1142-1162.

6. Steinman RM, Kaplan G, Witmer MD, & Cohn ZA (1979) Identification Of A Novel Cell Type In Peripheral Lymphoid Organs Of Mice .5. Purification Of Spleen Dendritic Cells, New Surface Markets, And Maintenance Invitro. *Journal Of Experimental Medicine* 149(1):1-16.

7. Steinman RM & Witmer MD (1978) Lymphoid Dendritic Cells Are Potent Stimulators Of Primary Mixed Leukocyte Reaction In Mice. *Proceedings Of The National Academy Of Sciences Of The United States Of America* 75(10):5132-5136.

8. Langerhans P (1868) Ueber die Nerven der menschlichen Haut. *Virchows Archiv* 44(2):325-337.

9. Patterson BK, *et al.* (2002) Susceptibility to Human Immunodeficiency Virus-1 Infection of Human Foreskin and Cervical Tissue Grown in Explant Culture. *Am J Pathol* 161(3):867-873.

10. de Witte L, *et al.* (2007) Langerin is a natural barrier to HIV-1 transmission by Langerhans cells. *Nat Med* 13(3):367-371.

11. Fearnley DB, Whyte LF, Carnoutsos SA, Cook AH, & Hart DNJ (1999) Monitoring human blood dendritic cell numbers in normal individuals and in stem cell transplantation. *Blood* 93(2):728-736.

12. Inaba K, *et al.* (1992) Generation Of Large Numbers Of Dendritic Cells From Mouse Bone-Marrow Cultures Supplemented With Granulocyte Macrophage Colony-Stimulating Factor. *Journal Of Experimental Medicine* 176(6):1693-1702.

13. Coombes JL & Powrie F (2008) Dendritic cells in intestinal immune regulation. *Nat Rev Immunol* 8(6):435-446.

14. Shortman K & Liu Y-J (2002) Mouse and human dendritic cell subtypes. *Nat Rev Immunol* 2(3):151-161.

15. Jarrossay D, Napolitani G, Colonna M, Sallusto F, & Lanzavecchia A (2001) Specialization and complementarity in microbial molecule recognition by human myeloid and plasmacytoid dendritic cells. *European Journal of Immunology* 31(11):3388-3393.

16. Barchet W, Cella M, & Colonna M (2005) Plasmacytoid dendritic cells--virus experts of innate immunity. *Seminars in Immunology* 17(4):253-261.

17. Sato K & Fujita S (2007) Dendritic cells: nature and classification. (Translated from eng) *Allergol Int* 56(3):183-191 (in eng).

18. Shi Y, Evans JE, & Rock KL (2003) Molecular identification of a danger signal that alerts the immune system to dying cells. *Nature* 425(6957):516-521.

19. Aliberti J, *et al.* (2003) Cutting Edge: Bradykinin Induces IL-12 Production by Dendritic Cells: A Danger Signal That Drives Th1 Polarization. *J Immunol* 170(11):5349-5353.

20. Gallucci S & Matzinger P (2001) Danger signals: SOS to the immune system. *Current Opinion in Immunology* 13(1):114-119.

21. Banchereau J & Steinman RM (1998) Dendritic cells and the control of immunity. (Translated from eng) *Nature* 392(6673):245-252 (in eng).

22. Randolph GJ, Angeli V, & Swartz MA (2005) Dendritic-cell trafficking to lymph nodes through lymphatic vessels. *Nat Rev Immunol* 5(8):617-628.

23. Sozzani S, *et al.* (1998) Cutting Edge: Differential Regulation of Chemokine Receptors During Dendritic Cell Maturation: A Model for Their Trafficking Properties. *J Immunol* 161(3):1083-1086.

24. Sozzani S, Allavena P, Vecchi A, & Mantovani A (2000) Chemokines and Dendritic Cell Traffic. *Journal of Clinical Immunology* 20(3):151-160.

25. Förster R, *et al.* (1999) CCR7 Coordinates the Primary Immune Response by Establishing Functional Microenvironments in Secondary Lymphoid Organs. 99(1):23-33.

26. Yanagihara S, Komura E, Nagafune J, Watarai H, & Yamaguchi Y (1998) EBI1/CCR7 Is a New Member of Dendritic Cell Chemokine Receptor That Is Up-Regulated upon Maturation. *J Immunol* 161(6):3096-3102.

27. Luther SA*, et al.* (2002) Differing Activities of Homeostatic Chemokines CCL19, CCL21, and CXCL12 in Lymphocyte and Dendritic Cell Recruitment and Lymphoid Neogenesis. *J Immunol* 169(1):424-433.

28. Forster R, Davalos-Misslitz AC, & Rot A (2008) CCR7 and its ligands: balancing immunity and tolerance. *Nat Rev Immunol* 8(5):362-371.

29. janeway CA, Jr., travers P, Walport M, & Shlomchik MJ (2001) *Immunobiology, The Immune System in Health and Disease* (Garland Science, New York).

30. Grakoui A*, et al.* (1999) The Immunological Synapse: A Molecular Machine Controlling T Cell Activation. *Science* 285(5425):221-227.

31. Bromley SK*, et al.* (2003) THE IMMUNOLOGICAL SYNAPSE. *Annual Review of Immunology* 19(1):375-396.

32. Jordan MS, Singer AL, & Koretzky GA (2003) Adaptors as central mediators of signal transduction in immune cells. (Translated from eng) *Nat Immunol* 4(2):110-116 (in eng).

33. Guermonprez P, Valladeau J, Zitvogel L, Théry C, & Amigorena S (2003) ANTIGEN PRESENTATION AND T CELL STIMULATION BY DENDRITIC CELLS. *Annual Review of Immunology* 20(1):621-667.

34. Kalinski P, Hilkens CMU, Wierenga EA, & Kapsenberg ML (1999) T-cell priming by type-1and type-2 polarized dendritic cells: the concept of a third signal. *Immunology Today* 20(12):561-567.

35. Zlotnik A & Yoshie O (2000) Chemokines: A New Classification System and Their Role in Immunity. *Immunity* 12(2):121-127.

36. Ohl L, Bernhardt G, Pabst O, & Förster R (2003) Chemokines as organizers of primary and secondary lymphoid organs. *Seminars in Immunology* 15(5):249-255.

37. Murdoch C & Finn A (2000) Chemokine receptors and their role in inflammation and infectious diseases. *Blood* 95(10):3032-3043.

38. Proudfoot AE (2002) Chemokine receptors: multifaceted therapeutic targets. (Translated from eng) *Nat Rev Immunol* 2(2):106-115 (in eng).

39. Ma Q, *et al.* (1998) Impaired B-lymphopoiesis, myelopoiesis, and derailed cerebellar neuron migration in CXCR4- and SDF-1-deficient mice. *Proceedings of the National Academy of Sciences of the United States of America* 95(16):9448-9453.

40. Strieter RM, *et al.* (1995) The Functional Role of the ELR Motif in CXC Chemokine-mediated Angiogenesis. *Journal of Biological Chemistry* 270(45):27348-27357.

41. Charo IF & Ransohoff RM (2006) The Many Roles of Chemokines and Chemokine Receptors in Inflammation. *New England Journal of Medicine* 354(6):610-621.

42. Yoshida R, *et al.* (1998) Secondary Lymphoid-tissue Chemokine Is a Functional Ligand for the CC Chemokine Receptor CCR7. *Journal of Biological Chemistry* 273(12):7118-7122.

43. Meili R & Firtel RA (2003) Two Poles and a Compass. 114(2):153-156.

44. Kohout TA, *et al.* (2004) Differential Desensitization, Receptor Phosphorylation, β-Arrestin Recruitment, and ERK1/2 Activation by the Two Endogenous Ligands for the CC Chemokine Receptor 7. *Journal of Biological Chemistry* 279(22):23214-23222.

45. Byers MA, *et al.* (2008) Arrestin 3 Mediates Endocytosis of CCR7 following Ligation of CCL19 but Not CCL21. *J Immunol* 181(7):4723-4732.

46. Sallusto F, *et al.* (1999) Distinct patterns and kinetics of chemokine production regulate dendritic cell function. (Translated from eng) *Eur J Immunol* 29(5):1617-1625 (in eng).

47. Johnson LA & Jackson DG (2008) Cell Traffic and the Lymphatic Endothelium. *Annals of the New York Academy of Sciences* 1131(The Lymphatic Continuum Revisited):119-133.

48. Stachowiak AN, Wang Y, Huang Y-C, & Irvine DJ (2006) Homeostatic Lymphoid Chemokines Synergize with Adhesion Ligands to Trigger T and B Lymphocyte Chemokinesis. *J Immunol* 177(4):2340-2348.

49. Ford RM & Lauffenburger DA (1991) Measurement of bacterial random motility and chemotaxis coefficients: II. Application of single-cell-based mathematical model. *Biotechnology and Bioengineering* 37(7):661-672.

50. Thelen M & Stein JV (2008) How chemokines invite leukocytes to dance. *Nat Immunol* 9(9):953-959.

51. Paoletti S, *et al.* (2005) A rich chemokine environment strongly enhances leukocyte migration and activities. *Blood* 105(9):3405-3412.

52. Chung CY, Funamoto S, & Firtel RA (2001) Signaling pathways controlling cell polarity and chemotaxis. *Trends in Biochemical Sciences* 26(9):557-566.

53. Pfeffer W (1884) *Unters Bot. Inst. Tubengen* 1(363):363.

54. Leber T (1888) *Med.* 6(460):460.

55. Boyden S (1962) THE CHEMOTACTIC EFFECT OF MIXTURES OF ANTIBODY AND ANTIGEN ON POLYMORPHONUCLEAR LEUCOCYTES. *The Journal of Experimental Medicine* 115(3):453-466.

56. Zigmond SH & Hirsch JG (1973) LEUKOCYTE LOCOMOTION AND CHEMOTAXIS. *The Journal of Experimental Medicine* 137(2):387-410.

57. Snyderman R, Altman LC, Hausman MS, & Mergenhagen SE (1972) Human Mononuclear Leukocyte Chemotaxis: A Quantitative Assay for Humoral and Cellular Chemotactic Factors. *J Immunol* 108(3):857-860.

58. Buettner HM, Lauffenburger DA, & Zigmond SH (1989) Measurement of leukocyte motility and chemotaxis parameters with the Millipore filter assay. *Journal of Immunological Methods* 123(1):25-37.

59. Nelson RD, Quie PG, & Simmons RL (1975) Chemotaxis Under Agarose: A New and Simple Method for Measuring Chemotaxis and Spontaneous Migration of Human Polymorphonuclear Leukocytes and Monocytes. *J Immunol* 115(6):1650-1656.

60. Foxman EF, Campbell JJ, & Butcher EC (1997) Multistep Navigation and the Combinatorial Control of Leukocyte Chemotaxis. *J. Cell Biol.* 139(5):1349-1360.

61. Zigmond SH (1977) Ability of polymorphonuclear leukocytes to orient in gradients of chemotactic factors. *The Journal of Cell Biology* 75(2):606-616.

62. Zicha D, Dunn G, & Brown A (1991) A new direct-viewing chemotaxis chamber. *J Cell Sci* 99(4):769-775.

63. Pujic Z, Mortimer D, Feldner J, & Goodhill GJ (2009) Assays for eukaryotic cell chemotaxis. (Translated from eng) *Comb Chem High Throughput Screen* 12(6):580-588 (in eng).

64. Jannat RA, Robbins GP, Ricart BG, & Hammer DA (2010) Neutrophil adhesion and chemotaxis depend on substrate mechanics. *Journal of Physics: Condensed Matter* 22(19):194117.

65. Lin F & Butcher EC (2006) T cell chemotaxis in a simple microfluidic device. *Lab on a Chip* 6(11):1462-1469.

66. Irimia D, *et al.* (2006) Microfluidic system for measuring neutrophil migratory responses to fast switches of chemical gradients. *Lab on a Chip* 6(2):191-198.

67. Lin F, *et al.* (2005) Neutrophil Migration in Opposing Chemoattractant Gradients Using Microfluidic Chemotaxis Devices. *Annals of Biomedical Engineering* 33(4):475-482.

68. Walker GM, *et al.* (2005) Effects of flow and diffusion on chemotaxis studies in a microfabricated gradient generator. *Lab on a Chip* 5(6):611-618.

69. Li Jeon N, *et al.* (2002) Neutrophil chemotaxis in linear and complex gradients of interleukin-8 formed in a microfabricated device. *Nat Biotech* 20(8):826-830.

70. Ricart BG, John B, Hunter CA, & Hammer DA (Dendritic Cell Chemotaxis in Engineered Chemokine Gradients. *Proc Natl Acad Sci U S A* In Preparation.

71. Haessler U, Kalinin Y, Swartz M, & Wu M (2009) An agarose-based microfluidic platform with a gradient buffer for 3D chemotaxis studies. *Biomedical Microdevices* 11(4):827-835.

72. Kim D, Lokuta MA, Huttenlocher A, & Beebe DJ (2009) Selective and tunable gradient device for cell culture and chemotaxis study. *Lab on a Chip* 9(12):1797-1800.

73. Shamloo A, Ma N, Poo M-m, Sohn LL, & Heilshorn SC (2008) Endothelial cell polarization and chemotaxis in a microfluidic device. *Lab on a Chip* 8(8):1292-1299.

74. Wang S-J, Saadi W, Lin F, Minh-Canh Nguyen C, & Li Jeon N (2004) Differential effects of EGF gradient profiles on MDA-MB-231 breast cancer cell chemotaxis. *Experimental Cell Research* 300(1):180-189.

75. Andrus J (1964) Office USP 3,122,817 (Mar 1964).

76. Moore GE (1965) Cramming more components onto integrated circuits. *Electronics* 38(8):114-117.

77. Xia Y & Whitesides GM (1998) Soft Lithography. *Annual Review of Materials Science* 28(1):153-184.

78. Napoli M, Eijkel JCT, & Pennathur S (2010) Nanofluidic technology for biomolecule applications: a critical review. *Lab on a Chip* 10(8):957-985.

79. Quake SR & Scherer A (2000) From Micro- to Nanofabrication with Soft Materials. *Science* 290(5496):1536-1540.

80. Ye H, Gu Z, & Gracias DH (2006) Kinetics of Ultraviolet and Plasma Surface Modification of Poly(dimethylsiloxane) Probed by Sum Frequency Vibrational Spectroscopy. *Langmuir* 22(4):1863-1868.

81. Rogers JA & Nuzzo RG (2005) Recent progress in soft lithography. *Materials Today* 8(2):50-56.

82. Jeon NL, *et al.* (2000) Generation of Solution and Surface Gradients Using Microfluidic Systems. *Langmuir* 16(22):8311-8316.

83. Lin F, *et al.* (2004) Generation of dynamic temporal and spatial concentration gradients using microfluidic devices. (Translated from eng) *Lab Chip* 4(3):164-167 (in eng).

84. Jiang X, Ng JM, Stroock AD, Dertinger SK, & Whitesides GM (2003) A miniaturized, parallel, serially diluted immunoassay for analyzing multiple antigens. (Translated from eng) *J Am Chem Soc* 125(18):5294-5295 (in eng).

85. Faure-Andre G, *et al.* (2008) Regulation of Dendritic Cell Migration by CD74, the MHC Class II-Associated Invariant Chain. *Science* 322(5908):1705-1710.

86. Weiger MC, *et al.* (2009) Spontaneous phosphoinositide 3-kinase signaling dynamics drive spreading and random migration of fibroblasts. *J Cell Sci* 122(3):313-323.

87. Lammermann T, *et al.* (2009) Cdc42-dependent leading edge coordination is essential for interstitial dendritic cell migration. *Blood* 113(23):5703-5710.

88. Van Keymeulen A, *et al.* (2006) To stabilize neutrophil polarity, PIP3 and Cdc42 augment RhoA activity at the back as well as signals at the front. *The Journal of Cell Biology* 174(3):437-445.

89. Lammermann T & Sixt M (2009) Mechanical modes of 'amoeboid' cell migration. (Translated from eng) *Curr Opin Cell Biol* 21(5):636-644 (in eng).

90. Wessels D, Lusche DF, Kuhl S, Heid P, & Soll DR (2007) PTEN plays a role in the suppression of lateral pseudopod formation during Dictyostelium motility and chemotaxis. *J Cell Sci* 120(15):2517-2531.

91. Hug C, *et al.* (1995) Capping protein levels influence actin assembly and cell motility in dictyostelium. 81(4):591-600.

92. Svitkina TM, Verkhovsky AB, McQuade KM, & Borisy GG (1997) Analysis of the Actin–Myosin II System in Fish Epidermal Keratocytes: Mechanism of Cell Body Translocation. *The Journal of Cell Biology* 139(2):397-415.

93. Small JV, Herzog M, & Anderson K (1995) Actin filament organization in the fish keratocyte lamellipodium. *The Journal of Cell Biology* 129(5):1275-1286.

94. Renkawitz J, *et al.* (2009) Adaptive force transmission in amoeboid cell migration. *Nat Cell Biol* 11(12):1438-1443.

95. Quast T, *et al.* (2009) Cytohesin-1 controls the activation of RhoA and modulates integrin-dependent adhesion and migration of dendritic cells. *Blood* 113(23):5801-5810.

96. Hannigan M, *et al.* (2002) Neutrophils lacking phosphoinositide 3-kinase γ show loss of directionality during N-formyl-Met-Leu-Phe-induced chemotaxis. *Proceedings of the National Academy of Sciences of the United States of America* 99(6):3603-3608.

97. Heit B, Tavener S, Raharjo E, & Kubes P (2002) An intracellular signaling hierarchy determines direction of migration in opposing chemotactic gradients. *J. Cell Biol.* 159(1):91-102.

98. Cronshaw DG, Owen C, Brown Z, & Ward SG (2004) Activation of Phosphoinositide 3-Kinases by the CCR4 Ligand Macrophage-Derived Chemokine Is a Dispensable Signal for T Lymphocyte Chemotaxis. *J Immunol* 172(12):7761-7770.

99. Shin EH, Lee HY, & Bae Y-S (2006) Leukotriene B4 stimulates human monocyte-derived dendritic cell chemotaxis. *Biochemical and Biophysical Research Communications* 348(2):606-611.

100. Srinivasan S, *et al.* (2003) Rac and Cdc42 play distinct roles in regulating PI(3,4,5)P3 and polarity during neutrophil chemotaxis. *The Journal of Cell Biology* 160(3):375-385.

101. Pestonjamasp KN, *et al.* (2006) Rac1 links leading edge and uropod events through Rho and myosin activation during chemotaxis. *Blood* 108(8):2814-2820.

102. Burns S, Thrasher AJ, Blundell MP, Machesky L, & Jones GE (2001) Configuration of human dendritic cell cytoskeleton by Rho GTPases, the WAS protein, and differentiation. *Blood* 98(4):1142-1149.

103. Leung T, Chen XQ, Manser E, & Lim L (1996) The p160 RhoA-binding kinase ROK alpha is a member of a kinase family and is involved in the reorganization of the cytoskeleton. (Translated from eng) *Mol Cell Biol* 16(10):5313-5327 (in eng).

104. Tamura M, *et al.* (1998) Inhibition of Cell Migration, Spreading, and Focal Adhesions by Tumor Suppressor PTEN. *Science* 280(5369):1614-1617.

105. Weiss P (1959) Cellular Dynamics. *Reviews of Modern Physics* 31(1):11.

106. Mudera V, *et al.* (2000) Molecular responses of human dermal fibroblasts to dual cues: Contact guidance and mechanical load. *Cell Motility and the Cytoskeleton* 45(1):1-9.

107. McBeath R, Pirone DM, Nelson CM, Bhadriraju K, & Chen CS (2004) Cell Shape, Cytoskeletal Tension, and RhoA Regulate Stem Cell Lineage Commitment. *Developmental Cell* 6(4):483-495.

108. Engler AJ, Sen S, Sweeney HL, & Discher DE (2006) Matrix Elasticity Directs Stem Cell Lineage Specification. *Cell* 126(4):677-689.

109. Oakes PW, *et al.* (2009) Neutrophil morphology and migration are affected by substrate elasticity. *Blood* 114(7):1387-1395.

110. Lee J, Leonard M, Oliver T, Ishihara A, & Jacobson K (1994) Traction forces generated by locomoting keratocytes. *The Journal of Cell Biology* 127(6):1957-1964.

111. Pelham RJ & Wang Y-l (1997) Cell locomotion and focal adhesions are regulated by substrate flexibility. *Proceedings of the National Academy of Sciences of the United States of America* 94(25):13661-13665.

112. Paszek MJ, *et al.* (2005) Tensional homeostasis and the malignant phenotype. *Cancer cell* 8(3):241-254.

113. Saunders R & Hammer D (2010) Assembly of Human Umbilical Vein Endothelial Cells on Compliant Hydrogels. *Cellular and Molecular Bioengineering* 3(1):60-67.

114. Pless DD, Lee YC, Roseman S, & Schnaar RL (1983) Specific cell adhesion to immobilized glycoproteins demonstrated using new reagents for protein and glycoprotein immobilization. (Translated from eng) *J Biol Chem* 258(4):2340-2349 (in eng).

115. Dembo M & Wang Y-L (1999) Stresses at the Cell-to-Substrate Interface during Locomotion of Fibroblasts. *Biophysical journal* 76(4):2307-2316.

116. Wang J & Lin J-S (2007) Cell traction force and measurement methods. *Biomechanics and Modeling in Mechanobiology* 6(6):361-371.

117. Smith LA, Aranda-Espinoza H, Haun JB, Dembo M, & Hammer DA (2007) Neutrophil Traction Stresses are Concentrated in the Uropod during Migration. 92(7):L58-L60.

118. Lemmon CA, *et al.* (2005) Shear force at the cell-matrix interface: enhanced analysis for microfabricated post array detectors. (Translated from eng) *Mech Chem Biosyst* 2(1):1-16 (in eng).

119. Beningo KA, Dembo M, Kaverina I, Small JV, & Wang Y-l (2001) Nascent Focal Adhesions Are Responsible for the Generation of Strong Propulsive Forces in Migrating Fibroblasts. *J. Cell Biol.* 153(4):881-888.

120. Hur SS, Zhao Y, Li YS, Botvinick E, & Chien S (2009) Live Cells Exert 3-Dimensional Traction Forces on Their Substrata. (Translated from Eng) *Cell Mol Bioeng* 2(3):425-436 (in Eng).

121. Maskarinec SA, Franck C, Tirrell DA, & Ravichandran G (2009) Quantifying cellular traction forces in three dimensions. *Proceedings of the National Academy of Sciences* 106(52):22108-22113.

122. Galbraith CG & Sheetz MP (1997) A micromachined device provides a new bend on fibroblast traction forces. *Proceedings of the National Academy of Sciences of the United States of America* 94(17):9114-9118.

123. Tan JL, *et al.* (2003) Cells lying on a bed of microneedles: An approach to isolate mechanical force. *Proceedings of the National Academy of Sciences of the United States of America* 100(4):1484-1489.

124. Yang MT & Chen CS (2009) Mechanotransduction and the Study of Cellular Forces. *Methods in Bioengineering: Microdevices in Biology and Medicine*, eds Nahmias Y & Bhatia SN (Artech House, Norwood, MA).

125. Yang M, Sniadecki N, & Chen C (2007) Geometric Considerations of Micro- to Nanoscale Elastomeric Post Arrays to Study Cellular Traction Forces. *Advanced Materials* 19(20):3119-3123.

Chapter 3: Dendritic Cell Motility in Uniform Chemokine Fields

Abstract

Dendritic cells (DCs) are potent initiators of the adaptive immune system, but they must migrate from peripheral tissue to lymphoid organs to perform their function. Thus motility is essential for DC function *in vivo*. Despite the prominent role of locomotion in DC function, it remains poorly understood and basic responses to chemokines have not been well characterized. In the present work, we examine DC response to uniform fields of chemoattractants and characterize this chemokinesis. We augment our understanding of DC motility by analyzing their adhesion to multiple extracellular matrix proteins and adhesion to chemokines directly (*i.e.* haptokinesis). We find that DCs show a biphasic response to chemokines in both adhesion and motility, and that fibronectin is preferred to collagen for integrin-dependent migration. This work lays the foundation for understanding basic DC motility and forms the basis of more advanced studies.

Introduction

Dendritic cells (DCs) acquire information about foreign antigens at sites of infection. They later deliver this informational cargo to T and B cells in secondary lymphoid organs (SLOs) (1-2). The transit from peripheral tissue to SLOs is central to DC function. While dendritic cells have been of increasing interest, we still lack basic information about their motility on common substrates.

Collagen and fibronectin represent two of the most physiologically relevant extracellular matrix (ECM) proteins. Collagen is found throughout the body, but especially in connective tissue and basement membranes (3). Fibronectin is more ubiquitous, being found in both a soluble plasma form, and in an insoluble cellular form; both are products of the same gene but undergo alternate splice patterns (4). Due to their physiological relevance and ease of use, these two ECM proteins are among the most widely studied for cell adhesion and migration. Collagen in particular has become popular for three-dimensional studies because it is readily polymerized into a 3D network (5-9). Fibronectin has received considerably less attention from DC researchers.

In addition to providing a substrate for integrin binding, ECM proteins can also signal into the cell. The primary function of ECM proteins is to form a lattice in which cells can adhere and grow, yet this relationship is complex because cells themselves produce ECM proteins and shape their patterns (4, 10). There is a secondary effect of binding ECM proteins, however. Activated integrins which bind ligands generate intracellular signals

in a process known as outside-in signaling (11). These signals ultimately activate Rac, Cdc42 and Rho (12), similar to chemokine signals. Thus it is unclear whether DCs receive migration signals from ECM proteins in addition to chemokines.

In this chapter we investigate the basic adhesion and migration of mature dendritic cells on two well studies ECM proteins, collagen and fibronectin. We apply standard engineering approaches to measure cell speed, random motility coefficient, and strength of adhesion on these substrates. Our results show that mature, bone marrow derived murine dendritic cells do not appreciably bind collagen, but are able to bind fibronectin. Further, we show that in the absence of integrin outside-in signaling, chemokines affect speed and random motility in a biphasic manner. We conclude that this biphasic response is primarily due to adaptation to high concentrations of chemokine and not increased adhesion to the substrate, because the adhesion response is a relatively weak function of chemokine stimulation.

Materials and Methods

Cell Culture

Dendritic cells were generated from murine bone marrow cells according to the procedure of Lutz *et al.* (13) with minor modifications. Briefly, bone marrow was flushed from the tibias and femurs of 8 to 10-week-old C57BL/6 mice and depleted of red blood cells using ammonium chloride lysis buffer. The cells were plated in 10-cm petri dishes (2×10^6 cells/ml; 10ml/plate) in RPMI-1640 supplemented with 10% heat-inactivated fetal bovine serum, 100 U/ml penicillin, 100 mg/ml streptomycin, 50 nM BME, and 20 ng/ml rmGM-CSF (Peprotech, Rocky Hill, NJ) at 37°C in 5% CO_2. On day 3 fresh media was added, and on day 6 half of the media was gently replaced. To mature DCs, 10 ng/ml TNF-α (PeproTech) and 1 μg/ml LPS (Sigma-Aldrich, St. Louis, MO) were added on day 6 and cells were used in experiments on day 7. On day 7, 80% or more of the non-adherent cells expressed the monocyte lineage marker CD11c as confirmed by flow cytometry.

Chemokinesis Assay

Migratory speed was measured by videomicroscopy. DCs suspended in growth medium were allowed to attach to collagen (PureCol, 550 ug/cm^2) or fibronectin (Sigma-Aldrich, 10 ug/cm^2) coated glass coverslips for 30 min. Protein coating was performed by first cleaning the coverslips with methanol, then incubating with the protein solution for 90 minutes at room temperature, followed by blocking with 1% BSA in PBS for 60 minutes at room temperature. Movement was recorded using a video camera attached to a Nikon

Inverted Eclipse TE300 microscope using a 10x objective for 2 h in a custom-built stage maintained at 37°C and 5% CO_2. Tracks of individual cells (100 or more cells) were captured using the Manual Tracking or ParticleTracker plugins for ImageJ (NIH, Bethesda, MD), and the data are presented as microns per hour. For automated tracking, cells were incubated with 5 uM CellTracker Red CMTPX (Invitrogen) for 30 min prior to imaging, and fluorescence images were captured using a Texas Red filter. The parameters that have been used to describe this random motility are the cell speed and persistence time according to the Dunn Equation (14): $\left\langle d^2 \right\rangle = nS^2\left[Pt - P^2\left(1 - e^{-t/P}\right)\right]$.

The random motility coefficient can be calculated by either $\mu = \frac{1}{n}S^2P$ or $\mu = \frac{\left\langle d^2 \right\rangle}{n^2 t}$ for t >> P. Each cell's persistence time (P) was fit using nonlinear least-squares regression in a custom-build MATLAB (The Mathworks, Natick, MA) program by inserting its speed (S) into a persistent random walk model for cell migration.

Haptokinesis Assay

Haptokinesis experiments were performed as chemokinesis experiments with a different adsorbed protein. Instead of using collagen or fibronectin, haptotaxis experiments used CCL19 or CCL21. The chemokine coating was performed on plastic non-tissue culture treated 96 well plates (Falcon, BD Biosciences, San Jose, CA), then incubating with the chemokine solution for 90 minutes at room temperature, followed by blocking with 1% BSA in PBS for 60 minutes at room temperature.

Adhesion Assay

Cell adhesion to protein-coated surfaces was measured using a centrifugation assay (15). Tissue culture polystyrene 96-well plates (Falcon 3077, BD, Franklin Lakes, NJ) were coated with bovine serum fibronectin (Sigma-Aldrich, 10 μg/ml) in PBS or type I collagen (PureCol, 550 μg/ml) in PBS for 1 h at room temperature. The protein-coating concentrations ranged from 0.015 to 45 $\mu g/cm^2$ in addition to a negative control with no adsorbed protein. Conditions were replicated in three separate columns on the same microplate. All wells were then blocked in 1% heat-denatured BSA for 1 h to prevent nonspecific cell adhesion. DCs (5×10^4 cells/well) were added to wells with CCL19 concentrations ranging from 0 to 100nM. The plates were incubated for 60 min at 37°C to allow adhesion. Each well was then carefully aspirated to remove floating cells and refilled with fresh HBSS for an initial cell count before detachment. The lid was removed, and the plate was covered with sealing tape (Nunc, Rochester, NY) and centrifuged upside down at a specified speed for 5 min on an Allegra 25R centrifuge (Beckman Coulter, Fullerton, CA) to detach the cells. The wells were carefully aspirated and refilled with fresh HBSS for a post-spin cell count. The post-spin data were normalized by the pre-spin data to obtain adherent fractions, which were plotted against protein-coating concentration to determine adhesion profiles. Alternatively, cells were fixed for 15 min at room temperature with 4% PFA and stained for 15 min with 0.5% crystal violet. The cells were then washed with PBS and read on a Tecan plate reader at 590 nm.

Results

Migratory cells are expected to display random motility in the absence of a chemotactic gradient. Mean squared displacement for dendritic cells migrating on a collagen/glass surface in the absence of chemokine has been plotted in Figure 3.1. By taking an average over the cell population, we can accurately fit our data to the Dunn Equation using least squares regression.

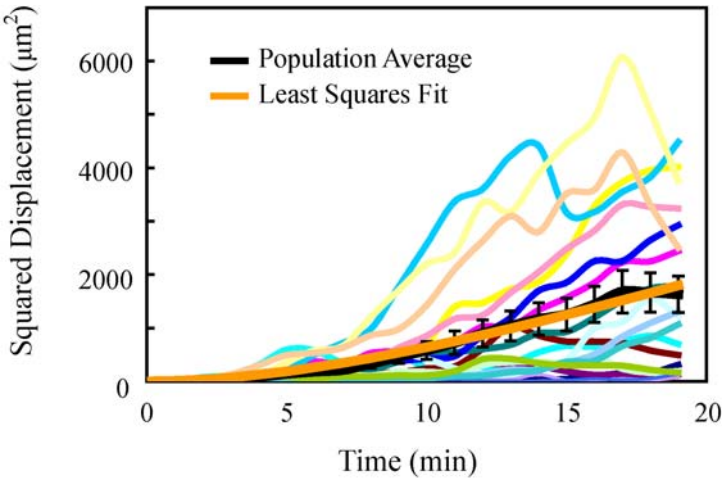

Figure 3.1. Trajectories of the squared displacement from initial location are plotted over time. The black line represents the mean of the displayed data, error bars indicate standard error of the mean. The orange line indicates the Dunn Equation curve fit by the parameters S = 3.0 μm/min, P = 9.0 min.

The resulting parameters are calculated to be 3.0 ± 0.3 μm/min for cell speed, 9.0 minutes for persistence time, and 24 μm^2/min for the random motility coefficient.

An inverse relationship has been observed between persistence time and cell speed for a variety of cells (see Figure 3.2). We show that dendritic cells obey the general inverse relationship between speed and persistence time (Figure 3.2).

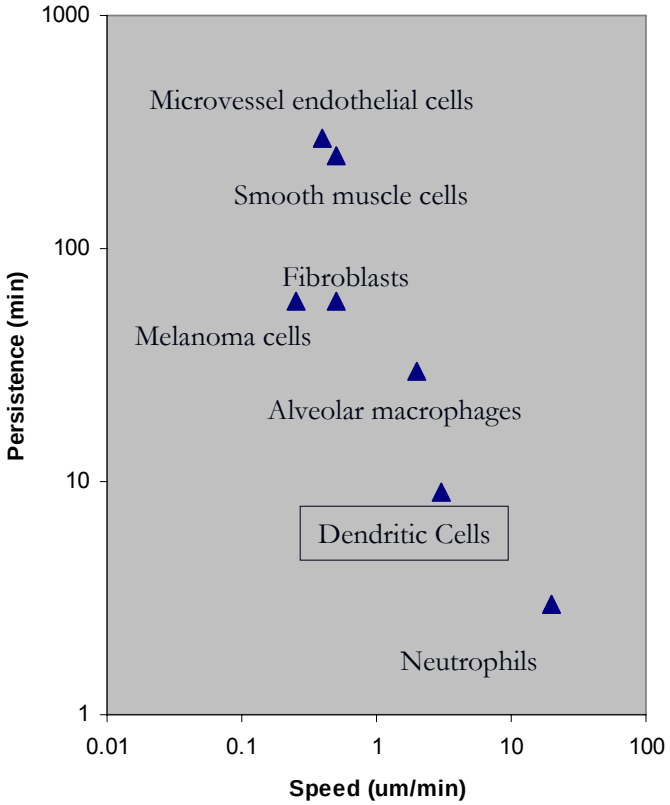

Figure 3.2 A demonstration of the inverse relationship between migratory speed and persistence time (reproduced from reference (16)). Datum for dendritic cells has been added from our observations.

Having calculated the baseline parameters of DC migration, we are now concerned with how they change upon activation by chemokines. We show here that dendritic cells modulate their migratory velocity in response to CCL19 and CCL21 (Figure 3.3). We find that on collagen substrates, the speed reaches a maximum of approximately double the resting velocity. On fibronectin coated substrates, however, the cells do not seem to respond to chemokine with any discernable pattern. On collagen, the random motility coefficient goes through a maximum at approximately 10 nM CCL19 or CCL21.

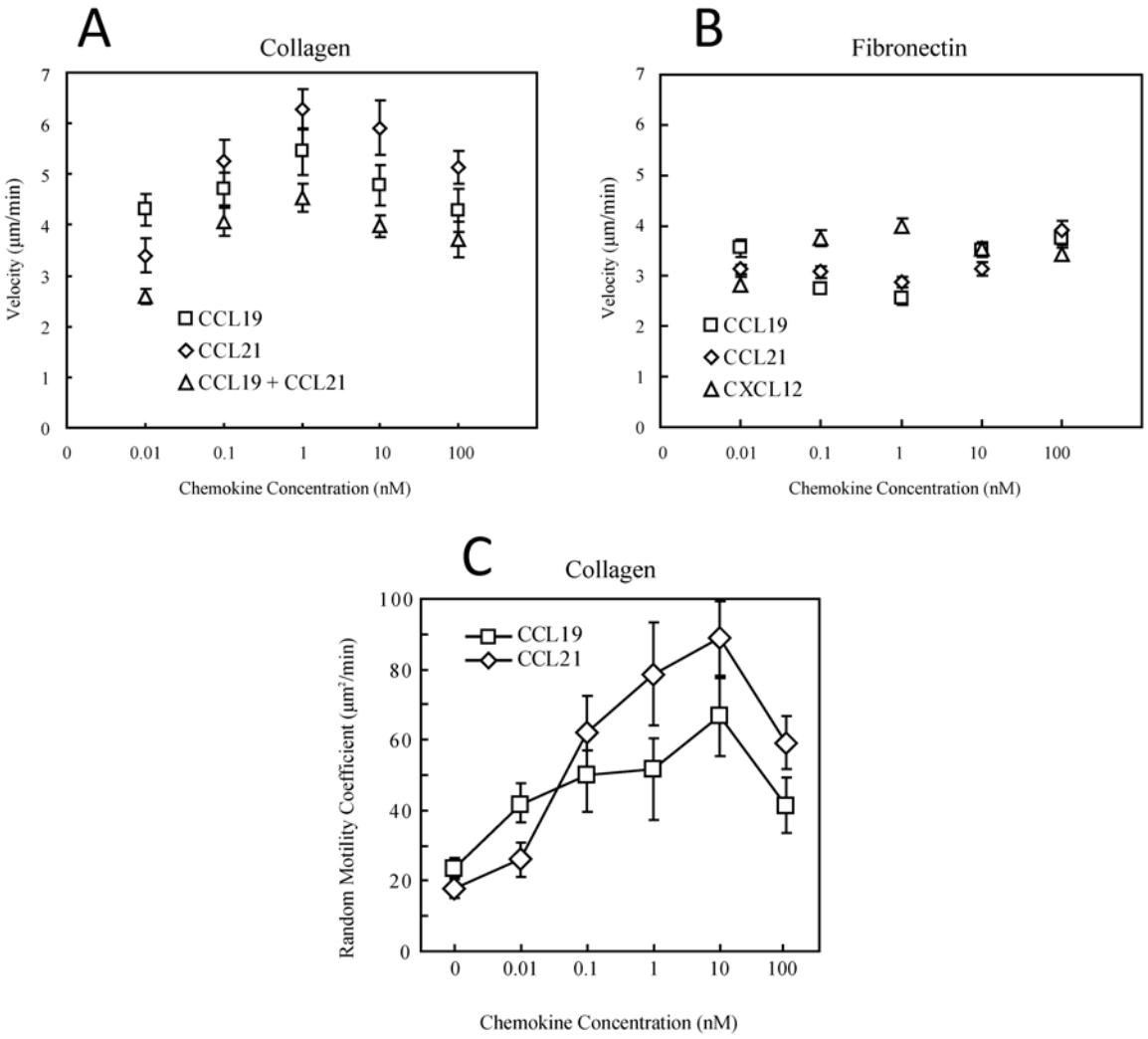

Figure 3.3. Velocity of dendritic cells on a glass surface functionalized with collagen Type 1 (A and C) or bovine fibronectin (B). For CCL19+21, the chemokine concentration is reported as the sum (total) concentration. Cells respond to chemokine on collagen, going through a maximum before adapting to large doses. On fibronectin, DCs do not respond to chemokine stimulation.

There are two important observations that we make regarding the response to increasing chemokine concentration. First, the response is biphasic, going through a maximum at ~1-10 nM, which is close to the K_D for these receptor/ligand pairs (17). Second, CCL21

exhibits a significantly stronger response than either CCL19 or CCL19 and CCL21 combined, especially at higher chemokine concentrations.

To understand whether chemokines need to be bound to the substrate to elicit chemokinetic signals, we coated the surface of 96-well plates with CCL19 or CCL21. Results are summarized in Figure 3.4.

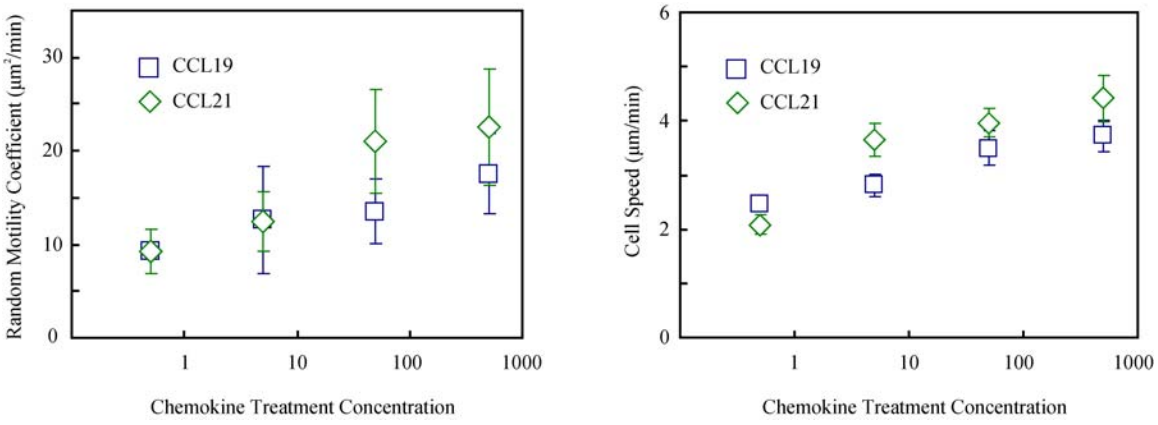

Figure 3.4. Mature dendritic cells exhibit haptokinesis on chemokine coated surfaces. Greater chemokine concentrations used to treat the surface resulted in higher cell speed and higher random motility coefficients. CCL21 triggers greater haptokinesis than CCL19.

It has been well established for a variety of cell types that a "goldilocks" level of adhesion is necessary for maximal motility (18). If cells are too weakly adherent, they cannot generate the traction needed to counteract protrusion. If the cells are too strongly adherent, they are unable to break integrin bonds at the uropod and become "stuck". Thus it is reasonable to expect that if chemokine signaling becomes too strong, it may inhibit migration.

To determine whether this correlation between motility and adhesion holds for dendritic cells, we conducted centrifugation experiments to assess adhesion at varying chemokine concentrations. Cells were plated on a fibronectin-coated 96-well plate, allowed to adhere for 1 hour, and then spun at 100RPM (~1.6 x g) for 5 minutes. As shown in Figure 3.5, adhesion strength is indeed a function of chemokine concentration. It appears that the adhesion goes through a maximum with chemokine concentration before adapting to high concentrations, as observed with cell speed.

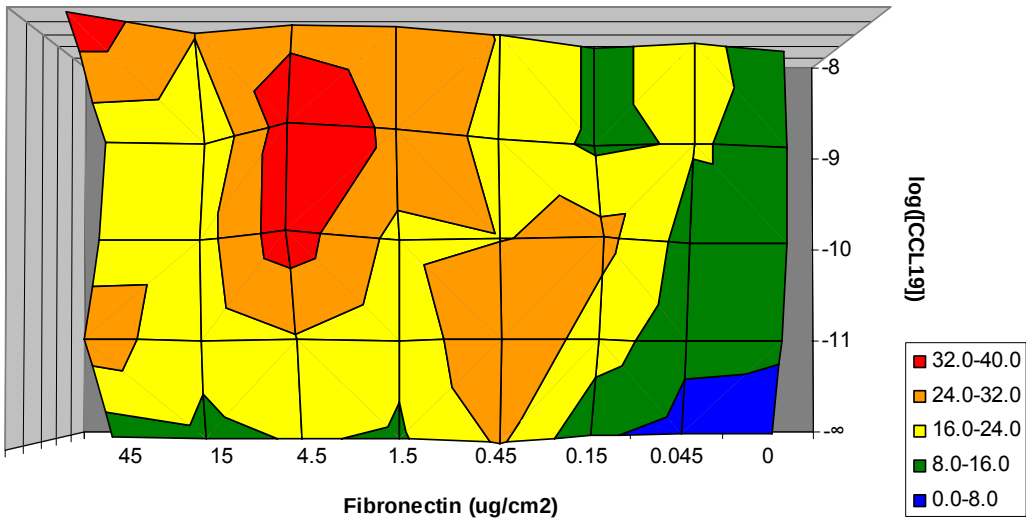

Figure 3.5. Adhesion of cells to a plastic TC surface functionalized with bovine fibronectin. Cells were allowed to adhere for 1h before being inverted and centrifuged at 1.6 x g. Data is reported as the percentage of cells that remain adhered after 5 minutes.

We can also use a centrifugation assay to determine the mean force required for detachment. In this assay, the cells are again allowed to adhere to 96-well plates coated with various concentrations of fibronectin for 1 hour. The plates are then inverted and

spun at various speeds ranging from 0 to 42 x g to generate a range of applied forces. The fraction of adhered cells was calculated for each fibronectin and force combination (Figure 3.6). From this data we calculate an applied force: $F_{applied} = \Delta\rho V\omega^2 R$. By assuming r_{cell} = 10 um, ρ_{cell} = 1.05 g/cm^3, ρ_{media} = 1.00 g/cm^3, and R (radius of centrifuge arm) = 15 cm, we are able to calculate the average force required to remove 50% of the cells to be 4 pN. This is significantly lower than traction forces observed for DCs (see Chapter 6), which may be due to variable adhesion during the 5 min spin. If the migrating cells lose adhesion while migrating during the assay, they will detach, leading to an artificially low value of F_{50}.

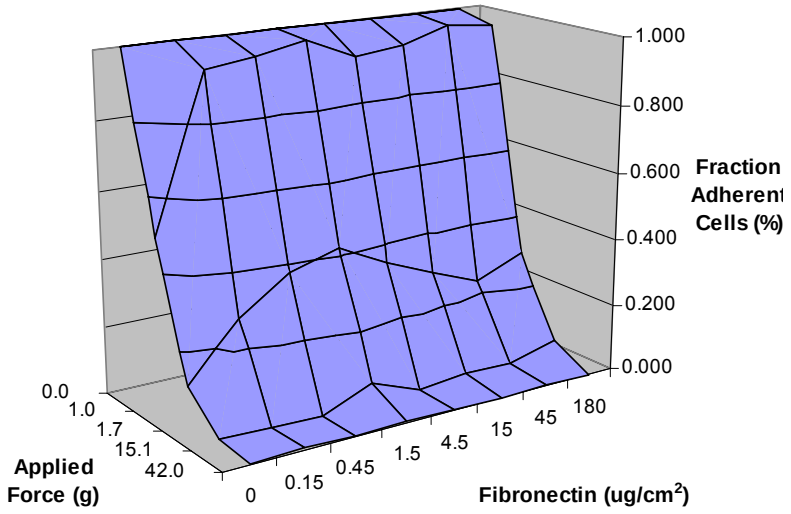

Figure 3.6. Adhesion of DCs on a plastic TC surface coated with various concentrations of fibronectin as a function of applied centrifugal force.

A crucial assay is to determine whether DCs use integrins to bind either collagen or fibronectin. Literature shows hints that fibronectin may be more potent than collagen for binding DCs (6). We coated 96 well plates with either fibronectin or collagen and observed the adhesion of cell to this simple substrate at 1 x g (9.8 m/s^2). To determine whether chemokine stimulation would affect adhesion, we dosed 0 to 100 nM CCL19 into the wells with the cells. We clearly observe that DCs are able to bind fibronectin, but have a negligible ability to bind collagen (Figure 3.7). There was a mild dependence on CCL19 concentration for fibronectin, with a characteristic maxima at 10 nM. Under no doses of chemokine were cells able to bind collagen. This is highly elucidative for understanding dendritic cell locomotion.

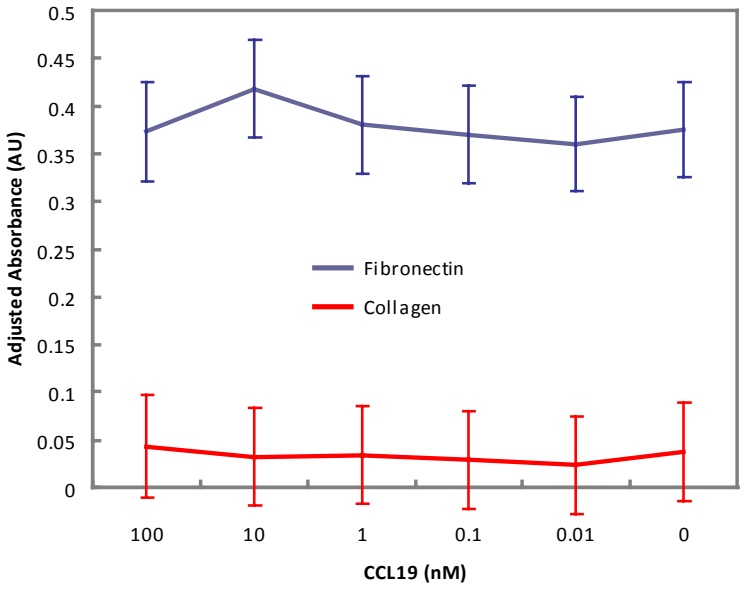

Figure 3.7. Mature dendritic cells are able to bind fibronectin, but not collagen. Wells in a 96-well plate were coated with either fibronectin or collagen. Cells were then introduced and allowed to bind for 30 minutes. Loose cells were removed by washing and adherent cells were fixed and stained. Background levels of absorbance were subtracted. Results are reported as absorbance at 590 nm as a function of chemokine (CCL19) concentration.

Discussion

The data for cell speed is in good agreement with published data for dendritic cells trafficking in the lymph node *in vivo*, which has been reported to be 3.8 μm/min in tissue near lymphatic vessels and 4.2 μm/min for dendritic cells within the lymph node (6). Persistence time for dendritic cells has not been reported to our knowledge; our group is the first to apply such an analysis to dendritic cell motility. Persistence time is related to cell polarity, because it allows a cell to retain a memory its direction of motion and it is thought to be related to the time-scale of the biological signaling processes that regulate polarity, but research in this area has not lead to conclusive models. Also, we are the first to quantify a random motility coefficient for dendritic cells. This parameter is analogous to a diffusion coefficient for the cells, expressing the time scale over which they will randomly "diffuse" away from their original position during random motion.

Mesenchymal cells generally are not required to move to perform their function; indeed, their motility is generally associated with abnormal states, such as traumatic wound healing (19), or growth of new blood vessels (20-21). These cells generally act in a coordinated, unidirectional fashion, which implies that a long persistence time is beneficial. White blood cells (WBCs) including macrophages and neutrophils must migrate to sites of infection to perform their function, thus they are highly motile (22-24). Additionally, they must be able to change direction to chase down mobile prey, such as bacteria (25). Thus they benefit from shorter persistence times. We expect dendritic cells to fall within the WBC regime because they are required to migrate quickly to

perform their function, but they signals they respond to (lymphatics, SLOs) are stationary. Indeed, we saw that they fall between mesenchymal cells and faster moving neutrophils.

Chemokines provide the directional signals for chemotaxis, but they may also elicit increased migratory response when presented in a uniform field by signaling through Gαi, PI3Ps (26), Rac, Cdc42 (7) and F-actin for protrusion (27), as well as G_{12} and G_{13} (28), which stimulate Rho, ROCK, and Myosin II for contraction. Indeed, we show that dendritic cells modulate their migratory velocity in response to CCL19 and CCL21. We submit that there are two possible explanations we observe a biphasic response to soluble chemokines on collagen surfaces. First, adhesion may be a function of chemokine concentration, as has been previously shown in rolling leukocytes that require chemokine signals to activate integrins, which allow them to firmly adhere to their substratum (see Figure 3.8).

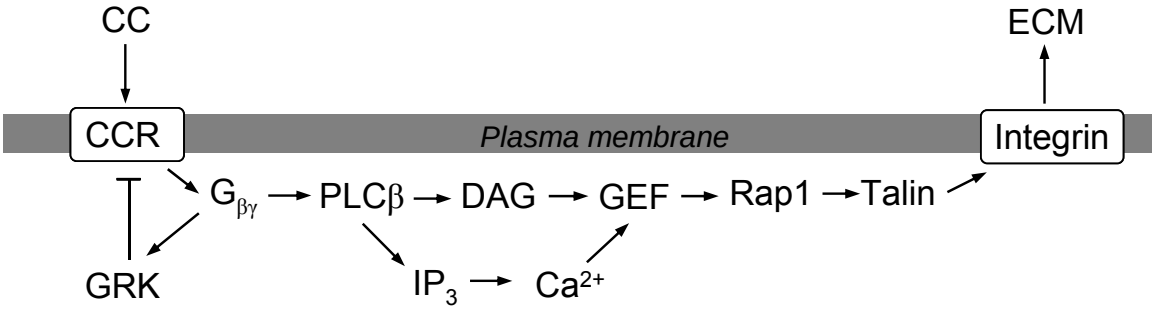

Figure 3.8. Signal cascade for chemokine ligation leading to integrin activation and binding to the extracellular matrix. Note that signaling proceeds though the βγ-subunit of an activated G protein.

The second justification for a biphasic response of DCs to chemokine concentration stems from receptor desensitization. A naïve observer may expect that the response would not be biphasic, since increasing the ligand concentration (L) should increase the number of occupied receptors (C), according to the simple one-step binding equilibrium equation: $[C] = \frac{R_T L}{L_T + K_D}$. This would lead to a sigmoidal saturation response. However, GRKs are known to phosphorylate active GPCRs, including CCR7. Once a receptor has been phosphorylated, it is considered unable to bind and activate G-proteins. Phosphorylated receptors can be bound by β-arrestins, which then recruit clathrin and ultimately lead to endocytosis (29). In the adhesion versus desensitization debate, we reason that desensitization is the likely explanation because we do not observe a significant increase in adhesion at high chemokine concentrations.

In the present work, we have identified the characteristic behavior of mature, bone-marrow derived murine dendritic cells. We examined their behavior on typical extracellular matrix proteins and found that they are able to bind fibronectin but not collagen. On fibronectin surfaces, integrins are likely activating motility, so no increase is observed upon chemokine stimulation. On collagen surfaces, chemokines increase random motility with a maximal effect at approximately 10 nM. We also show that DCs are able to migrate on chemokine surfaces, with CCL21 eliciting a greater effect than CCL19, consistent with current reports in the literature (30). Thus studies using collagen matrices are likely to show no traction forces, but with fibronectin-based substrates, DC traction forces may be significant.

References

1. Grakoui A, *et al.* (1999) The Immunological Synapse: A Molecular Machine Controlling T Cell Activation. *Science* 285(5425):221-227.
2. Bromley SK, *et al.* (2003) THE IMMUNOLOGICAL SYNAPSE. *Annual Review of Immunology* 19(1):375-396.
3. Pflicke H & Sixt M (2009) Preformed portals facilitate dendritic cell entry into afferent lymphatic vessels. *J. Exp. Med.*:jem.20091739.
4. Mao Y & Schwarzbauer JE (2005) Fibronectin fibrillogenesis, a cell-mediated matrix assembly process. *Matrix Biology* 24(6):389-399.
5. Quast T, *et al.* (2009) Cytohesin-1 controls the activation of RhoA and modulates integrin-dependent adhesion and migration of dendritic cells. *Blood* 113(23):5801-5810.
6. Lammermann T, *et al.* (2008) Rapid leukocyte migration by integrin-independent flowing and squeezing. *Nature* 453(7191):51-55.
7. Lammermann T, *et al.* (2009) Cdc42-dependent leading edge coordination is essential for interstitial dendritic cell migration. *Blood* 113(23):5703-5710.
8. Haessler U, Kalinin Y, Swartz M, & Wu M (2009) An agarose-based microfluidic platform with a gradient buffer for 3D chemotaxis studies. *Biomedical Microdevices* 11(4):827-835.
9. Gunzer M, *et al.* (2000) Migration of dendritic cells within 3-D collagen lattices is dependent on tissue origin, state of maturation, and matrix structure and is maintained by proinflammatory cytokines. *J Leukoc Biol* 67(5):622-629.
10. Wierzbicka-Patynowski I & Schwarzbauer JE (2003) The ins and outs of fibronectin matrix assembly. (Translated from eng) *J Cell Sci* 116(Pt 16):3269-3276 (in eng).
11. Giancotti FG & Ruoslahti E (1999) Integrin signaling. (Translated from eng) *Science* 285(5430):1028-1032 (in eng).
12. Harburger DS & Calderwood DA (2009) Integrin signalling at a glance. *J Cell Sci* 122(2):159-163.

13. Lutz MB, *et al.* (1999) An advanced culture method for generating large quantities of highly pure dendritic cells from mouse bone marrow. *Journal of Immunological Methods* 223(1):77-92.

14. Dunn GA (1983) Characterising a kinesis response: time averaged measures of cell speed and directional persistence. (Translated from eng) *Agents Actions Suppl* 12:14-33 (in eng).

15. Reyes CD & García AJ (2003) A centrifugation cell adhesion assay for high-throughput screening of biomaterial surfaces. *Journal of Biomedical Materials Research Part A* 67A(1):328-333.

16. Lauffenburger DA & Linderman JJ (1996) *Receptors: Models for Binding, Trafficking, and Signaling* (Oxford University Press, New York) p 376.

17. Yoshida R, *et al.* (1998) Secondary Lymphoid-tissue Chemokine Is a Functional Ligand for the CC Chemokine Receptor CCR7. *Journal of Biological Chemistry* 273(12):7118-7122.

18. Palecek SP, Loftus JC, Ginsberg MH, Lauffenburger DA, & Horwitz AF (1997) Integrin-ligand binding properties govern cell migration speed through cell-substratum adhesiveness. (Translated from eng) *Nature* 385(6616):537-540 (in eng).

19. Mudera V, *et al.* (2000) Molecular responses of human dermal fibroblasts to dual cues: Contact guidance and mechanical load. *Cell Motility and the Cytoskeleton* 45(1):1-9.

20. Saunders R & Hammer D (2010) Assembly of Human Umbilical Vein Endothelial Cells on Compliant Hydrogels. *Cellular and Molecular Bioengineering* 3(1):60-67.

21. Strieter RM, *et al.* (1995) The Functional Role of the ELR Motif in CXC Chemokine-mediated Angiogenesis. *Journal of Biological Chemistry* 270(45):27348-27357.

22. Jannat RA, Robbins GP, Ricart BG, & Hammer DA (2010) Neutrophil adhesion and chemotaxis depend on substrate mechanics. *Journal of Physics: Condensed Matter* 22(19):194117.

23. Sengupta K, Aranda-Espinoza H, Smith L, Janmey P, & Hammer D (2006) Spreading of Neutrophils: From Activation to Migration. 91(12):4638-4648.

24. Foxman EF, Campbell JJ, & Butcher EC (1997) Multistep Navigation and the Combinatorial Control of Leukocyte Chemotaxis. *J. Cell Biol.* 139(5):1349-1360.

25. Weiner OD, *et al.* (1999) Spatial control of actin polymerization during neutrophil chemotaxis. *Nat Cell Biol* 1(2):75-81.

26. Van Keymeulen A, *et al.* (2006) To stabilize neutrophil polarity, PIP3 and Cdc42 augment RhoA activity at the back as well as signals at the front. *The Journal of Cell Biology* 174(3):437-445.

27. Renkawitz J, *et al.* (2009) Adaptive force transmission in amoeboid cell migration. *Nat Cell Biol* 11(12):1438-1443.

28. Meili R & Firtel RA (2003) Two Poles and a Compass. 114(2):153-156.

29. Ferguson SSG (2001) Evolving Concepts in G Protein-Coupled Receptor Endocytosis: The Role in Receptor Desensitization and Signaling. *Pharmacological Reviews* 53(1):1-24.

30. Schumann K, *et al.* (2010) Immobilized Chemokine Fields and Soluble Chemokine Gradients Cooperatively Shape Migration Patterns of Dendritic Cells. *Immunity* 32(5):703-713.

Chapter 4: Dendritic Cell Chemotaxis in Engineered Gradients

Adapted from: **Dendritic Cells Distinguish Individual Chemokine Signals Through CCR7 and CXCR4**

Brendon G. Ricart, Beena John, Dooyoung Lee, Christopher A. Hunter and Daniel A. Hammer

Submitted to *The Journal of Immunology*

Abstract

Dendritic cells (DCs) respond to chemotactic signals to migrate from sites of infection to secondary lymphoid organs where they initiate the adaptive immune response. The key chemokines directing their migration are CCL19, CCL21 and CXCL12, but how signals from these chemokines are integrated by migrating cells is poorly understood. Using a microfluidic device, we present both single and competing chemokine gradients to murine bone-marrow derived DCs in a controlled, time-invariant microenvironment. Experiments performed with counter gradients reveal that CCL19 is 10 to 100 fold more potent than CCL21 or CXCL12. Interestingly, when the chemoattractive potencies of opposing gradients are matched, cells "home" to a central region in which the signals from multiple chemokines are balanced; in this region, cells are motile but display no net displacement. Actin and myosin inhibitors affected the speed of crawling, but not directed motion, while pertussis toxin inhibited directed motion, but not speed. These results provide fundamental insight into the processes that DCs use to migrate toward and position themselves within secondary lymphoid organs.

Introduction

Dendritic cells (DCs) are widely accepted to be the most potent and versatile antigen presenting cells in the immune system (1). In peripheral tissues, these cells are highly motile (2), possess superior capacity for acquiring and processing antigens for presentation to T lymphocytes, and within SLO have the potential to express high levels of the co-stimulatory molecules that direct and fine-tune T-cell activation (3-5). These characteristics are essential components of DC biology that allow them to act as the intermediary between local sites of infection and the SLOs where interactions with T and B cells take place.

Compartmental segregation of lymphoid tissues, which facilitates both efficient surveillance and targeted cellular response, relies on the precise trafficking of immune cells between the circulation, tissues, and SLOs. Specific responses, however, require directed cell migration that DCs accomplish through selective expression of chemokine receptors, coupled with generation of specific chemokines in immune organs. Immature DCs (iDCs), which often reside in or traffic through peripheral tissue, express a variety of chemokine receptors that confer responsiveness to inflammatory chemokines and direct DC migration towards inflammatory stimuli and peripheral tissues (6). Specifically, iDCs express the chemokine receptors CCR1, CCR2, CCR5 and CCR6 as well as CXCR3 and CXCR4, which direct their pattern of migration throughout the body (7-8). However, upon exposure to signals such as inflammatory chemokines or cytokines (such as IL-8 or TNF-alpha) (9-10) and foreign antigens (LPS, TLR ligands, etc) (11-12), DCs

mature and down-regulate most chemokine receptors, with the exception of CXCR4, while up-regulating the crucial receptor CCR7 (13). CXCR4 binds the widely-expressed CXCL12 (SDF1-α) which allows iDCs access to many peripheral tissues; however, its role for guiding the motility of mature DCs (mDCs) is unclear. CCR7 has two cognate ligands, CCL19 (ELC, MIP-3 β) and CCL21 (SLC, 6Ckine, Exodus-2), which are highly expressed in SLOs (14). In mice lacking CCR7, the organization of lymphoid organs is compromised and mature DCs fail to migrate to SLOs (15).

It is generally accepted that CCR7-dependent migration is primarily directed by a chemotactic gradient of CCL21 (16), a molecule expressed by afferent lymphatic vessels. Evidence for this interaction is based on histological studies which show CCL21 co-localizes with lymphatic endothelial cells (17), and upregulation of CCL21 on those cells during inflammation (18). An alternative hypothesis, however, suggests that DCs secrete chemokines (including CCL19) following activation and during migration (7, 19). In this model, the local extracellular gradient of CCL19 will be weakly influenced by interstitial flow velocities, which are typically on the order of 1 μm/s near the cell (20). Thus, motile DCs may respond to extrinsic or intrinsic, self-generated gradients of chemokine to direct their chemotaxis to draining lymph nodes (1), or use a combination of paracrine and autocrine signaling to home to appropriate locations.

Investigation of fundamental modes of DC chemotaxis requires the creation of well-defined gradients on biologically relevant length-scales from tens to hundreds of microns. Unfortunately, creation of these gradients has proven to be a substantial experimental

challenge (21). Transwell assays (Boyden chamber assays) are commonly used for chemotaxis (6, 8, 22) because they are easily employed, but present limitations for the interpretation of results because the chemotactic gradient is non-linear and varies with time and results are difficult to quantify (23). Simple methods for generating gradients in solution, such as secreting chemokine using a micropipette or delivering chemokine from a reservoir in a gel cannot be designed to deliver a time-independent gradient of chemokine. Even recent advances in three dimensional methods limit the shape of gradients that can be created, because they rely on diffusion of the chemical species between a "source" and a "sink" (2, 24-25). Thus, these techniques cannot fully meet the challenges of quantifying chemotactic migration.

To address these challenges, we and others previously developed a method to deliver linear, time-invariant gradients of chemokine using microfluidic chambers made by microfabrication (26-28). While neutrophils have been studied extensively using microfluidic chambers (29-30), Butcher and co-workers were the first to extend the use of simple microfluidic gradients to T cells (31). In their study, T cells were presented with overlapping microfluidic gradients of two homeostatic chemokines, CCL19 and CXCL12. This experiment uncovered a subtle preference of naïve T lymphocytes for the CCR7 ligand CCL19. In the current work, we extend the use of such a device to dendritic cells; since dendritic cells have a different role in the immune system, there is no reason to expect their response to be identical to that of T-cells. This system allows us to address questions about how DCs integrate chemotactic signals and provides insight on how they may navigate *in vivo* to reach SLOs. We find that mDCs are at least an order of

magnitude more sensitive to CCL19 than to CCL21 or CXCL12. Additionally, when opposing gradients have similar potency, we observe a central homing behavior in which the net flux of DCs is zero. Using inhibitors, we found that actin and myosin inhibition affected the speed of crawling, but not directed motion, while pertussis toxin inhibited directed motion, but not speed. Overall, our fundamental understanding of how multiple chemokine signals are coordinated by DCs may explain accumulation at specific locations *in vivo* and may be exploited for *ex vivo* immune therapy.

Materials and Methods

Cell isolation and culture conditions

Dendritic cells were generated from murine bone marrow cells according to the procedure of Lutz *et al.* (32) with minor modifications. Briefly, bone marrow was flushed from the tibias and femurs of 8 to 10-week-old C57BL/6 mice and depleted of red blood cells using ammonium chloride lysis buffer. The cells were plated in 10-cm petri dishes (2×10^6 cells/ml; 10ml/plate) in RPMI-1640 supplemented with 10% heat-inactivated fetal bovine serum, 100 U/ml penicillin, 100 mg/ml streptomycin, 50 nM BME, and 20 ng/ml rmGM-CSF (Peprotech, Rocky Hill, NJ) at 37°C in 5% CO_2. On day 3 fresh media was added, and on day 6 half of the media was gently replaced. Immature DCs were used in experiments on day 7. For mature DCs, 10 ng/ml TNF-α (PeproTech) and 1 μg/ml LPS (Sigma-Aldrich, St. Louis, MO) were added on day 6 and cells were used in experiments on day 7. On day 7, 80% or more of the non-adherent cells expressed the monocyte lineage marker CD11c as confirmed by flow cytometry. When inhibitors were used, they were added to cell culture 1 hour prior to imaging, with the exception of pertussis toxin, which was added 24 hours prior. All inhibitors were supplied by Sigma-Alrich, St. Louis, MO. Inhibitors were PD-98059 (100μM), LY-294002 (50μM), Latrunculin A (150nM, 1μM), blebbistatin (10, 50 μM), Y-27632 (10 μM), and pertussis toxin (100 ng/ml).

Western blotting

Fully matured DCs were treated with 50 μM LY-294002 or 100 μM PD-98059 for 90 minutes with or without addition of 20 nM CCL19 at 60 minutes. DCs (10^5/sample) washed in PBS were pelleted and then lysed in NuPAGE SDS LDS Sampler Buffer (Invitrogen, Carlsbad, CA) at 100°C for 20 minutes. Lysates were loaded on a SDS-PAGE gel and blots were transferred on a PVDF membrane (Invitrogen). A mixture of anti-phospho Akt rabbit polyclonal antibody (Cell Signaling Technology, Danvers, MA) and anti-GAPDH mouse monoclonal antibody (Ambion, Austin, TX) or a mixture of anti-phospho Erk1/2 rabbit monoclonal antibody (Cell Signaling Technology, Danvers, MA) and anti-GAPDH antibody was added to detect the protein blots on the membrane. GAPDH was used as a loading control. Fluorescently labeled blots were detected using ODYSSEY Infrared Imaging System (LICOR, Lincoln, NE). The membranes were immersed with 0.2 M NaOH for 30 minutes to strip the antibodies and antibody against total Akt or total Erk1/2 was applied to the membrane. The expression levels of proteins on the blots were evaluated using the Gel Analyzer in ImageJ software (NIH, http://rsbweb.nih.gov/ij/). Antibodies against mouse phospho-Akt (Ser473) (Cat #9271), total Akt (Cat #9272), phospho-Erk1/2 (p44/42 MAPK) (Thr202/Tyr204) (Cat #4377) and total Erk1/2 (Cat #4695) were purchased from Cell Signaling Technology (Danvers, MA).

Fabrication of microfluidic device

A microfluidic gradient generator was fabricated in polydimethylsiloxane (PDMS) using soft lithography as described previously (33). Briefly, a high-resolution printer was used to generate a mask from a CAD file. The mask was used in 1:1 contact photolithography with SU-8-2050 photoresist (MicroChem, Newton, MA) to generate a negative master, consisting of patterned photoresist on a 3-inch Si wafer. Positive replicas with embedded channels were fabricated by molding PDMS (Sylgard 184, Dow Corning, Midland, MI) against the master. The PDMS replica and a glass microscope slide were activated by oxygen plasma treatment (15 sec, 30 W, 600 mTorr O_2), then irreversibly contact-bonded; this assembly produced the required systems of microfluidic channels. Inlet and outlet ports were punched out of the PDMS using a 20-gauge blunt end needle. The adhesion surface was functionalized by incubation with fibronectin (Sigma, 10 μg/ml) for 1h at 20°C and blocked with BSA (Sigma, 1%) in PBS for 2h at 20°C. Inlet flow was controlled by a syringe pump (Harvard Apparatus, South Natick, MA).

Chemotaxis Assay

The chemotaxis assay was performed as described previously (34) with modifications. Additional information for the microfluidic device can be found in Figure 4.1.

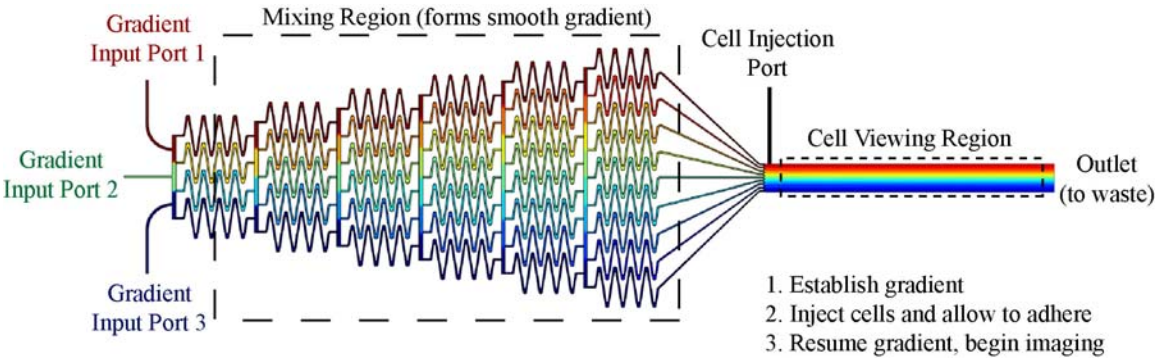

Figure 4.1. Schematic of the microfluidic device. Top-down view of microfluidic device used to present controlled gradients of chemokine to dendritic cells. The chamber is initially filled with PBS. Chemokine solutions are introduced at the inlet ports (left) and flow through a mixing region to form a smooth gradient in the viewing region. Cells are introduced via a side port and allowed to adhere to the migration surface in the cell viewing region. The gradient is then restarted and held constant for the duration of the experiment.

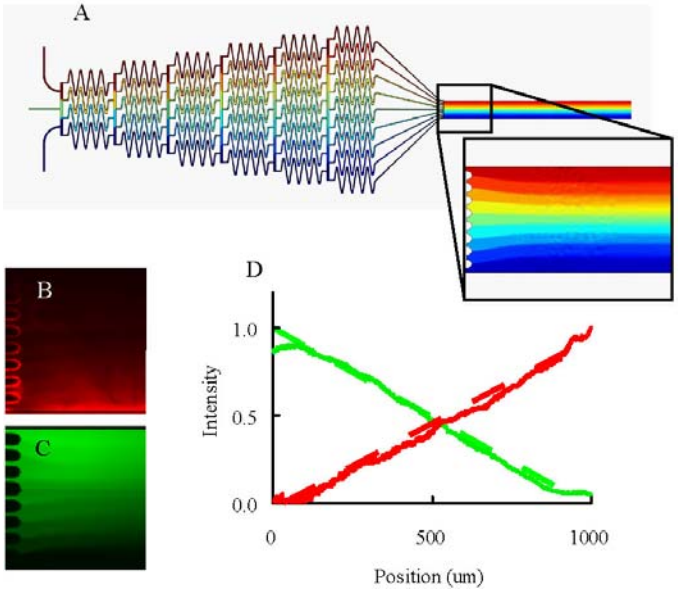

Figure 4.2. Flow profiles and chemokine gradients in a microfluidic device were modeled using COMSOL Multiphysics (A). A minimum flow of 9 μL/min was required to maintain a stable gradient in the chamber (A, inset). Using this flowrate, fluorescence images of tracer dyes were captured at 10× magnification at the inlet to the viewing chamber. Fluorescent intensity of rhodamine (B) and fluorescein (C) were quantified and showed linear, overlapping gradients (D, solid line), closely matching theoretical predictions (D, dashed line).

Assembled microfluidic devices were submerged in PBS and filled under vacuum. Chemoattractant solutions of CCL19, CCL21 or CXCL12 (Peprotech, Rocky Hill, NJ) in complete culture media were prepared for each of the three inlets. Fluorescein (Fluka) was added to one inlet at 10^{-5} M final concentration to aid visualization of the gradient and to confirm its persistence during the experiment. Sterile, 1-ml syringes were loaded with chemoattractant solutions and connected to the inlet ports while submerged to prevent the formation of air bubbles. A 1-ml syringe was loaded with mature dendritic cells at 10^6 cells/ml and connected to the side inlet. To complete assembly, tubing with an in-line valve was connected to the outlet, and the device was mounted in a custom-built microscope enclosure at 37°C and 5% CO_2. The total flowrate within the chamber was maintained at 9 μL/min using a syringe pump, resulting in a wall shear rate of 6 s^{-1}. After the gradient was visually established, the flow was stopped, and cells were injected via the side port and allowed to adhere for 10 min before resuming flow. Using custom built LabView (National Instruments, Austin, TX) software, 8-12 fields of view were imaged at 10X magnification by phase and green-channel fluorescence microscopy on a Nikon Eclipse TE300 (Nikon Inc., Melville, NY). Images were captured every 60 seconds for 60 minutes. Cell trajectories were captured using the ImageJ ManualTracking plugin (http://rsbweb.nih.gov/ij), and chemotactic parameters were calculated using a custom-written MATLAB (Mathworks, Natick, MA) script. Chemokine concentrations (a) are non-dimensionalized according to the relevant receptor dissociation constant as $\alpha = \frac{a}{K_D}$ (see Table 4.1 for K_D).

Receptor	Ligand	K_D
CCR7	CCL19	10 nM (35)
CCR7	CCL21	10 nM (35)
CXCR4	CXCL12	3-15 nM (36-37)

Table 4.1. Dissociation constants for chemokine receptor/ligand pairs involved in dendritic cell chemotaxis.

Additionally, the percent difference in concentration across a cell is defined by the parameter $\varepsilon = \frac{\Delta a}{\bar{a}}$ where Δa represents the difference in concentration between front and rear of the cell and $\bar{a}$ represents the mean concentration over the cell. The chemotactic index (CI) is a ratio of the displacement of the cell up the gradient (Δy) to the total path length (L_{path}). CI can be related to the persistence time, P,

$CI = \frac{\Delta y}{L_{path}} \left\{ 1 - \left(\frac{P}{t} \right) \left[1 - e^{-t/P} \right] \right\}^{-1}$ (38) which includes a correction for the period of time over which the cell was tracked. The persistence time can be calculated (P) by a one-parameter fit to the Langevin-type equation for random cell motility from the mean squared dispacement of cells $\left\langle d^2 \right\rangle = 2S^2 \left[Pt - P^2 \left(1 - e^{-t/P} \right) \right]$. The persistence length (P_L) and random motility coefficient (μ) are then calculated as $P_L = PS$ and $\mu = 2S^2 P$ (39).

COMSOL Modeling of Microfluidic Device

CAD renderings of the original microfluidic device mask were imported in COMSOL Multiphysics (COMSOL, Inc., Burlington, MA). Boundary conditions for the Navier-Stokes (NS) flow problem were no-slip at the walls and 3 μL/min at each of the three inlet ports with an atmospheric-pressure outlet condition. Boundary conditions for the convection-diffusion (CD) problem were no flux at the walls, 0, 10 and 20 nM at the 3 inlets and convective flux at the outlet.

Optimization of microfluidic chamber gradients

The microfluidic device was designed to facilitate generation and maintenance of stable chemokine gradients required for DC chemotaxis experiments. Since mature DCs are only weakly adherent, a low flow rate is required to minimize the effect of hydrodynamic shear on migration paths. At low enough flow rates, however, the relative rate of diffusion over convection is sufficient to dissipate the magnitude of the gradient. Thus, a moderate flow rate (corresponding to $Pe = \frac{vL_{chamber}}{D_{chemokine}} >> 1$) is required to maintain a consistent gradient within the viewing area. A COMSOL simulation determined that the minimum flow rate required to achieve less than 5% variance in gradient steepness within the chamber was 9 μL/min (Figure 4.2, A). The results of the simulation were then experimentally verified using two fluorescent tracers. Antiparallel gradients of

fluorescein and rhodamine were generated at 9 μL/min, and fluorescence intensities compared favorably to simulated concentrations (Figure 4.2, B-D).

Results

Dendritic cell expression of CXCR4 and CCR7

To determine relative receptor expression levels on several populations of BMDCs, we analyzed $CD11b^+/CD11c^+$ cells for CCR7, CXCR4, MHC Class II and CD86 expression by flow cytometry (Figures 4.3, 4.4). CCR7 expression was highest on mature DCs, which is essential for their migration to and within SLOs. Slightly elevated CCR7 expression was observed on a subset of immature DCs, which is associated with constitutive trafficking to lymph nodes and induction of tolerance (40). As expected, CCR7 knockout cells showed no expression of CCR7 on immature or mature cells. CXCR4, a ubiquitous monocyte/lymphocyte receptor, was observed in all $CD11c^+$ populations. Importantly, expression of CXCR4 on either immature or mature cells was not altered by knocking out CCR7, indicating that expression of these receptors is independently controlled. Additionally, CXCR4 expression is increased upon maturation for both the *wt* and CCR7 knockout DCs, suggesting a role for CXCR4 in mDC trafficking.

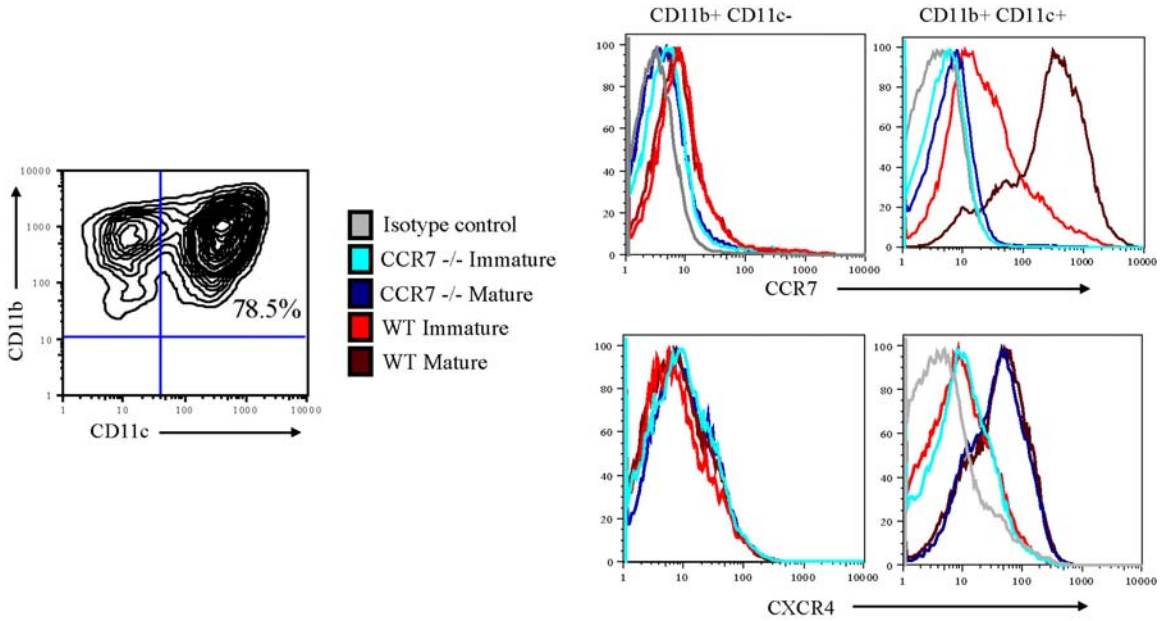

Figure 4.3. Flow cytometry results for BMDCs. Cells were gated on $CD11c^{hi/low}$ and analyzed for CXCR4 and CCR7 expression. $CD11c^{-}$ cells do not express CXCR4 or CCR7 in either mature or immature states. $CD11b^{+}/CD11c^{+}$ DCs express higher levels of CXCR4 upon maturation. No difference in CXCR4 expression is observed between $CCR7^{-/-}$ and *wt*. CCR7 is upregulated upon maturation and is absent in knockout cells.

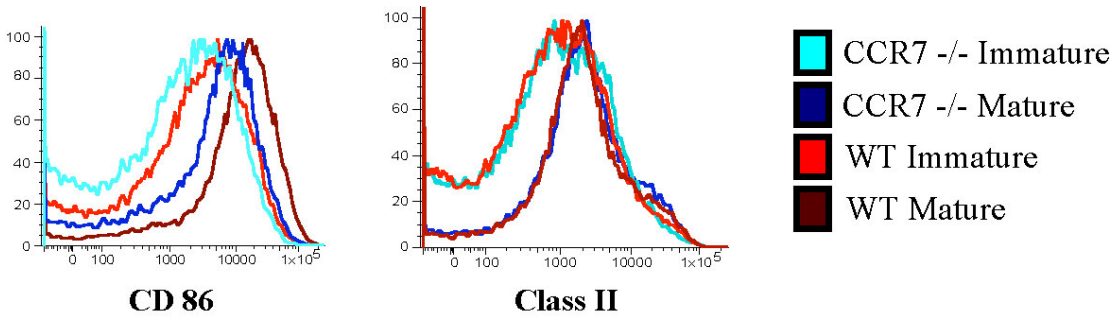

Figure 4.4. MHC Class II and CD86 expression on DCs. DCs upregulate both CD86 and MHC Class II expression upon maturation. This upregulation was observed regardless of CCR7 expression.

CCL19, CCL21 and CXCL12 induce directed DC migration

When placed in a uniform concentration of chemoattractant without an imposed gradient DCs exhibit chemokinesis (purely random motion). Chemokinesis can be described by a characteristic speed and persistence time. On a fibronectin surface in the absence of chemokine, mDCs migrated at 7.3 +/- 0.3 μm/min with a persistence time of 4.5 minutes, giving a random motility coefficient of 120 μm^2/min. Empirical observations show that speed and persistence time are inversely correlated across a variety of cell types (38), and these data for mDCs are consistent with this relationship, with mDCs crawling slower than lymphocytes/neutrophils but faster than macrophages/mesenchymal cells (38).

When DCs experience a gradient of chemoattractant, their ability to respond is governed by levels of receptor expression. Single gradients of 2 K_D/mm steepness ($\bar{a} = K_D$) were used to measure the chemotactic response of both mature and immature DCs. This gradient was chosen because in shallow gradients, few ligands are available, leading to sub-optimal signal generation while in steep gradients, receptors become saturated. Thus, the optimal chemotactic response is given when ligand concentrations are near the K_D for the receptor/ligand pair (Figure 4.5, A). Directional migration is quantified using the chemotactic index, which is the ratio of the cell displacement up the gradient to the total path length, with a correction for the temporal duration of the trajectory (38). Immature DCs showed no response to the CCR7 ligands, CCL19 and CCL21 (Figure 4.5,B) but strongly migrated toward the CXCR4 ligand, CXCL12, despite lower receptor expression levels of CXCR4 compared to mature cells (8, 41). Mature DCs migrated strongly

toward CCR7 ligands and weakly toward the CXCR4 ligand with a typical bell-shaped response curve, consistent with results from transwell assays and with their receptor expression (8). Mature DCs migrated with significantly greater velocity than immature DCs (Figure 4.5, D), which are often sessile within tissue until matured by the presence of a pathogen.

We used CCR7 knockout cells to confirm that CCL19 and CCL21 act only through the CCR7 receptor. Indeed, cells lacking this receptor were not able to respond to a gradient of either CCR7 ligand, but maintained their ability to migrate toward the CXCR4 ligand CXCL12 (Figure 4.5, B). Further, in mDCs the lack of CCR7 increased chemotactic response to CXCR4 ligand, despite no change in CXCR4 expression levels. We observe that DC chemotaxis is governed by receptor expression levels, but may be enhanced by the absence of non-cognate receptors.

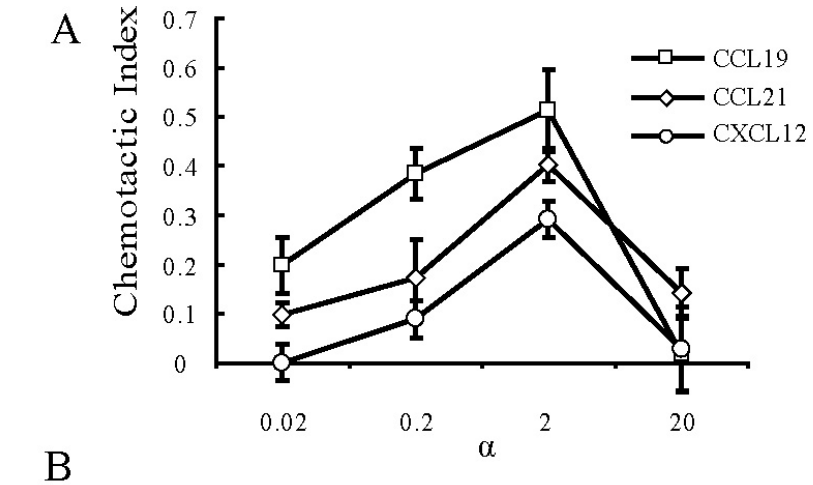

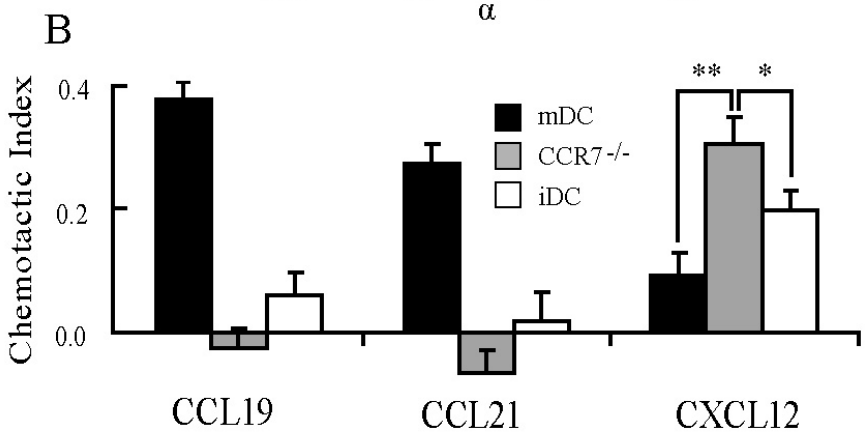

C

Cell Type	CXCR4	CCR7
Immature wt	+	-
Mature wt	+	+
Mature ccr7 -/-	+	-

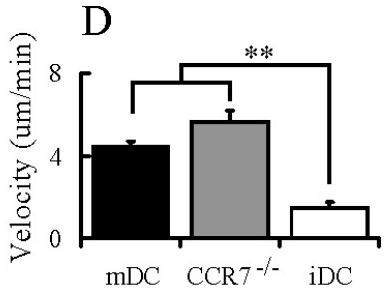

Figure 4.5. Response of BMDCs to chemokines CCL19, CCL21 and CXCL12 measured by chemotactic index. Mature DC chemotaxis toward chemokines was measured as a function of maximum chemokine concentration (A). Mature DCs (black bars), Immature DCs (grey bars) and Mature CCR7 knockout DCs (white bars) were presented with a single gradient of $\alpha = 0 - 2$ in a microfluidic device (B). Response was determined by the receptor expression profile (C). Mature DCs migrated with higher average velocity than immature DCs (D, data pooled from all experiments shown in B). Values are represented as the mean +/- S.E.M. * $p < 0.03$, ** $p < 0.001$ (Student's t-test).

Chemotaxis for a given gradient depends on the average chemoattractant concentration

Under a linear gradient of chemokine, migrating cells experience a constant difference in absolute ligand concentration between front and rear (Δa), but a varying average ligand concentration ($\bar{a}$). Therefore, we examined the chemotactic response of cells as a function of cell position within the gradient, parameterized by $\varepsilon = \frac{\Delta a}{\bar{a}}$. As the cell migrates toward higher concentrations of a, ε decreases. Regardless of chemokine, the migratory response was a strong function of ε (Figure 4.6). At high ε, migrating cells were able to coordinate a strong chemotactic response due to a high difference in receptor occupancy between the front and rear of the cell. However, as cells migrate up the gradient into higher chemokine concentrations and correspondingly lower ε, their ability to follow the gradient is diminished due to receptor saturation. Cells were significantly better able to adapt to the CCL19 gradient, but responses to CCL21 and CXCL12 were similar. Despite the change of chemotactic index as a function of chemokine concentration, the cell speed remained unchanged in all regions.

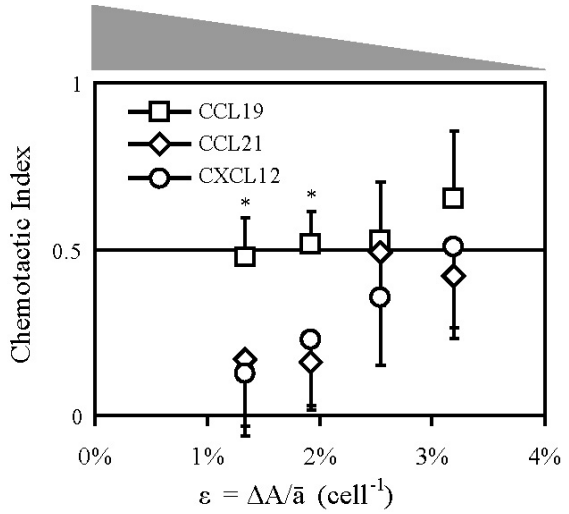

Figure 4.6. Chemotactic index is a function of position within the gradient. Cells were presented with a stable gradient of α = 0 - 2 CCL19 (triangles), CCL21 (squares) or CXCL12 (circles) in a microfluidic device. Response depended on the change in chemokine concentration across a cell length (ΔA/cell) compared to the local average concentration ($\bar{a}$). Greater differential in signal lead to a super-linear increase in chemotactic index. CCL19 shows superior ability to adapt to higher chemokine concentrations. Values are represented as the mean +/- S.E.M. * $p < 0.001$, (Student's t-test).

CCL19 antagonism by CCL21 and CXCL12

In order to simultaneously interrogate the way cells integrate multiple chemotactic signals and search for possible hierarchies of chemotactic signaling, cells were presented with opposing gradients of two different chemokines. When mDCs were presented with two opposing gradients, each with $\bar{a} = K_D$, they migrated more strongly to higher concentrations of CCL19 over either CCL21 or CXCL12 (Figure 4.7, A-C). Despite better adaptation to CCL19 at lower ε, this behavior was unexpected due to strong chemotactic responses to CCL21 and CXCL12 at high ε. To validate this response, we used CCR7 knockout cells in counter gradients of CCR7 and CXCR4 ligands. In these experiments, DCs responded only to the gradient of CXCR4 ligand and ignored the gradients of CCR7 ligands (unpublished data), verifying that the response CCL19 and CCL21 was specific for CCR7. When wild-type cells were placed in opposing gradients of CCL21 and CXCL12, the potencies were well-matched and no net preference and no net directional motion was observed. To determine the conditions of equipotency between CCL19 and the other chemokines, we lowered the gradient magnitude of CCL19 until a net balance was achieved. To reach equipotency against $\bar{a} = K_D$ CXCL12 and CCL21 gradients, we needed to lower the CCL19 gradients to $\bar{a} = 0.1(K_D)$ and $\bar{a} = 0.01(K_D)$, respectively (Figure 4.7, D-E) indicating a cell preference of 10 (CXCL12) to 100 fold (CCL21) for CCL19.

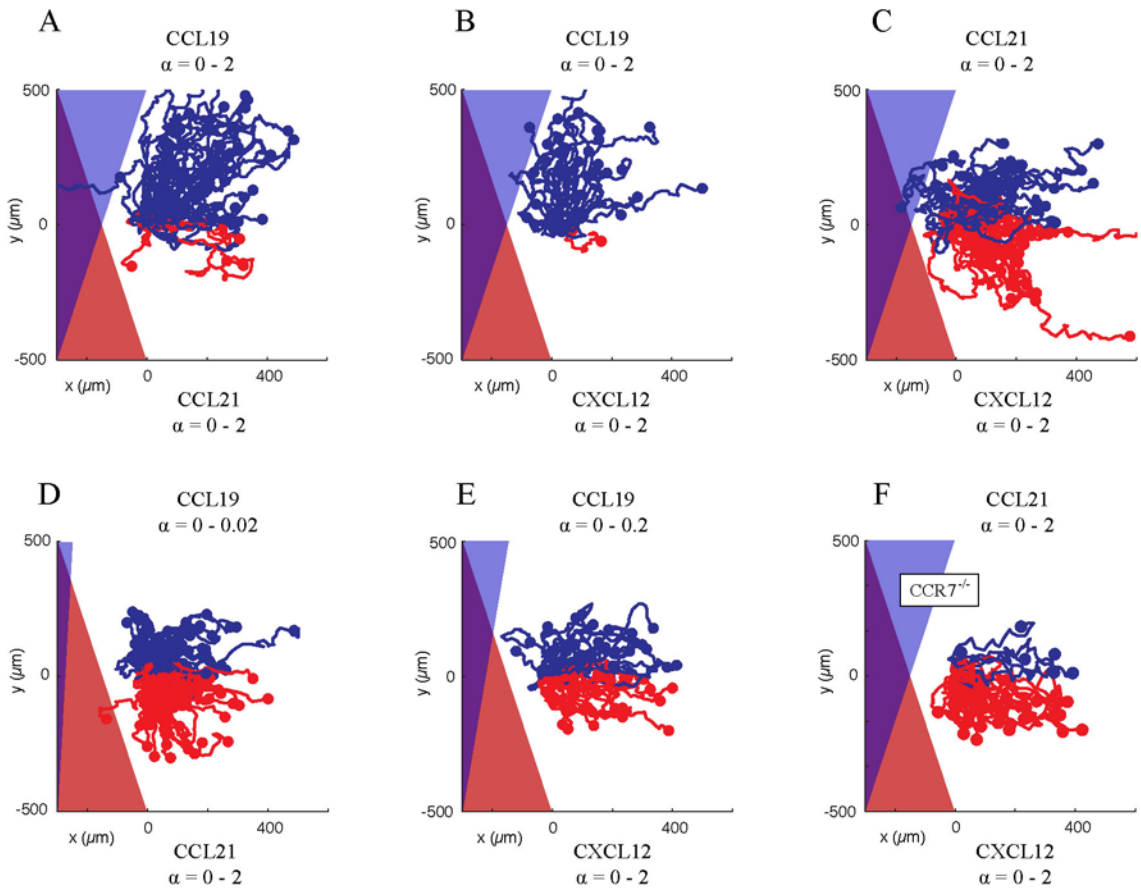

Figure 4.7. CCL19 attracts mDCs more potently than CCL21 or CXCL12 in competition assays. Trajectories of individual cells are plotted for α = 0 - 2 gradients of CCL19 against CCL21 (A), CCL19 against CXCL12 (B) and CCL21 against CXCL12 (C). The gradient of CCL19 was lowered until there was no net cell flux in the direction of the gradient. For CCL19 against CCL21 (D) and CXCL12 (E), the gradient of CCL19 was lowered to α = 0 – 0.2 and 0 – 0.02 respectively.

Cell homing in competing gradients

When equipotent antiparallel gradients of two chemokines were simultaneously presented to mDCs there is no net displacement, but surprisingly, individual cells continued to migrate. Cells collected at a midline at which the chemotactic signals from the two chemokines led to no preferential directed motion. Cells located initially far from the midline migrated toward the midline with long persistence times, sometimes greater than 100 μm (Figure 4.8). Upon reaching a central location where the effect of each gradient was equal (where the ε of each gradient was the same), the cells displayed random migration (Figure 4.8). The persistence length in the region near the midline shortened to approximately 25 μm, indicating the cells turned much more frequently as cells could not maintain orientation toward either gradient. The motion in this region was not directed but was also not truly random, because the mean squared displacement tended toward zero; thus, the motion was not chemokinetic, but rather, the cells were constrained chemically to remain within a narrow band. Interestingly, speed did not vary between regions, and speeds were similar to when the cells were undergoing chemokinesis at approximately 7 μm/min. This behavior was recreated in counter gradients of CCR7 ligands against the CXCR4 ligand and also surprisingly with counter gradients of CCL19 and CCL21, despite the fact that each bind the same receptor. This observation indicates that the cell is able to differentiate not only between signals from different receptors, but also between two ligands binding to the same receptor.

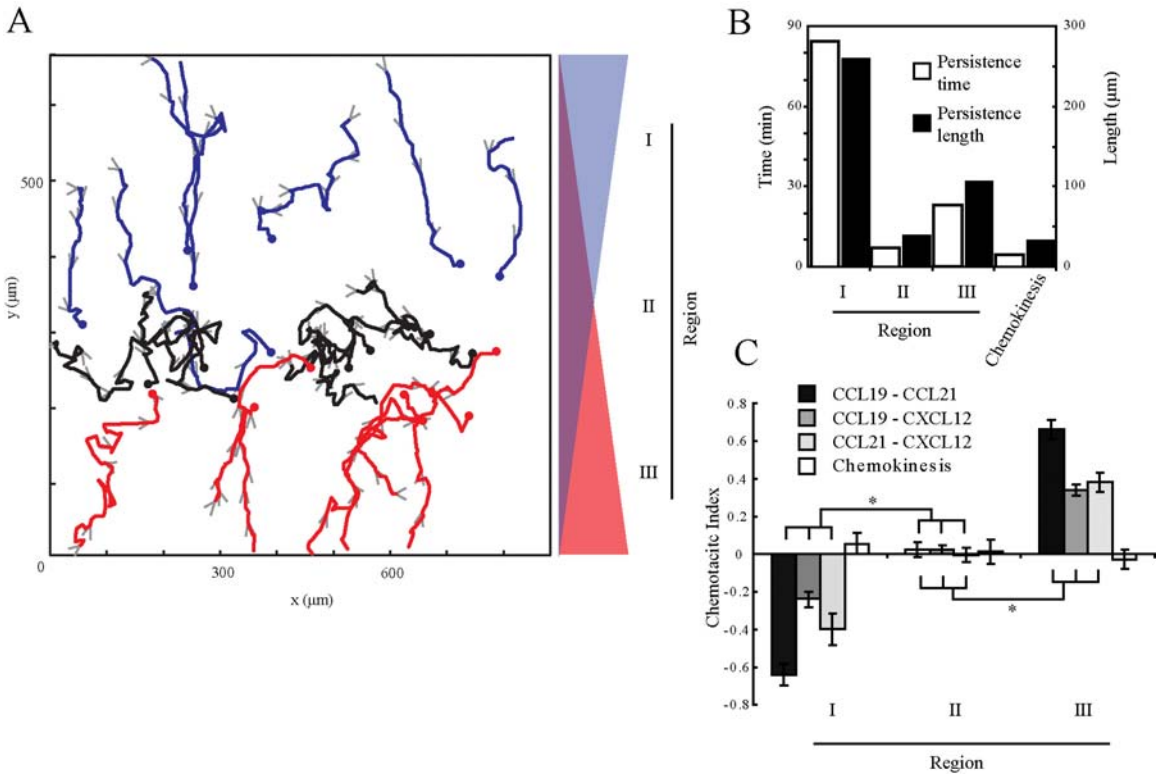

Figure 4.8. Homing behavior was observed in competing chemokine gradients. (A) Traces of cells responding to a distant CXCL12 gradient (blue, Region I), cells responding to a distant gradient of CCL19 (red, Region III), and cells retained in the central focusing region (black) are plotted with arrows (grey, Region II) indicating direction of motion at 10 minute intervals. Persistence times and persistence lengths are longer outside the focusing region (B). In the focusing region, persistence is similar to chemokinesis. Chemotactic indices are higher outside the focusing region (C). Values are represented as the mean +/- S.E.M. * = $p < 0.001$ (Student's t-test).

Chemical inhibitors alter speed or directional sensing

A number of chemosensory and structural molecules have been implicated in the motility of amoeboid cells, and we used pharmacological inhibitors to understand which of these was responsible for directed DC migration. To determine which molecular pathways are relevant for DC chemotaxis, we used chemical inhibitors to knock down a variety of intracellular targets. Since the Ras/Raf/MEK/ERK pathway has been implicated in cell migration (42-43), we used PD-98059 to inhibit MEK1. Even at high doses, this inhibitor did not affect cell migration (Figures 4.9, B and 4.10). Phosphoinositide 3-kinase (PI3K) is important for neutrophil polarization and migration (44), and has been implicated in controlling signaling at the leading edge through chemokine receptors, so we used the inhibitor LY-294002 to determine its role in DC migration. Surprisingly, knocking down this pathway also had no effect on DC speed or ability to move in a CCL19 gradient (Figures 4.9, C and 4.10). These data indicate that the MEK/ERK and PI3K pathways are not required for DC chemotaxis.

Chemokines signal through 7-transmembrane G-protein coupled receptors, so we used PTX to lock $G\alpha_i$ in its inactive state. As expected, PTX-treated cells were not able to sense the chemokine gradient, and migrated randomly (Figure 4.9, G;H). Speed was not decreased in the absence of G-protein signaling, demonstrating that on fibronectin surfaces, DCs are motile in the absence of chemokine stimulation.

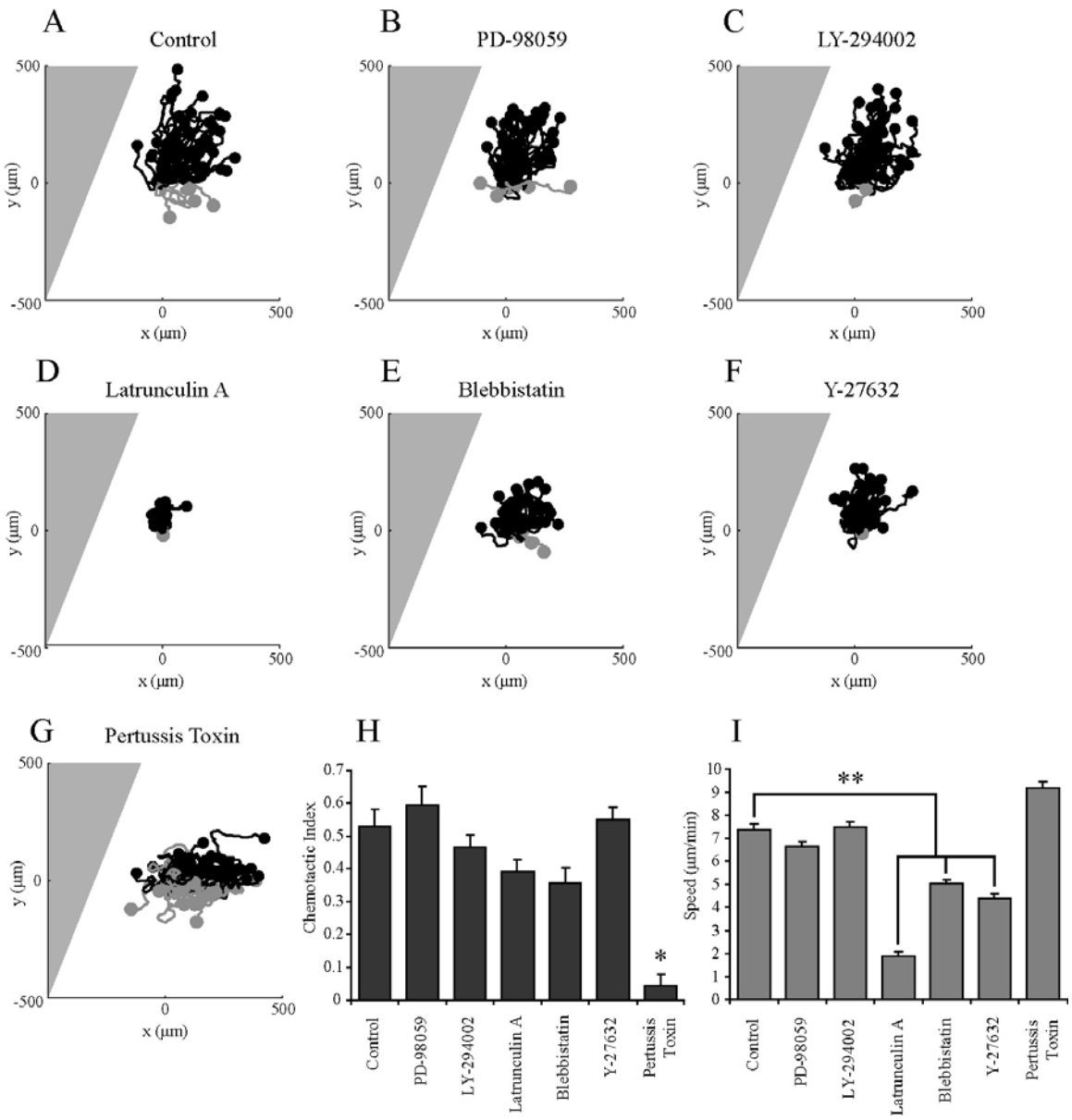

Figure 4.9. Effect of chemical inhibitors of DC chemotaxis. Cells were dosed with inhibitor for 1 hour (24 hours for PTX), then observed in an optimal gradient of CCL19 ($\alpha = 0 - 2$). Cell trajectories for a 60 minute experiment are shown (A-G) with final positions toward the gradient (blue) or away from the gradient (red). Inhibitors of actin/myosin showed no change in chemotactic index (H), but decreased migration speed (I). PTX blocked chemotactic sensing, but not speed. P13K and MEK inhibitors did not affect speed or chemotactic index. * = $p < 0.001$, ** = $p < 0.001$ (Student's t-test).

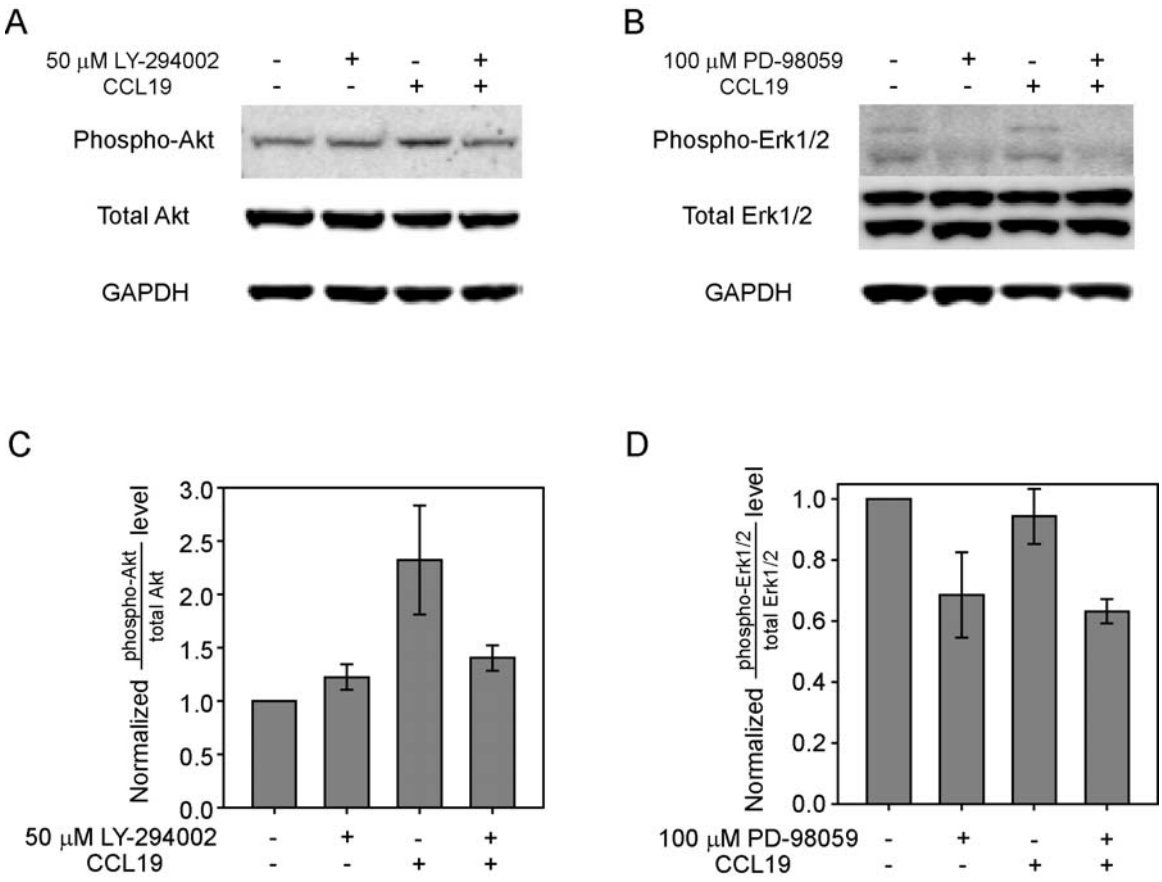

Figure 4.10. CCL19 stimulation in DCs increases the level of phospho-Akt but not phospho-Erk1/2. (A) Phospho-Akt and total Akt expression in DCs under the CCL19 stimulation without or with 50 □M LY-294002. (B) Phospho-Erk1/2 and total Erk1/2 expression in DCs under the CCL19 stimulation without or with 100 □M PD-98059. GAPDH was used as a loading control. Normalized phospho-Akt/total Akt (C) or phospho-Erk1/2/total Erk1/2 (D) level measured from the Western blots. The level of phospho Akt/total Akt or phospho-Erk1/2/total Erk1/2 in a control (which is a set without a inhibitor nor CCL19) was set to 1 and relative protein levels were calculated.

Actin polymerization occurs at the leading edge of migrating DCs, and it has been previously shown that actin polymerization alone can propel DC migration *in vitro* (45). When DCs in the most potent gradient of CCL19 ($\bar{a} = K_D$) were preincubated with Latrunculin A to inhibit actin polymerization, they developed a spherical phenotype with few protrusions. At low doses, the cells were able to move directionally toward the chemokine gradient, but with reduced speed (unpublished data). At higher doses, cell migration was completely abrogated (Figure 4.9, D;H;I). Myosin II produces contractile forces that are thought to propel the nucleus and exert traction forces (2). We used blebbistatin to inhibit myosin II, which lead to a highly branched morphology characterized by several stable lamellipodia, but treated cells had difficulty detaching adhesions. This led to a decrease in cell speed, and a small decrease in chemotactic index (Figure 4.9, E;H;I). Rho is an upstream effector of myosin II, which we blocked with the compound Y-27632. This produced an effect similar to blebbistatin (Figure 4.9, F), with a highly branched morphology, reduced speed, but no effect on chemotactic index. Overall, inhibition of actin or myosin did not affect gradient sensing, but did affect migration speed.

We extended the use of inhibitors to counter-gradients, to determine whether signal from one ligand may be differentially processed through a specific pathway. For example, it has been shown that CCL19 shows greater ERK phosphorylation than CCL21, so we used PD-98059 at conditions where CCL19 and CCL21 were equipotent. However, we did not observe a significant difference from the control (Figure 4.11). We also used the PI3K inhibitor LY-294002 and the ROCK inhibitor Y-27632 in counter-gradients of

CCL19 and CCL21, but did not observe any change in chemotactic behavior from the control experiment (Figure 4.11), though Y-27632 did reduce speed, as seen in a single-gradient. We conclude that the PI3K and ERK pathways are not critical for bone marrow DC chemotaxis.

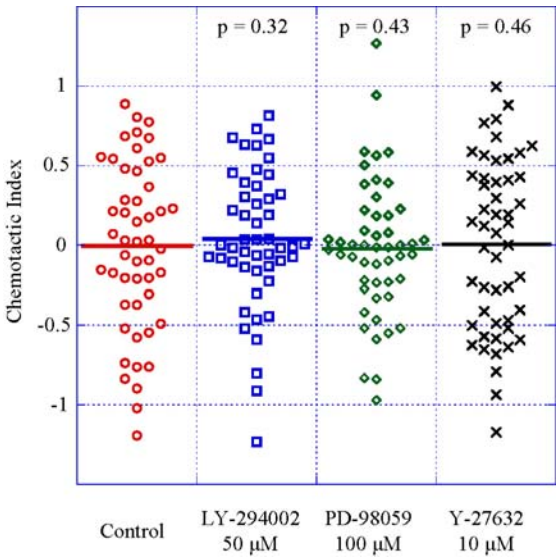

Figure 4.11. Dendritic cells migrating in CCL19-CCL21 counter gradients with inhibitors (Left). Cells were simultaneously exposed to 0-200 pM CCL19 and 20-0 nM CCL21 and treated (or not) with LY-294002, PD-98059 or Y-27632. No significant difference was observed from control (Student's T-test). See Methods section for experimental procedure. Each data point represents a unique cell migration path.

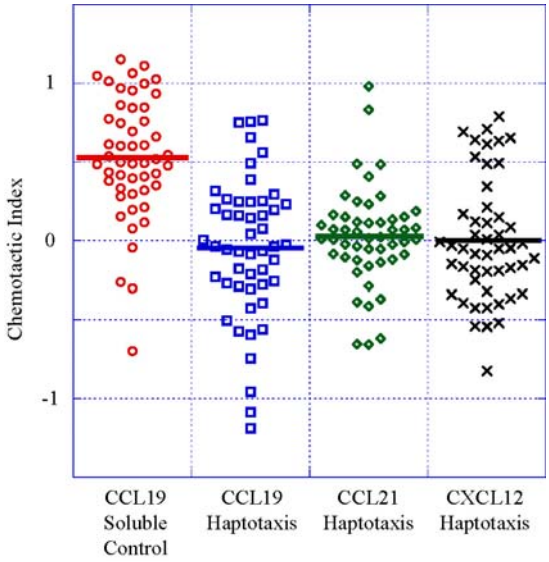

Figure 4.12. Investigation of haptotaxis due to "bound" chemokine (Right). Chemokine gradients were flowed through the microfluidic device for 60 minutes, simulating a typical experiment. The flow was then stopped, the chamber flushed, and cells introduced. Cells were allowed to migrate for 60 minutes, but did not show directional migration ($|CI| < 0.02$), indicating chemokine binding to migration surface did not affect trajectories. Each data point represents a unique cell migration path.

Discussion

The tissue microenvironment near and within SLOs presents multiple chemotactic stimuli to numerous cells involved in immune surveillance, including antigen-presenting DCs. Because DCs must navigate complex chemokine environments to perform their function, we studied their response to multiple soluble ligands (some which bind the same receptor) in a controlled environment. We presented cells with single and multiple oppositely oriented chemokine gradients generated by a custom-built microfluidic device which allowed us to investigate quantitatively the relationship between multiple spatial chemokine gradients and directional motion. The device is especially well suited to studying moderately-adhesive cell types such as mDCs, T cells and B cells due to the low shear stresses generated within the chamber while still providing a linear gradient which is stable in space and time. It should be noted that while we minimized shear forces, hydrodynamic flow did affect cell trajectories. However, since the direction of flow is orthogonal to the gradient, the resulting effects can be treated independently. The presentation of multiple gradients mimics the *in vivo* environments where mDCs must correctly integrate both extrinsic and intrinsic signals in order to leave a site of inflammation, navigate to a proximal lymph node, and seek a final position within the lymph node for antigen presentation.

We first demonstrated chemotaxis of mature mouse bone-marrow derived DCs in single gradients of CCR7 ligands CCL19, CCL21 and the CXCR4 ligand CXCL12. Although DC migration in confined microchannels has been demonstrated (46), this is the first experiment demonstrating DC chemotaxis to chemokines in an engineered two

dimensional microenvironment. We showed that mDCs respond more strongly to CCR7 ligands than CXCR4 ligands, which is most likely related to higher receptor expression levels of CCR7. Using a CCR7 knockout mouse, we observed that when CCR7 is not present, the response through CXCR4 is increased. Since both receptors signal through G-proteins, the lack of CCR7 may increase the supply of G-proteins available to CXCR4 to generate signal. Similarly, although CXCR4 expression is upregulated during maturation, its fraction of all receptors may be decreased due to high CCR7 expression, leading to the ultimate decrease in chemotactic response to CXCR4 ligands.

In competition assays, CCL19 outperformed CCL21 and CXCL12 in its ability to attract mDCs. *In vivo*, CCL21 coats afferent lymphatic vessels, and while both CCL19 and CCL21 are expressed within SLOs, CCL19 is approximately 100 fold less prevalent in lymph nodes (14). Matrix-binding of CCL21 has been shown to affect DC migration (47), but in our reductionist system, we did not observe adsorbed chemokine leading to haptotaxis (Figure 4.12). Our data indicates that CCL19 is approximately 100 fold more potent, so despite the lower abundance of CCL19, both chemokines can be expected to play a role in positioning within a lymph node. Our findings also agree with previous reports of calcium activation in T cells (35) in response to CCL21 as well as the physiological observation that mDCs first encounter CCL21 in the lymphatics (1) but do not stall in the subcapsular sinus once they reach the CCL19-rich lymph node.

We find that CXCL12 is equally as potent as CCL21. *In vivo*, deletion of CCR7 or deletion of its ligands CCL19 and CCL21 (as in the *plt* mouse) does not fully impair DC migration to lymph nodes (48-49), implying that the process is complex and that

CXCL12 may also be involved in trafficking to the afferent lymphatics. Although CCL19 is approximately 10 times more potent than CXCL12, both chemoattractants are highly expressed in specific zones of SLOs. CCL19 is expressed on stromal cells in the T-cell rich paracortex of lymph nodes while CXCL12 is expressed on the high endothelial venules (HEVs) (15). Similarly, CCL19 is found in the T-dependent areas of white pulp in the spleen, while CXCL12 is in the red pulp and marginal bridging channels (50). Mature DCs may integrate these competing signals to find their correct final positioning within SLOs.

With the use of temporally stable gradients, we demonstrate "central homing" of a cell population in competing gradients. To our knowledge, this is the first demonstration of cells seeking and remaining within a central zone which can be tuned based on the gradients presented. Previous reports have indicated that PMNs and T lymphocytes are able to respond to distant gradients, but were not able to identify a central collecting region (31, 51). Despite CCL19 and CCL21 binding the same receptor, our studies and several others (7, 52-53) have shown that the cell perceives them as unique entities. In cross-desensitization studies, CCL19 inhibits CCL21 signaling, but not vice-versa (35, 53), and despite similar G-protein activation and calcium mobilization, differences have been shown in receptor desensitization, internalization, and recycling (52-55). In our direct competition assays between CCL19 and CCL21, opposing gradients of equal concentrations resulted in a biased response toward CCL19. Further, when equal potency gradients were used, the cells displayed the same central homing behavior observed when two different chemokines engage multiple receptors. The central homing mechanism

may be exploited by several leukocytes to find their highly specific spatial positions within the complex chemokine environment of SLOs. For example, expression of CCR7 and CXCR5 by B lymphocytes is known to draw them into a boundary zone between the lymph node B-cell follicle and T-cell zone (56). Thus, this may serve as a common mechanism to ensure the spatial restriction of immune cells at their targets, thus allowing for effective cell-cell communication.

We used a microfluidic device to measuring chemotaxis and chemokinesis in dendritic cells in response to chemokines. We tracked individual DC chemotaxis within a stable, well defined environment which allowed a detailed, compartmentalized analysis of cell behavior as a function of the surrounding chemokine gradient(s). We were able to study signal integration using single and multiple, competing chemoattractant gradients to tease out a hierarchy of receptor signaling in mDCs where CCL19 > CCL21 > CXCL12; however, each ligand can promote effective DC trafficking. Finally, we observed a unique homing phenomenon in which murine bone-marrow derived DCs collected in a spatially restructed region that balanced the signal of competing chemoattractants. The homing behavior was generalizable to all competing gradients we studied, and was observed even when chemoattractants bound the same receptor. We suggest that this ability to simultaneously respond to overlapping gradients may be used by leukocytes to find their final position within secondary lymphoid organs, and conversely exploited by SLOs to direct interactions between multiple leukocyte subpopulations.

Acknowledgements

We thank Eric Johnston for technical support, Dr. Gudrun Debes for providing CCR7 knockout mice, Calixte Monast and Christopher Furcht for consultations and Drs. Michael Beste and Gregory Robbins for critical reading of this chapter.

References

1. Randolph GJ, Angeli V, & Swartz MA (2005) Dendritic-cell trafficking to lymph nodes through lymphatic vessels. *Nat Rev Immunol* 5(8):617-628.

2. Lammermann T, *et al.* (2008) Rapid leukocyte migration by integrin-independent flowing and squeezing. *Nature* 453(7191):51-55.

3. Banchereau J & Steinman RM (1998) Dendritic cells and the control of immunity. (Translated from eng) *Nature* 392(6673):245-252 (in eng).

4. Lanzavecchia A & Sallusto F (2000) Dynamics of T lymphocyte responses: intermediates, effectors, and memory cells. (Translated from eng) *Science* 290(5489):92-97 (in eng).

5. Quaratino S, Duddy LP, & Londei M (2000) Fully competent dendritic cells as inducers of T cell anergy in autoimmunity. (Translated from eng) *Proc Natl Acad Sci U S A* 97(20):10911-10916 (in eng).

6. Jung ID, *et al.* (2007) Sphingosine kinase inhibitor suppresses dendritic cell migration by regulating chemokine receptor expression and impairing p38 mitogen-activated protein kinase. *Immunology* 121(4):533-544.

7. Sallusto F, *et al.* (1999) Distinct patterns and kinetics of chemokine production regulate dendritic cell function. (Translated from eng) *Eur J Immunol* 29(5):1617-1625 (in eng).

8. Vecchi A, *et al.* (1999) Differential responsiveness to constitutive vs. inducible chemokines of immature and mature mouse dendritic cells. *J Leukoc Biol* 66(3):489-494.

9. Luster AD, Weinshank RL, Feinman R, & Ravetch JV (1988) Molecular and biochemical characterization of a novel gamma-interferon-inducible protein. (Translated from eng) *J Biol Chem* 263(24):12036-12043 (in eng).

10. Proudfoot AE (2002) Chemokine receptors: multifaceted therapeutic targets. (Translated from eng) *Nat Rev Immunol* 2(2):106-115 (in eng).

11. De Smedt T, *et al.* (1996) Regulation of dendritic cell numbers and maturation by lipopolysaccharide in vivo. *J. Exp. Med.* 184(4):1413-1424.

12. Stockwin LH, McGonagle D, Martin IG, & Blair GE (2000) Dendritic cells: Immunological sentinels with a central role in health and disease. *Immunol Cell Biol* 78(2):91-102.

13. Yanagihara S, Komura E, Nagafune J, Watarai H, & Yamaguchi Y (1998) EBI1/CCR7 Is a New Member of Dendritic Cell Chemokine Receptor That Is Up-Regulated upon Maturation. *J Immunol* 161(6):3096-3102.

14. Luther SA, *et al.* (2002) Differing Activities of Homeostatic Chemokines CCL19, CCL21, and CXCL12 in Lymphocyte and Dendritic Cell Recruitment and Lymphoid Neogenesis. *J Immunol* 169(1):424-433.

15. Förster R, *et al.* (1999) CCR7 Coordinates the Primary Immune Response by Establishing Functional Microenvironments in Secondary Lymphoid Organs. 99(1):23-33.

16. Gunn MD, *et al.* (1999) Mice Lacking Expression of Secondary Lymphoid Organ Chemokine Have Defects in Lymphocyte Homing and Dendritic Cell Localization. *J. Exp. Med.* 189(3):451-460.

17. Gunn MD, *et al.* (1998) A chemokine expressed in lymphoid high endothelial venules promotes the adhesion and chemotaxis of naive T lymphocytes. *Proceedings of the National Academy of Sciences of the United States of America* 95(1):258-263.

18. Martin-Fontecha A, *et al.* (2003) Regulation of Dendritic Cell Migration to the Draining Lymph Node: Impact on T Lymphocyte Traffic and Priming. *J. Exp. Med.* 198(4):615-621.

19. Radstake TRDJ, *et al.* (2005) Increased expression of CCL18, CCL19, and CCL17 by dendritic cells from patients with rheumatoid arthritis, and regulation by Fc gamma receptors. *Ann Rheum Dis* 64(3):359-367.

20. Chary SR & Jain RK (1989) Direct measurement of interstitial convection and diffusion of albumin in normal and neoplastic tissues by fluorescence photobleaching. (Translated from eng) *Proc Natl Acad Sci U S A* 86(14):5385-5389 (in eng).

21. Wilkinson PC (1998) Assays of leukocyte locomotion and chemotaxis. *Journal of Immunological Methods* 216(1-2):139-153.

22. Ledgerwood LG, *et al.* (2008) The sphingosine 1-phosphate receptor 1 causes tissue retention by inhibiting the entry of peripheral tissue T lymphocytes into afferent lymphatics. *Nat Immunol* 9(1):42-53.

23. Buettner HM, Lauffenburger DA, & Zigmond SH (1989) Measurement of leukocyte motility and chemotaxis parameters with the Millipore filter assay. *Journal of Immunological Methods* 123(1):25-37.

24. Haessler U, Kalinin Y, Swartz M, & Wu M (2009) An agarose-based microfluidic platform with a gradient buffer for 3D chemotaxis studies. *Biomedical Microdevices* 11(4):827-835.

25. Kim D, Lokuta MA, Huttenlocher A, & Beebe DJ (2009) Selective and tunable gradient device for cell culture and chemotaxis study. *Lab on a Chip* 9(12):1797-1800.

26. Jannat RA, Robbins GP, Ricart BG, & Hammer DA (2010) Neutrophil adhesion and chemotaxis depend on substrate mechanics. *Journal of Physics: Condensed Matter* 22(19):194117.

27. Herzmark P, *et al.* (2007) Bound attractant at the leading vs. the trailing edge determines chemotactic prowess. *Proceedings of the National Academy of Sciences* 104(33):13349-13354.

28. Irimia D, *et al.* (2006) Microfluidic system for measuring neutrophil migratory responses to fast switches of chemical gradients. *Lab on a Chip* 6(2):191-198.

29. Li Jeon N, *et al.* (2002) Neutrophil chemotaxis in linear and complex gradients of interleukin-8 formed in a microfabricated device. *Nat Biotech* 20(8):826-830.

30. Lin F, *et al.* (2005) Neutrophil Migration in Opposing Chemoattractant Gradients Using Microfluidic Chemotaxis Devices. *Annals of Biomedical Engineering* 33(4):475-482.

31. Lin F & Butcher EC (2006) T cell chemotaxis in a simple microfluidic device. *Lab on a Chip* 6(11):1462-1469.

32. Lutz MB, *et al.* (1999) An advanced culture method for generating large quantities of highly pure dendritic cells from mouse bone marrow. *Journal of Immunological Methods* 223(1):77-92.

33. Xia Y & Whitesides GM (1998) Soft Lithography. *Annual Review of Materials Science* 28(1):153-184.

34. Jannat R, Ricart, Dembo, Hammer (2010) Neutrophil adhesion and chemotaxis depend on substrate mechanics. *J. Phys.: Condens. Matter - CM* in press.

35. Yoshida R, *et al.* (1998) Secondary Lymphoid-tissue Chemokine Is a Functional Ligand for the CC Chemokine Receptor CCR7. *Journal of Biological Chemistry* 273(12):7118-7122.

36. Oberlin E, *et al.* (1996) The CXC chemokine SDF-1 is the ligand for LESTR/fusin and prevents infection by T-cell-line-adapted HIV-1. *Nature* 382(6594):833-835.

37. Laguri C, *et al.* (2007) The Novel CXCL12γ Isoform Encodes an Unstructured Cationic Domain Which Regulates Bioactivity and Interaction with Both Glycosaminoglycans and CXCR4. *PLoS ONE* 2(10):e1110.

38. Lauffenburger DA & Linderman JJ (1996) *Receptors: Models for Binding, Trafficking, and Signaling* (Oxford University Press, New York) p 376.

39. Ford RM & Lauffenburger DA (1991) Measurement of bacterial random motility and chemotaxis coefficients: II. Application of single-cell-based mathematical model. *Biotechnology and Bioengineering* 37(7):661-672.

40. Steinman RM, Turley S, Mellman I, & Inaba K (2000) The Induction of Tolerance by Dendritic Cells That Have Captured Apoptotic Cells. *The Journal of Experimental Medicine* 191(3):411-416.

41. Robbiani DF, *et al.* (2000) The Leukotriene C4 Transporter MRP1 Regulates CCL19 (MIP-3[beta], ELC)-Dependent Mobilization of Dendritic Cells to Lymph Nodes. *Cell* 103(5):757-768.

42. Chernyavsky AI, Arredondo J, Karlsson E, Wessler I, & Grando SA (2005) The Ras/Raf-1/MEK1/ERK Signaling Pathway Coupled to Integrin Expression Mediates Cholinergic

Regulation of Keratinocyte Directional Migration. *Journal of Biological Chemistry* 280(47):39220-39228.

43. Vindis C, Cerretti DP, Daniel TO, & Huynh-Do U (2003) EphB1 recruits c-Src and p52Shc to activate MAPK/ERK and promote chemotaxis. *The Journal of Cell Biology* 162(4):661-671.

44. Yoo SK, *et al.* (2010) Differential Regulation of Protrusion and Polarity by PI(3)K during Neutrophil Motility in Live Zebrafish. *Developmental Cell* 18(2):226-236.

45. Renkawitz J, *et al.* (2009) Adaptive force transmission in amoeboid cell migration. *Nat Cell Biol* 11(12):1438-1443.

46. Faure-Andre G, *et al.* (2008) Regulation of Dendritic Cell Migration by CD74, the MHC Class II-Associated Invariant Chain. *Science* 322(5908):1705-1710.

47. Schumann K, *et al.* (2010) Immobilized Chemokine Fields and Soluble Chemokine Gradients Cooperatively Shape Migration Patterns of Dendritic Cells. *Immunity* 32(5):703-713.

48. Mori S, *et al.* (2001) Mice Lacking Expression of the Chemokines Ccl21-Ser and Ccl19 (plt Mice) Demonstrate Delayed but Enhanced T Cell Immune Responses. *J. Exp. Med.* 193(2):207-218.

49. Junt T, *et al.* (2004) Impact of CCR7 on Priming and Distribution of Antiviral Effector and Memory CTL. *J Immunol* 173(11):6684-6693.

50. Ohl L, Bernhardt G, Pabst O, & Förster R (2003) Chemokines as organizers of primary and secondary lymphoid organs. *Seminars in Immunology* 15(5):249-255.

51. Foxman EF, Campbell JJ, & Butcher EC (1997) Multistep Navigation and the Combinatorial Control of Leukocyte Chemotaxis. *J. Cell Biol.* 139(5):1349-1360.

52. Kohout TA, *et al.* (2004) Differential Desensitization, Receptor Phosphorylation, β-Arrestin Recruitment, and ERK1/2 Activation by the Two Endogenous Ligands for the CC Chemokine Receptor 7. *Journal of Biological Chemistry* 279(22):23214-23222.

53. Britschgi MR, Link A, Lissandrin TKA, & Luther SA (2008) Dynamic Modulation of CCR7 Expression and Function on Naive T Lymphocytes In Vivo. *J Immunol* 181(11):7681-7688.

54. Otero C, Groettrup M, & Legler DF (2006) Opposite Fate of Endocytosed CCR7 and Its Ligands: Recycling versus Degradation. *J Immunol* 177(4):2314-2323.

55. Byers MA, *et al.* (2008) Arrestin 3 Mediates Endocytosis of CCR7 following Ligation of CCL19 but Not CCL21. *J Immunol* 181(7):4723-4732.

56. Reif K, *et al.* (2002) Balanced responsiveness to chemoattractants from adjacent zones determines B-cell position. *Nature* 416(6876):94-99.

Chapter 5: Application of Microfluidic Techniques to HS1 Knockout DCs

Adapted from: **HS1 Functions in Concert with WASp to Promote Podosome Organization and Chemotaxis in Dendritic Cells**

Deborah A. Klos Dehring, Fiona Clarke, Brendon G. Ricart, Yanping Huang, Daniel A. Hammer and Janis K. Burkhardt

Submitted to *The Journal of Immunology*

Abstract

Dendritic cells (DCs) are professional antigen presenting cells that reside in peripheral tissues and survey the body for pathogens. Upon activation by pathogen products, DCs undergo a maturation process and migrate to lymphoid organs where they present pathogen-derived antigens to T cells. DC function depends heavily on actin-regulatory proteins to reprogram the actin cytoskeleton during this switch from antigen surveillance to migration. We investigated the role of the actin-regulatory protein HS1, the hematopoietic homologue of cortactin, in reprogramming DCs. We find HS1 localizes to actin rich-structures associated with adhesion and migration, including podosomes and lamellipodial protrusions. Immature DCs from $HS1^{-/-}$ mice formed recognizable podosomes, but the arrays were loosely packed and improperly localized within the cell. Loss of HS1 did not affect actin turnover within preexisting podosomes or podosome function as sites of matrix metalloproteinase deposition, but did slow the rate of new podosome formation. Analysis of mature DCs, which lack podosomes, showed HS1 is not required for migration in transwell or in vivo migration assays, but is required for persistent chemotaxis in a chemokine gradient. Together, these results support a model in which HS1 functions to stabilize actin structures in DCs, allowing efficient migration in response to chemokine.

Introduction

Dendritic cells (DCs) are professional antigen presenting cells that play a unique role in bridging innate and adaptive immunity (reviewed in (1-3)). DCs reside in peripheral tissues and and continually sample the environment for pathogens. In response to pathogen-derived inflammatory molecules, these cells undergo a maturation program that induces their migration to lymphoid organs, where they present antigens obtained in the periphery to naïve T cells to initate an adaptive immune response. DC function is critically dependent on the ability to migrate long distances, traverse barriers, and navigate diverse tissues with variable surface characteristics (3). DCs achieve this by mechanical adaptation of cytoskeletal dynamics. Depending upon the nature of the substrate with which they are interacting, DCs can move by integrin-independent amoeboid protrusion into an open space within a 3D matrix, or by pushing against integrin-based adhesive contacts with extracellular substrates (4-5). In this latter mode, movement is driven by the combined force of actin polymerization and myosin contractility, pushing against integrin-dependent contacts. This mechanism is characterized by extension of an actin-rich lamellipodium at the front of the cell, often accompanied by the formation of adhesive contacts termed podosomes just behind the edge of this protrusion. Podosomes are short-lived structures comprised of actin-rich cores surrounded by adhesion molecules, including vinculin, talin and integrins (reviewed in (6-9). While the exact function of podosomes is still unclear, these structures serve as sites of matrix metalloproteinase deposition and are are thought to facilitate adhesion and migration through tissue barriers such as the lymphatic endothelium. In addition,

podosomes may function as part of the mechanosensing mechanism that allows DCs and other hematopoietic cells to alter their cytoskeletal dynamics in response to changing substrates.

The plasticity of DC migration is mediated by tightly regulated changes in actin dynamics. Several individual actin regulatory proteins have been shown to be important for controlling specific aspects of DC migration. One key protein is WASp, the protein defective in the immunodeficiency disorder Wiskott Aldrich Syndrome. DCs deficient for WASp (or for WIP, a WASp binding protein that protects WASp from degradation) show an almost complete lack of migratory capacity (10-14). WASp and WIP co-localize with F-actin in podosome cores and are essential for the formation of podosomes (15-18). WASp functions by activating the Arp2/3 complex, a 7-subunit protein complex that promotes actin polymerization by generating new actin on the sides of pre-existing filaments (19). Two other proteins that have been shown to be important for DC migration, CDC42 and Vav1, also function to activate Arp2/3-dependent actin polymerization (20-21). Formation of branched actin filaments is important for generating lameillipodial protrusions as well as for generating podosome cores, which turn over rapidly and exchange actin continuously (18, 22-23).

Another important actin regulatory protein in DCs is hematopoietic cell specific lyn substrate 1 (HS1) (24). HS1 is the hematopoietic homologue of cortactin, a protein involved in adhesion, spreading, endocytosis and migration in many cell types (25-28). Cortactin is upregulated or hyperphosphorylated in a number of metastatic cancers, and

plays an important role in the formation of invadopodia, stuctures that resemble, but are distinct from, podosomes (29-31). Cortactin stabilizes branched actin filaments *in vitro* (32-33), and enhances the persistence of actin-rich lamellipodial protrusions in fibroblasts (25). Like cortactin, HS1 is involved in the stabilization of branched actin filaments (34). Both of these proteins have a modular structure, with an N-terminal region that binds Arp2/3 complex and actin filaments, and a C-terminal adaptor region that can connect multiple proteins within the actin network, including Lck, Itk, Vav1, WASp, WIP and Nck (35-38). HS1 promotes lamellipodial protrusion in T cells (35-36), and regulates adhesion and migration in NK cells and B cells (39-40). Thus, HS1 and cortactin appear to carry out homologous functions in hematopoietic and non-hematopoietic cells, respectively. Though HS1 has recently emerged as an important actin-regulatory protein in hematopoietic cells, its role in DC function has not been investigated.

In this study, we show that HS1 is the sole cortactin family member expressed in murine BMDCs. HS1 localizes to actin-rich structures involved in cell migration, including lamellipodia and podosomes, and localization of HS1 to podosomes requires SH3-domain dependent interaction with WASp. Side-by-side analysis of DCs singly- and doubly-deficient for HS1 and WASp reveals that these proteins play distinct roles: WASp is essential for podosome formation, while HS1 is necessary to organize the podosome array within the cell. Similarly, while WASp is required for overall migration of DCs, HS1 is required for directional persistence during chemotaxis. These studies show that HS1 functions to fine-tune DC cytoarchitecture and direct cell migration.

Materials and Methods

Reagents and Antibodies

All flow cytometry antibodies were from Biolegend, unless specified. Rabbit anti-human HS1 (35) and rabbit anti-mouse HS1 (36) were previously described. Mouse anti-HS1 (3A3) was from Stressgen Bioreagents. Anti-GAPDH was from Calbiochem. Anti-cortactin (GK18), anti-vinculin and lipopolysaccharide (LPS) were from Sigma. Anti-green fluorescent protein (GFP), Alexa Fluor 594 phalloidin, anti-mouse IgG_1 Alexa Fluor 488, anti-mouse IgG Alexa Fluor 594, anti-rat Alexa Fluor 488, anti-rabbit IgG Alexa Fluor 488, anti-goat IgG Alexa Fluor 488 and FITC-gelatin were from Invitrogen. Anti- cortactin (4F11), anti-phosphotyrosine (4G10) and anti-WASp were from Upstate Biotechnology. Anti-β2-integrin (CD18, C71/16) was from BD Pharmingen. Anti-talin (C-20) was from Santa Cruz. Type B CpG oligonucleotide ODN 1668 and control oligonucleotide for murine TLR9 ligand 1668 were from Invivogen.

Recombinant HS1 was made as previously described (41). To generate recombinant cortactin, full-length human cortactin cDNA was subcloned into pGEX-4T-2 vector (GE Healthcare) and expressed in BL21-DE3 bacteria. The recombinant cortactin was purified using glutathione Sepharose 4B (GE Healthcare).

Mice

$HS1^{-/-}$ mice on the C57Bl/6J background have been previously described (42), and WASp knockout mice were from The Jackson Laboratory. To generate HS1 and WASp double knockout (DKO) mice, $HS1^{+/-}$ and $WASp^{-/y}$ mice were bred and the F1 progeny were then interbred. All mice were housed under pathogen-free conditions in the Children's Hospital of Philadelphia animal facility. All studies involving animals were reviewed and approved by the CHOP Institutional Animal Care and Use Committee.

BMDC Primary Culture

Granulocyte-monocyte colony-stimulating factor (GM-CSF) was produced from the B78Hi/GMCSF.1 cell line provided by T. Laufer (U. Penn.). Bone marrow was isolated from leg bones, cleaned of muscle tissues and sterilized in 70% EtOH using IMDM (Gibco) containing 1% FBS (Atlanta Biologicals). The cells were centrifuged at 1600 rpm and 4°C for 10 min and resuspended in DC culture media (IMDM, 10% FBS, penicillin/streptomycin, GlutaMax, 55 μM β-mercaptoethanol, 3% supernatant GM-CSF) at a concentration of $1x10^6$ cells/ml. 1 ml of cell suspension was added to wells of 24 well plates and supplemented with 1 ml of media on day 2. Starting on day 5, 1 ml of media was replaced daily. Differentiation into DCs was verified on day 6 by flow cytometric analysis of surface CD11c levels (typically 70-80%). Cultures were used between days 6 and 9. To induce maturation, DCs between days 6 and 8 were cultured with 100 ng/ml LPS for 24 hours.

DNA Constructs, Retroviral Production and Transduction

Vector expressing the GFP-variant Venus [Venus/pCS2, (43)] was provided by A. Miyawaki (Brain Science Institute, RIKEN, Yokohama). Human HS1 cDNA was provided by D. Billadeau (Mayo Clinic, Rochester, MN) (35). Human HS1 and Venus were amplified and ligated into the pMSCV2.1 retroviral vector (provided by W. Pear, U. Penn.). GFP-Actin (Clontech) was amplified and ligated in place of existing GFP in the MiGR retroviral vector (provided by W. Pear, U. Penn.). Retrovirus was produced by calcium phosphate co-transfection of 293T cells with 30 μg of the DNA of interest, the constructs encoding the viral envelope protein for mouse ectopic virus and the gag and pol genes. Supernatant was harvested at 24 and 30 hours post transfection and titered using NIH-3T3 fibroblast cells.

BMDCs were transduced by spin infection with retrovirus expressing Venus-HS1, GFP-WASp or GFP-Actin on day 2 of culture. Retrovirus and 4 μg/ml Polybrene (Sigma) were added to the wells of a 24 well culture plate and centrifuged at 2000 rpm and 32°C for 2 hours. Retrovirus-containing media was then replaced with DC culture media and the cultures were cared for as described above. Transduction efficiency (typically 45% or better) was determined on day 6 by detection of Venus or GFP expression by flow cytometry.

RAW/LR5 cells were a gift from D. Cox (Albert Einstein College of Medicine) and were cultured and transduced as previously described (18). Cells were either transduced with

control virus or virus to knockdown HS1. HS1 knockdown was verified by western blotting.

Flow Cytometry

BMDCs were harvested and $2x10^5$ cells were labeled for each condition. Fc receptors on the BMDCs were blocked using 2.4G2 antibody, made from the 2.4G2 hybridoma (provided by T. Laufer, U. Penn.). Cells were stained with anti-CD11c-PE alone or with anti-CD80-FITC, anti-CD86-FITC, anti-CD40-FITC or anti-mouse I-A/I-E-Alexa Fluor 488. Alternatively, cells were labeled with CD11c-APC alone or with anti-H-$2K^b$/H-$2D^b$-PE. Live cells were identified by exclusion of 7-AAD (Invitrogen). Cells were collected on a FACS Calibur flow cytometer and analyzed using FlowJo (Treestar).

Transwell Migration Assay

96 well transwell plates, 5 μm pore size, were from NeuroProbe Inc. Immature and mature WT and $HS1^{-/-}$ BMDCs were harvested, pelleted at 1500 rpm and RT for 5 minutes and resuspended at $2x10^6$ cells/ml. Migration media alone (IMDM, 1% serum) or containing chemokine (200 ng/ml CXCL12 (Peprotech, Inc) or 500 ng/ml CCL21 (R&D Systems)) was added to the bottom well. $5x10^4$ cells were placed on the filter and the plate was incubated at 37°C for 3 hours. The filter was removed and the cells in the bottom well were counted using a hemocytometer. The percentage of migrated cells was calculated by dividing the number of cells in the bottom well by the number of input

cells. Chemokine receptor expression and cell maturation were verified by flow cytometry of input cells.

Western Blotting

For analysis of cortactin, HS1 and WASp expression, cells were lysed in lysis buffer (20 mM Hepes pH 7.5, 1% NP-40, 0.5% deoxycholate, 0.1% SDS, 50 mM NaCl, 5 mM EDTA, 10 μg/ml leupeptin, 500 mM AEBSF, 1 mM Na_3VO_4 and 5 mM NaF) on ice, cleared by centrifugation, and protein concentration was determined by BCA Assay (Pierce). Lysates were resolved on 4-12% NuPage gels (Invitrogen) (Fig. 1) or tris-glycine SDS-PAGE gels (Fig. 3F and 4A), transferred to nitrocellulose membranes, blocked in 5% milk in PBS and probed with primary antibodies in TBST followed by secondary antibodies (goat anti-mouse IgG-Alexa Fluor 680 (Invitrogen) or goat anti-rabbit IgG-IR Dye 800 (Rockland)). Proteins were visualized and analyzed ratiometrically using the Licor Odyssey infrared fluorescence system, taking care to remain within the linear range.

Immunofluorescence Microscopy

BMDCs were harvested and cultured on coverslips at $2x10^5$ cells/well in 6 well plates overnight. The coverslips were washed in HBSS followed by fixation in 3% paraformaldehyde/PBS. Cells were permeabilized with 0.3% Triton X-100, and blocked with 0.05% Saponin/1.25% fish skin gelatin in TBS. Cells were labeled for F-actin with

Alexa Fluor 594-phalloidin and with primary antibodies followed by appropriate fluorescently-tagged secondary antibodies. For endogenous HS1 staining, cells were fixed and permeabilized simultaneously using a protocol from (44). For visualization of Venus or GFP tagged proteins, anti-GFP was used followed by anti-Rabbit IgG Alexa Fluor 488.

Cells were imaged using a Zeiss Axiovert 200 microscope equipped with Perkin Elmer Ultraview ERS6 spinning disk confocal system and a 63x 1.4 NA objective. Images were collected using an Orca ER camera (Hamamatsu) and analyzed using Volocity v.5 software (Improvision).

Podosome Analysis

For array analysis, images were collected without bias using spinning disk confocal imaging. Cell profiles were determined using the "find object" function in Volocity, and the borders of each podosome array were drawn by hand. The areas were calculated in Volocity. The percentage of the total area of individual cells covered by podosome arrays was then calculated. To determine the number of podosomes per cell, the actin cores were identified and counted using the "find object" function in Volocity, with verification and correction by eye.

For analysis of array localization and packing, slides were blinded to experimental conditions. Cell polarization was determined based on the presence of an actin-rich,

spread lamellipodium. The number of arrays per cell was counted and placed into one of the following groups: touching the leading edge (touch), behind the leading edge but not touching it (behind), in the middle of the cell not touching an edge (middle), opposite of the leading edge (back), lateral to the leading edge (side) or circular rosettes (rosette). Array packing was based upon the tightness of podosome packing within individual arrays, with cells scored as tight if most of the podosomes contacted one another in a regular pattern, and loose if gaps were evident between many of the podosomes. Approximately 200 cells were analyzed per experiment.

For the add-back experiments, approximately 100 cells from each condition were blindly counted to determine if the cells had podosomes, whether the arrays were loosely packed and finally, whether HS1 or WASp were in the podosome cores. Graphs are averages from 3-5 independent experiments.

Podosome Reformation Assay and FRAP analysis

Reformation of podosomes was assayed based on a modification of (18). Briefly, BMDCs were cultured on coverslips overnight. DC culture media containing 1 μM cytochalasin D (Calbiochem) was added for 30 minutes at 37°C. The cells were then washed twice with warm DC culture media and incubated for the indicated times at 37°C, fixed and labeled for actin and vinculin. Slides were blinded and approximately 200 cells were scored for the presence or absence of podosome arrays.

To measure actin turnover within podosomes, BMDCs transduced with GFP-actin were cultured in four-well Lab-Tek II chambered coverglasses (Nalge Nunc) at $5x10^4$ cells/chamber overnight. Fresh media was added and overlayed with mineral oil before imaging. Cells were imaged by spinning disk confocal microscopy using the Volocity v.5 FRAP plugin. The cells were imaged every 3 seconds before bleaching. A 20 μm^2 area within the podosome array of each cell was then bleached for 50 cycles, and images were captured at the fastest speed for 15 seconds, every second for 45 seconds and every 3 seconds for 180 seconds. Analysis was conducted using a single constrained exponential algorithm. Results are shown as $\tau_{1/2}$, the time required for fluorescence to recover to half the original value.

Analysis of MMP Secretion

For zymography, $2.5x10^6$ BMDCs were cultured in serum-free media in bacteriological 10 cm dishes for 24 hours. Supernatant was concentrated using a <30kDa cutoff centrifugal filter device (Millipore). Proteins were separated on tris-glycine gels containing 1 mg/ml gelatin (Sigma). The gel was then incubated in renaturation buffer (2.5% v/v Triton X-100, 50 mM Tris-HCl, 0.05% NaN_3) for 3 hours at 37°C and in developing buffer (50 mM-Tris HCl, 150 mM NaCl, 10 mM $CaCl_2$, 0.05% NaN_3) at 37°C overnight. Non-degraded gelatin was visualized by Coomassie blue staining and imaged on a Licor Odyssey fluorescence scanner.

FITC-gelatin degradation assays were performed as described in (45). Briefly, coverslips were acid-washed, coated with 2% FITC-gelatin (Invitrogen) and quenched in serum-free media for 1 hour at 37°C. BMDCs were cultured on coverslips overnight, washed and fixed. Cells were labeled for actin and imaged by spinning disk confocal microscopy.

Fabrication of microfluidic device

A microfluidic gradient generator was fabricated in polydimethylsiloxane (PDMS, Sylgard 184, Dow Corning) using soft lithography as described previously (46) with modifications. Briefly, soft lithography was used to create an SU-8-2050 photoresist (MicroChem) on silicon master. Positive replicas with embedded channels were fabricated by molding PDMS against the master. The PDMS replica and a glass microscope slide were activated by oxygen plasma treatment then irreversibly contact-bonded. The adhesion surface was functionalized by incubation with 10 μg/ml fibronectin (Sigma) for 1 hour at 20°C and blocked with 1% BSA (Sigma) in PBS for 2 hours at 20°C.

Chemotaxis Assay

The chemotaxis assay was performed as previously described (46) with the following changes. BMDCs were cultured as described in (47) and matured for 24 hours with 100 ng/ml LPS, harvested by pipetting and loaded into a syringe. The chemoattractant solution used was CCL19 (Peprotech).

Results

HS1, but not cortactin, is expressed in dendritic cells

The structural changes associated with DC migration are orchestrated by several actin-regulatory proteins, including Rho family GTPases, Vav1, and WASp (10, 13, 20-21, 48). The cortactin homologue HS1 functions as part of this actin regulatory complex in lymphocytes and NK cells (35-36, 39-40), but its role in DCs has not been addressed. HS1 and cortactin usually exhibit mutually exclusive expression patterns, with HS1 expressed in hematopoietic lineage cells and cortactin expressed in other cell types. However, DCs have been reported to express both proteins (16). Thus, we initiated our studies by carefully characterizing the expression patterns of these two proteins in bone marrow-derived dendritic cells (BMDCs). In addition to testing BMDCs from WT mice, we tested BMDCs generated from $HS1^{-/-}$ mice, to ask if cortactin expression is upregulated to compensate for loss of HS1. BMDCs lacking HS1 differentiate normally in culture and upregulate co-stimulatory molecules (CD80 and CD86), CD40, and MHC Class I and II similarly to WT BMDCs upon maturation with lipopolysaccharide (LPS) (YPH, DKD and JKB, manuscript in preparation). As shown in Figure 5.1, a polyclonal anti-mouse HS1 antibody raised in our lab reacted with recombinant human HS1 but not cortactin, and with lysates from hematopoietic cells (T cells and DCs) from WT mice, but not $HS1^{-/-}$ mice. As expected, this antibody failed to interact with lysates from non-hematopoietic cell types (mouse 3T3 and human 293T). This reagent binds human HS1 weakly, as indicated by its ability to detect recombinant human HS1, but not HS1 in human Jurkat T cells. Additionally, a polyclonal anti-human HS1 antibody reacts

specifically with human HS1 as a recombinant protein or from Jurkat T cells, but not with mouse HS1 (DCs and T cells). Several commercially available antibodies tested displayed different patterns of HS1 and cortactin recognition. A monoclonal anti-cortactin antibody, 4F11, reacted with mouse and human cortactin (3T3 and 293T cells, respectively), but failed to detect HS1 as a recombinant protein or from mouse T cells or DCs. However, another antibody, GK-18, previously used to show that DCs express cortactin (16), cross-reacted with HS1 and cortactin in all cell types tested and both recombinant proteins. These findings demonstrate that murine DCs express HS1, but not cortactin. Furthermore, they verify that DCs from $HS1^{-/-}$ mice lack HS1 expression and show that these cells do not exhibit compensatory upregulation of cortactin.

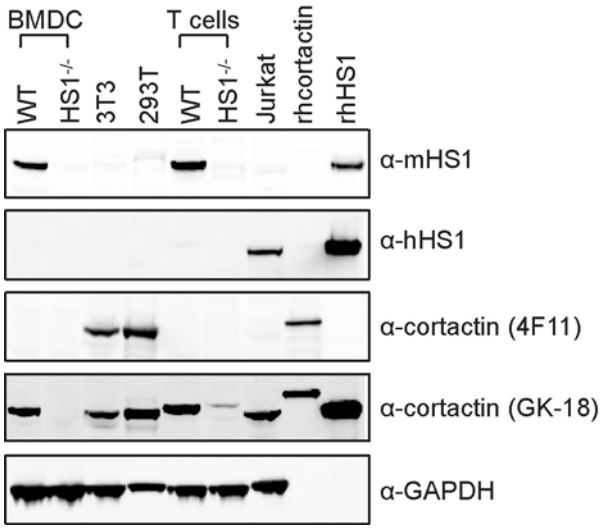

Figure 5.1. HS1 is the only cortactin family member expressed in murine BMDCs. BMDCs and T cells were cultured from WT or HS1$^{-/-}$ mice, and whole cell lysates were analyzed by immunoblotting with anti-HS1 or anti-cortactin antibodies. Lysates from the non-hematopoietic cell lines 3T3 and 293T were loaded as positive controls for mouse and human cortactin, respectively. Lysate from Jurkat T cells was loaded as a positive control for human HS1. Recombinant human cortactin and HS1 were loaded as positive controls for antibody specificity. GAPDH was used to verify equal loading.

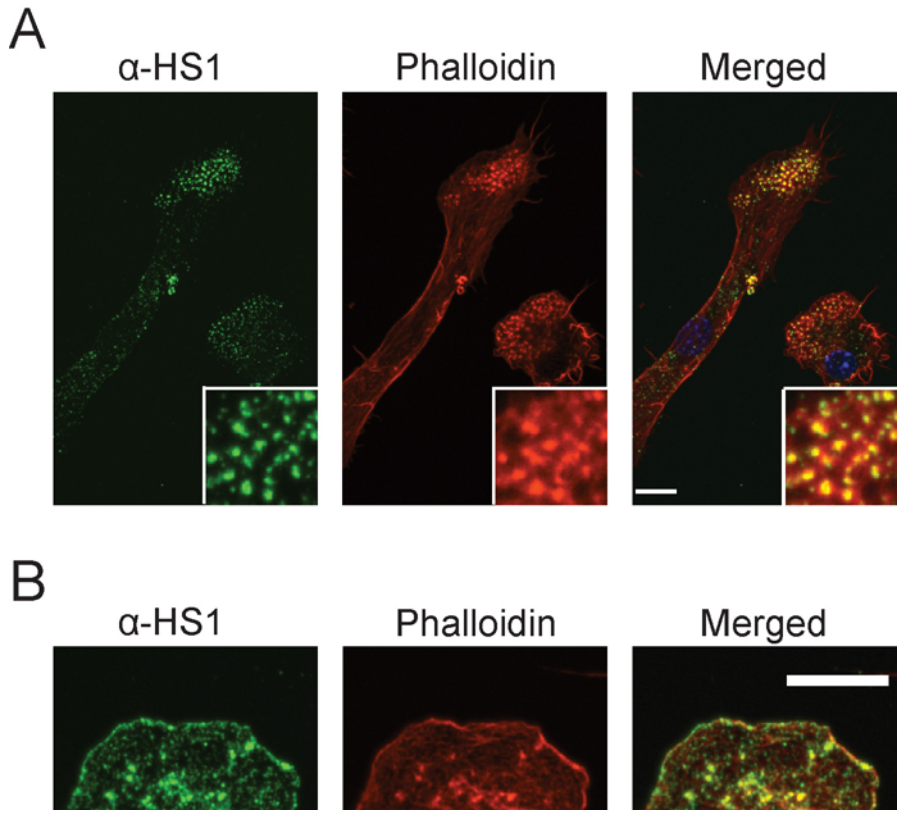

Figure 5.2. HS1 colocalizes with F-actin in structures associated with cell migration. BMDCs were cultured overnight on coverslips, fixed and stained with anti-HS1 to (green) and phalloidin to visualize F-actin structures (red). Colocalization of HS1 with F-actin in podosomes (A) and lamellipodial edges (B) is shown. Scale bars equal 10 μm.

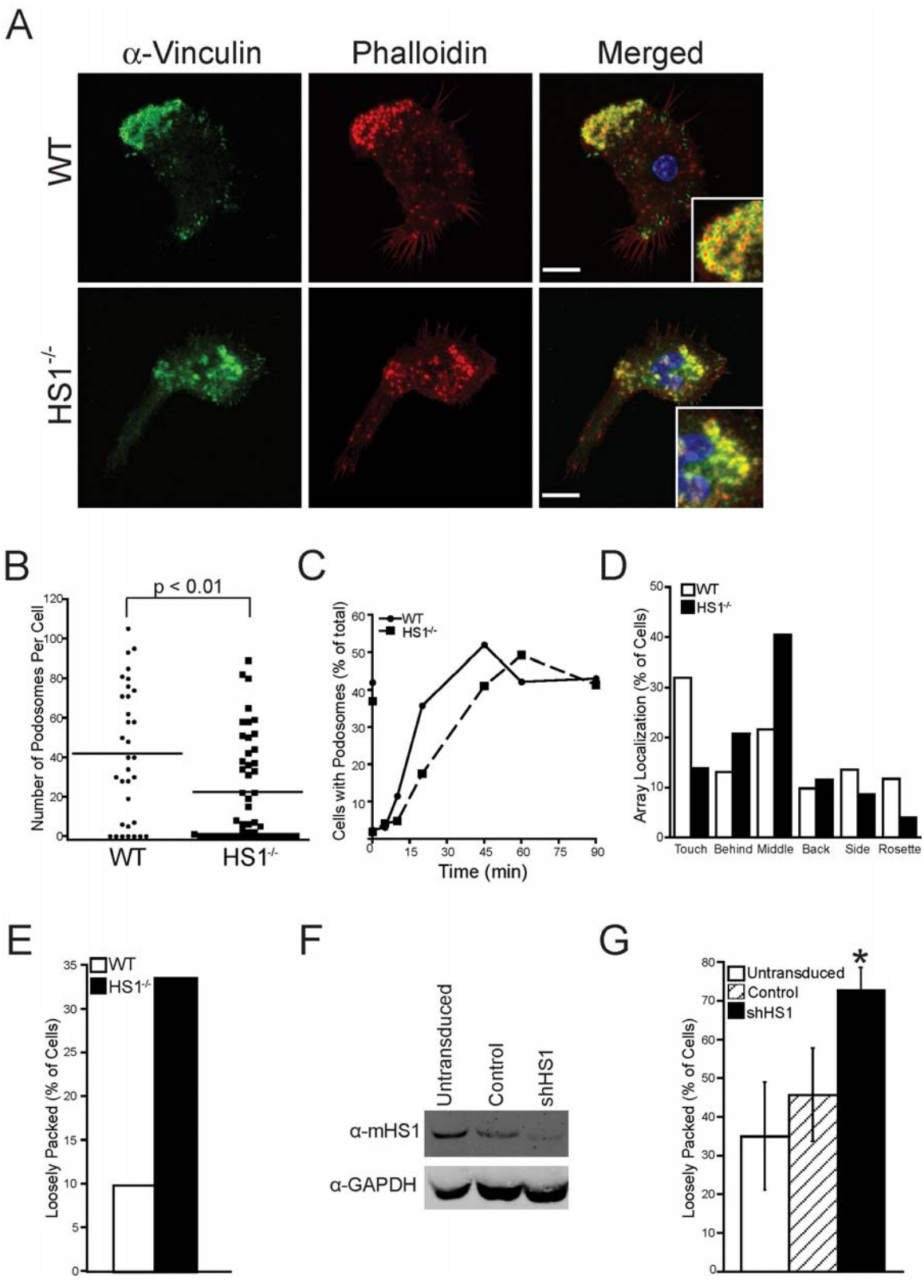
A
α-Vinculin
Phalloidin
Merged
WT
HS1-/-
B
p < 0.01
Number of Podosomes Per Cell
WT
HS1-/-
C
Cells with Podosomes (% of total)
WT
HS1-/-
Time (min)
D
WT
HS1-/-
Array Localization (% of Cells)
Touch
Behind
Middle
Back
Side
Rosette
E
WT
HS1-/-
Loosely Packed (% of Cells)
F
Untransduced
Control
shHS1
α-mHS1
α-GAPDH
G
Untransduced
Control
shHS1
Loosely Packed (% of Cells)
*

Figure 5.3. HS1 is required for efficient localization and organization of podosome arrays. A. WT and HS1$^{-/-}$ BMDCs were cultured on coverslips overnight, fixed and stained with phalloidin (red) and anti-vinculin (green) to visualize podosome cores and rings, respectively. DAPI (blue) was used to stain the nucleus. Images were captured by confocal microscopy. Arrows mark the leading edge of the cells. Scale bars equal 10 μm. B. Cells were prepared as in A. The number of podosomes per cell was counted as described in Materials and Methods; each dot represents a single cell. C. WT and HS1$^{-/-}$ BMDCs cultured overnight on coverslips were treated for 30 min at 37°C with cytochalasin D, after which time the drug was washed out and cells were allowed to recover. At the indicated times, cells were fixed and labeled with phalloidin and anti-vinculin, and the percentage of cells containing podosome arrays was determined. ($n \geq$ 200 cells/timepoint) D and E. Cells were scored for position and organization of the podosome array as described in Materials and Methods. F. Whole cell lysates were made from RAW/LR5 cells that were untransfected or transfected with control or shHS1 RNA and immunoblotted with anti-HS1 antibodies. GAPDH was used to verify equal loading. G. RAW/LR5 cells transduced as in F were prepared as in A and the organization of the podosome arrays was determined as described in Materials and Methods. (*$p<0.05$)

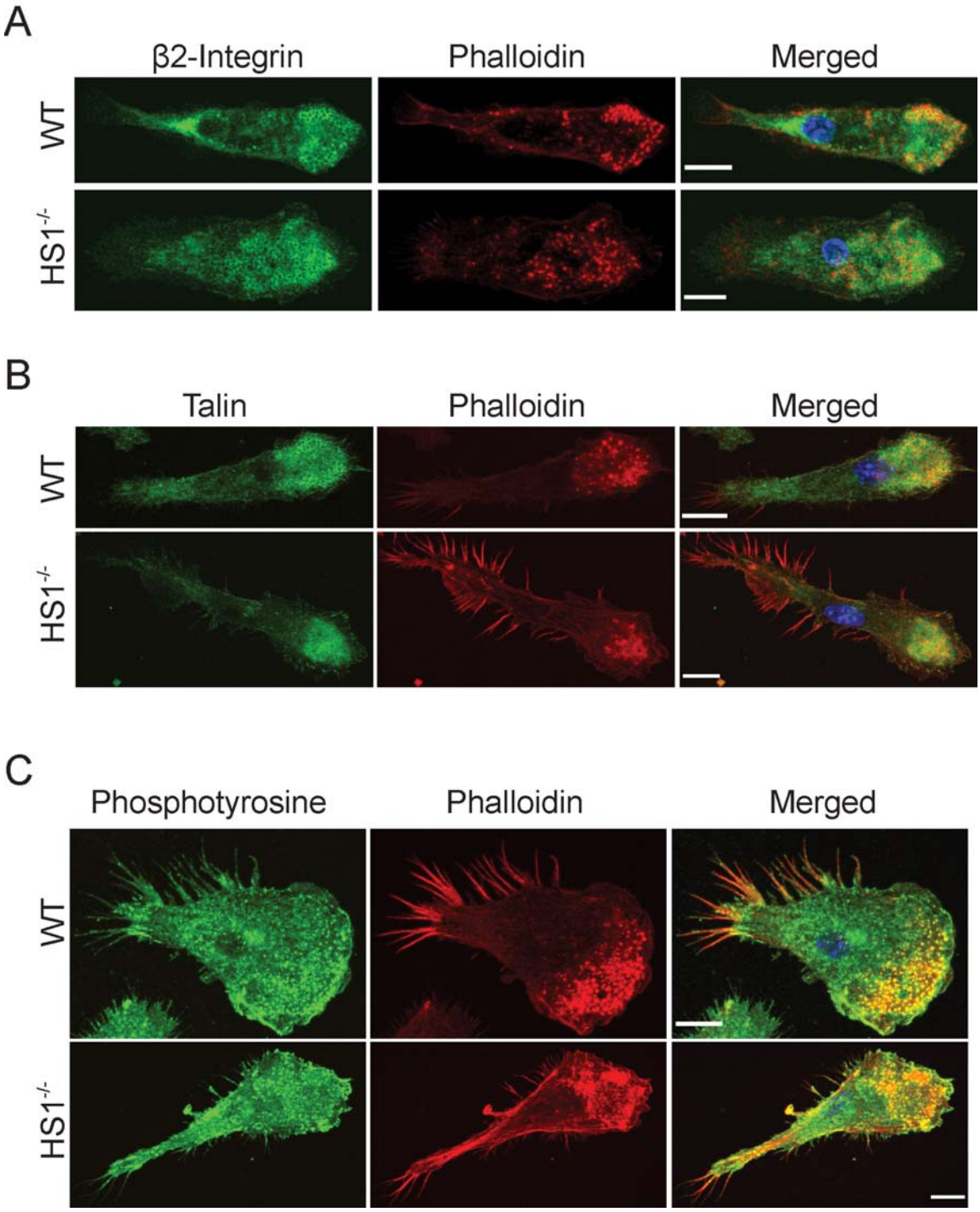

Figure 5.4. Podosomes of HS1$^{-/-}$ BMDCs are comprised of characteristic proteins. WT and HS1$^{-/-}$ BMDCs were cultured on coverslips, fixed and stained with phalloidin (red) to label F-actin and with anti-β2-integrin (green, A), anti-talin (green, B) or anti-phosphotyrosine (green, C). Scale bars equal 10 μm.

HS1 localizes to podosomes, but is dispensable for podosome formation

Using the anti-mouse HS1 antibody, we next investigated HS1 localization in murine BMDCs. As shown in Figure 5.2A, HS1 colocalized with F-actin in podosome cores. We also observed HS1 colocalization with F-actin at the edges of lamellipodia (Fig. 5.2B). This distribution is consistent with the localization of cortactin in non-hematopoietic cells (49), and with the idea that HS1 functions to regulate actin-rich structures associated with cell migration.

To ask if HS1 is required to organize DC cytoarchitecture, WT and $HS1^{-/-}$ DCs were plated onto coverslips and the actin cytoskeleton was analyzed by immunofluorescence microscopy. Adhesion and spreading of $HS1^{-/-}$ DCs on both fibronectin-coated and uncoated coverslips was grossly normal, although cells exhibiting multiple lamellipodial protrusions were somewhat more frequent among $HS1^{-/-}$ DCs (data not shown). Labeling with phalloidin and anti-vinculin revealed that both WT and $HS1^{-/-}$ DCs were able to make podosomes with actin-rich cores surrounded by vinculin rings (Fig. 5.3A). No differences were observed in the number of cells with arrays or the number of arrays per cell (data not shown). Moreover, other markers of podosomes, including talin, β2-integrin, and phosphotyrosine (50), localized normally within the podosomes of $HS1^{-/-}$ DCs (Fig. 5.4). In addition to exhibiting normal composition, the podosomes of $HS1^{-/-}$ DCs were functionally competent as sites of extracellular matrix degradation. Supernatants from WT and $HS1^{-/-}$ DCs contained similar levels of functional matrix metalloproteinases (MMPs) (Fig. 5.5A). Moreover, when WT or $HS1^{-/-}$ DCs were

cultured on FITC-gelatin-coated coverslips, there was no difference in the size, placement or frequency of holes formed in the matrix (Fig. 5.5B). We conclude that HS1 is not required for the formation of recognizable podosomes containing many of the characteristic proteins.

Podosome number and organization are perturbed in the absence of HS1

Although the organization of podosome arrays varies widely, even among WT cells, we observed clear differences in the podosome arrays of WT and HS1$^{-/-}$ DCs. One difference was that HS1$^{-/-}$ DCs exhibited significantly fewer podosomes per cell (Fig. 5.3B). Since HS1 stabilizes branched actin filaments, we hypothesized that loss of HS1 would decrease the stability of podosome cores. To test this idea, WT and HS1$^{-/-}$ DCs were transduced with retrovirus expressing GFP-actin and the exchange of actin molecules within podosomes was assessed by fluorescence recovery after photobleaching (FRAP) (Fig. 5.5C). No significant differences were observed, showing that loss of HS1 does not affect actin turnover within pre-existing podosomes. To determine if HS1 promotes podosome formation, WT or HS1$^{-/-}$ DCs were treated with cytochalasin D to dissolve podosomes. After drug washout, the cells were allowed to recover for varying times, and the number of cells with podosome arrays was assessed (Fig. 5.3C). Prior to treatment a similar number of WT and HS1$^{-/-}$ DCs exhibited podosomes (Fig. 5.3C, points on the y-axis). In both cell types, podosomes were lost upon drug treatment, and actin cores recovered within 30-60 minutes of drug washout (Fig. 5.3C). However, recovery of podosome cores in HS1$^{-/-}$ DCs was slightly, but consistently delayed. In both WT and

HS1$^{-/-}$ cells, recovery of vinculin into rings was not observed until after actin cores were formed (data not shown), consistent with the idea that a viable actin core is needed for recruitment of ring proteins (14). These data indicate that HS1 accelerates the early stages of podosome genesis, but is not essential for podosome formation.

HS1 is important for organizing the podosome array

The most striking cytoarchitectural defects we observed in HS1$^{-/-}$ DCs involved podosome array organization. Podosomes in the HS1$^{-/-}$ DCs were not packed as tightly as those in WT DCs and the arrays were more randomly distributed throughout the cell (Fig. 5.3A and Fig. 5.4). To assess differences in the positioning of podosome arrays, cells were categorized into one of several groups (Fig. 5.6): touching the leading edge (touch), behind the leading edge (behind), centrally located within the cell (middle), opposite the leading edge (back), lateral to the leading edge (side) or forming rosettes within the center of the cell not adjacent to any edges (rosettes). Whereas WT DCs more frequently showed arrays that touched the leading edge, arrays in HS1$^{-/-}$ DCs tended to be further behind the leading edge (Fig. 5.3D). In addition to array localization, array packing was affected (Fig. 5.3E). Whereas podosomes in WT DCs tended to be tightly packed within the array, HS1$^{-/-}$ DCs showed an increased number of cells with loosely packed podosome arrays (increased space between adjacent podosomes). This qualitative finding is consistent with our quantitative data showing that HS1$^{-/-}$ DCs have fewer podosomes than WT DCs, distributed in arrays that occupy a similar area (Fig 5.3B and 5D).

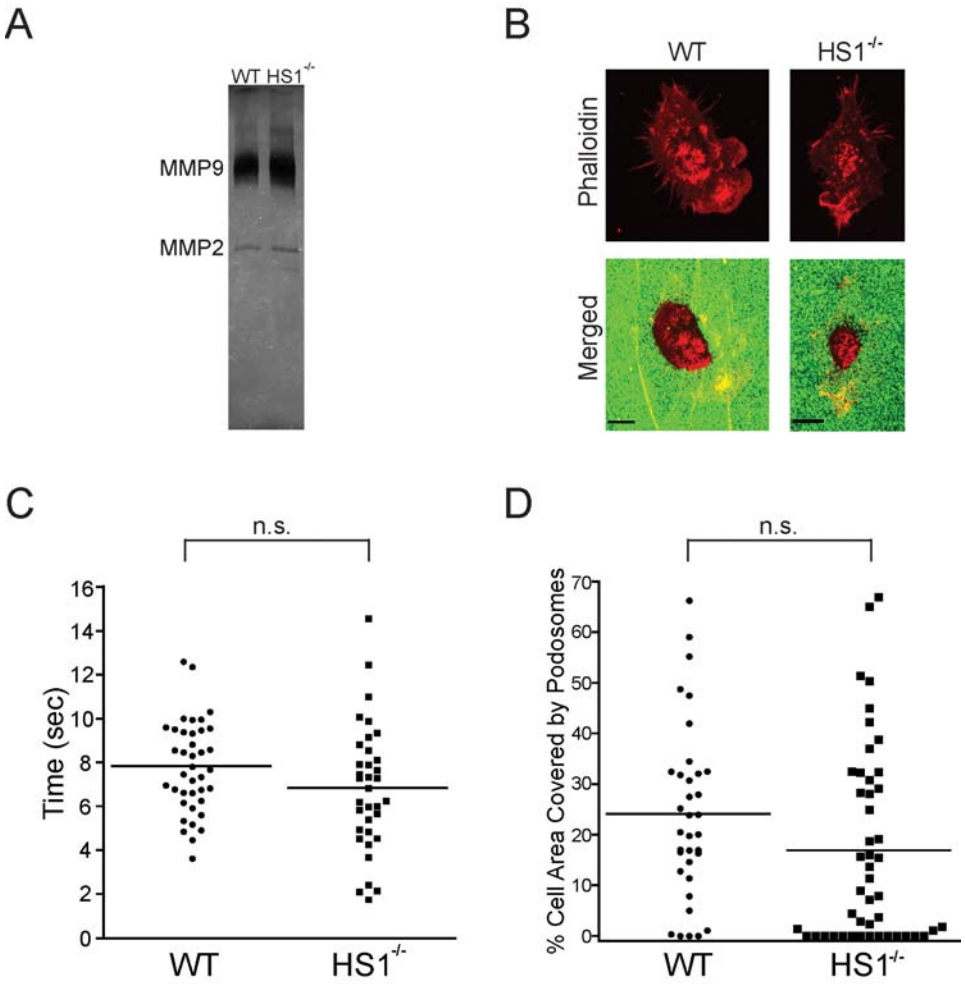

Figure 5.5. Analysis of podosomes in HS1$^{-/-}$ BMDCs. A. Culture supernatants from WT and HS1$^{-/-}$ BMDCs were harvested. Proteins were concentrated and separated on an SDS-PAGE gel supplemented with 1 mg/ml gelatin. The gel was renatured and stained with Coomassie Blue to determine regions of degraded gelatin. B. WT and HS1$^{-/-}$ BMDCs were cultured on coverslips coated with gelatin containing 2% FITC-labeled gelatin (green) overnight. Cells were fixed and stained with phalloidin (red) to visualize podosomes. Scale bars equal 10 μm. C. WT and HS1$^{-/-}$ BMDCs were transduced with GFP-Actin, cultured overnight on chambered coverglasses and imaged live by spinning disk confocal microscopy. A region of interest within the podosome array was bleached and monitored for recovery of fluorescence, and the half-life ($\tau_{1/2}$) for fluorescence recovery within the ROI was measured. Each dot represents a single cell. D. Cells were prepared as in figure 5.3A. The percent of cell area covered by podosomes was determined as described in Materials and Methods; each dot represents a single cell.

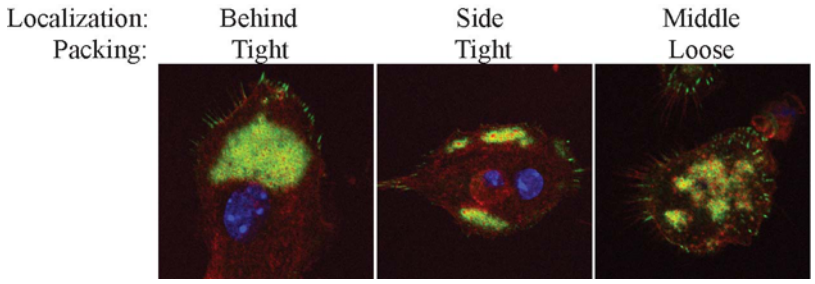

Figure 5.6. Examples of scoring categories used for analysis of podosome array localization and packing in Figure 5.3D and E. BMDCs were prepared as in Figure 5.3A. Scoring of localization and packing of arrays is noted above each picture.

To verify that the phenotypes we observe do not reflect developmental changes in the $HS1^{-/-}$ mice, and to ask if these results extend to other myeloid cell types, HS1 function was tested in RAW/LR5 macrophages, a cell line that efficiently forms podosomes (18, 51). Figure 5.3F shows that HS1 could be efficiently silenced in these cells using shRNA. HS1-suppressed RAW/LR5 cells were able to form podosomes with normal frequency (data not shown), but the podosome array in these cells became more loosely packed (Fig. 5.3G). We conclude that HS1 is not required for podosome formation in myeloid cells, but is required for proper organization of podosome arrays.

HS1 and WASp carry out distinct roles in podosome formation and organization

HS1 interacts with WASp, another actin regulatory protein involved in podosome formation, and in other systems, HS1 is thought to stabilize branched actin filaments generated by WASp and the related protein WAVE2 (34-35). To investigate the relationship between HS1 and WASp in DCs, we compared the phenotypes of DCs cultured from mice lacking HS1 alone, WASp alone, or both proteins. DCs cultured from these mice exhibit loss of the appropriate proteins, and knockout of one has no effect on the expression levels of the other (Fig. 5.7A). As shown in the filled bars in Fig 5.7B, $HS1^{-/-}$ and $WASp^{-/y}$ DCs differed with respect to the proportion of cells exhibiting podosomes. While significantly fewer WASp-deficient cells displayed podosomes, HS1-deficiency had no effect on this parameter (the slight increase relative to WT cells in this experiment was not reproducible). The defect in podosome formation in $WASp^{-/y}$ DCs is

consistent with previous reports (10, 52), though the magnitude of the defect is somewhat less severe in our hands. DCs deficient for both HS1 and WASp were indistinguishable from cells deficient for WASp alone. We next compared the effects of loss of HS1 or WASp with respect to podosome organization. As shown in the filled bars in Fig. 5.7C, $HS1^{-/-}$ DCs showed defective packing of the podosome array, but this phenotype was not observed in WASp-deficient cells. Podosome packing in DCs deficient in both HS1 and WASp was indistinguishable from packing in cells lacking HS1 alone. Taken together, these results show that WASp is required for efficient formation of podosomes, while HS1 is important for organizing the podosome array.

To confirm these findings, and to ask if HS1 and WASp show interdependent function, DCs lacking these proteins individually or together were transduced with WASp, HS1, or with an HS1 SH3 domain mutant (W465Y) that abrogates interaction between the two proteins. As shown in Fig. 5.7B (hatched bars), ectopic expression of WASp in either $WASP^{-/y}$ or double-deficient DCs restores the number of cells displaying podosomes to WT levels. In contrast, expression of HS1 (gray bar) in double deficient DCs does not rescue this defect, supporting the idea that WASp, but not HS1, is essential for efficient podosome formation. Expression of the SH3 domain mutant (open bar) actually suppressed podosome formation somewhat when expressed in $HS1^{-/-}$ DCs, which may represent a mild dominant negative effect of this mutant.

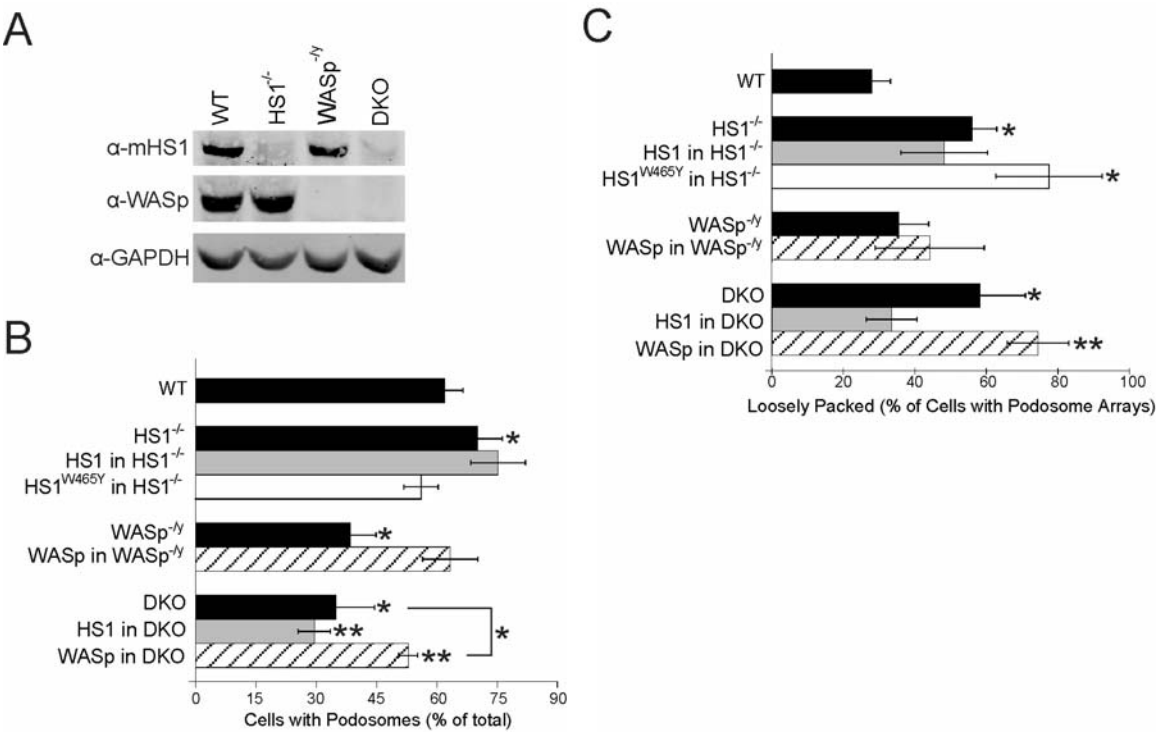

Figure 5.7. HS1 and WASp cooperate to form organized podosome arrays. A. BMDCs were cultured from WT, HS1$^{-/-}$, WASp$^{-/y}$ or HS1$^{-/-}$ WASp$^{-/y}$ (DKO) mice, and whole cell lysates were analyzed by immunoblotting with anti-HS1 or anti-WASp antibodies. GAPDH was used to verify equal loading. B and C. WT, HS1$^{-/-}$, WASp$^{-/y}$ or DKO cells were untransduced or transduced with Venus-HS1 (HS1$^{-/-}$ and DKO, gray), GFP-WASp (WASp$^{-/y}$ and DKO, hatched) or Venus-HS1^{W465Y} (HS1$^{-/-}$, white) and prepared as in figure 5.3A. Cells were scored for the presence of podosomes (B) and array organization in cells containing podosomes (C) as described in Materials and Methods. (*$p<0.05$; **$p<0.01$)

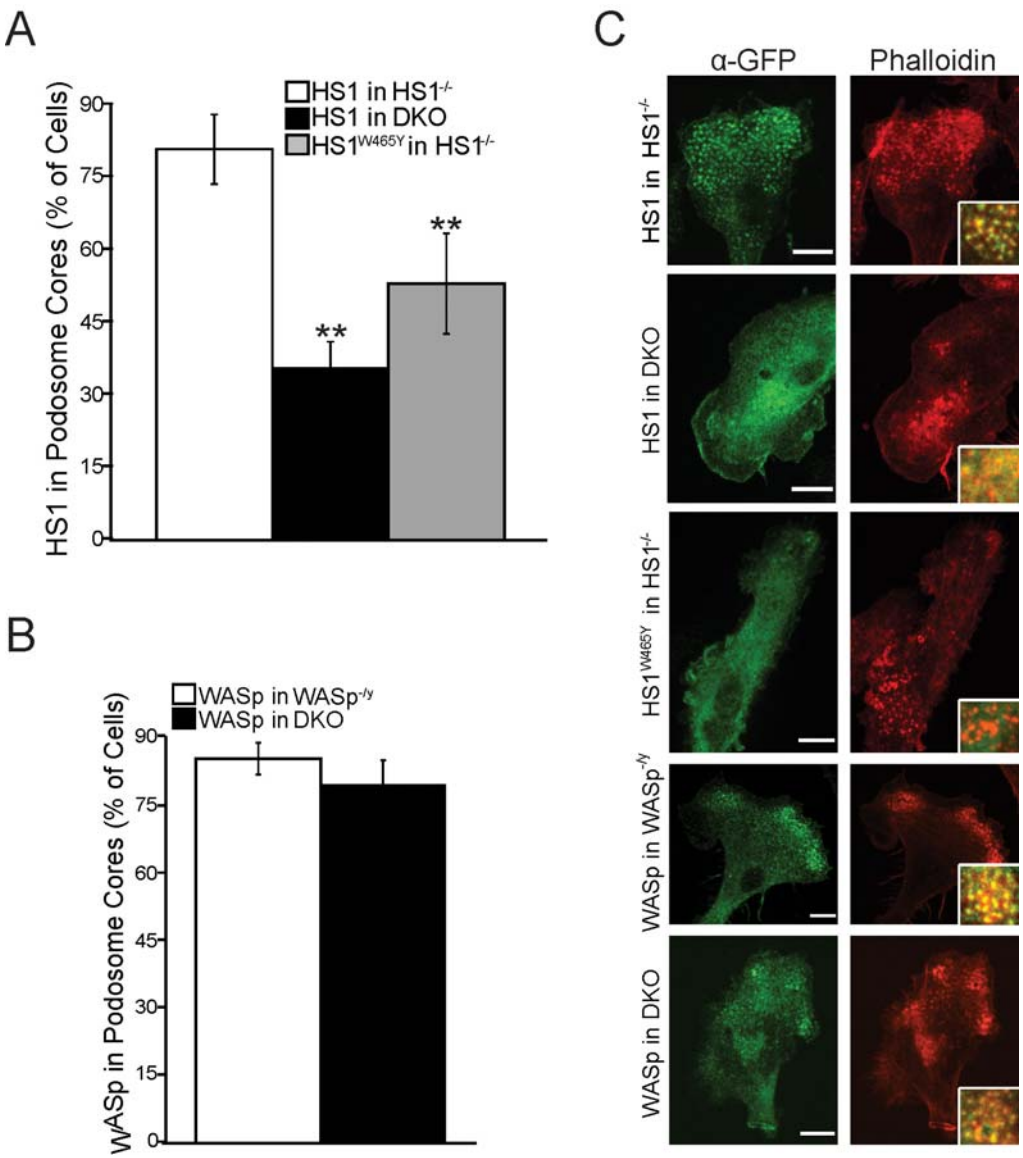

Figure 5.8. HS1 requires WASp for localization to podosome cores, but WASp localizes independently of HS1. $HS1^{-/-}$, $WASp^{-/y}$ or DKO cells were untransduced or transduced with Venus-HS1 ($HS1^{-/-}$ and DKO), GFP-WASp ($WASp^{-/y}$ and DKO) or Venus-$HS1^{W465Y}$ ($HS1^{-/-}$). Cells were prepared as in figure 5.3A, but staining with anti-GFP to visualize the transduced proteins. A. Cells were scored for the presence of HS1 in podosome cores as described in Materials and Methods. (**$p<0.05$) B. Cells were scored for the presence of WASp in podosome cores as described in Materials and Methods. C. Colocalization of HS1 or WASp with phalloidin staining in podosomes cores was visualized by confocal microscopy. Scale bars equal 10 μm.

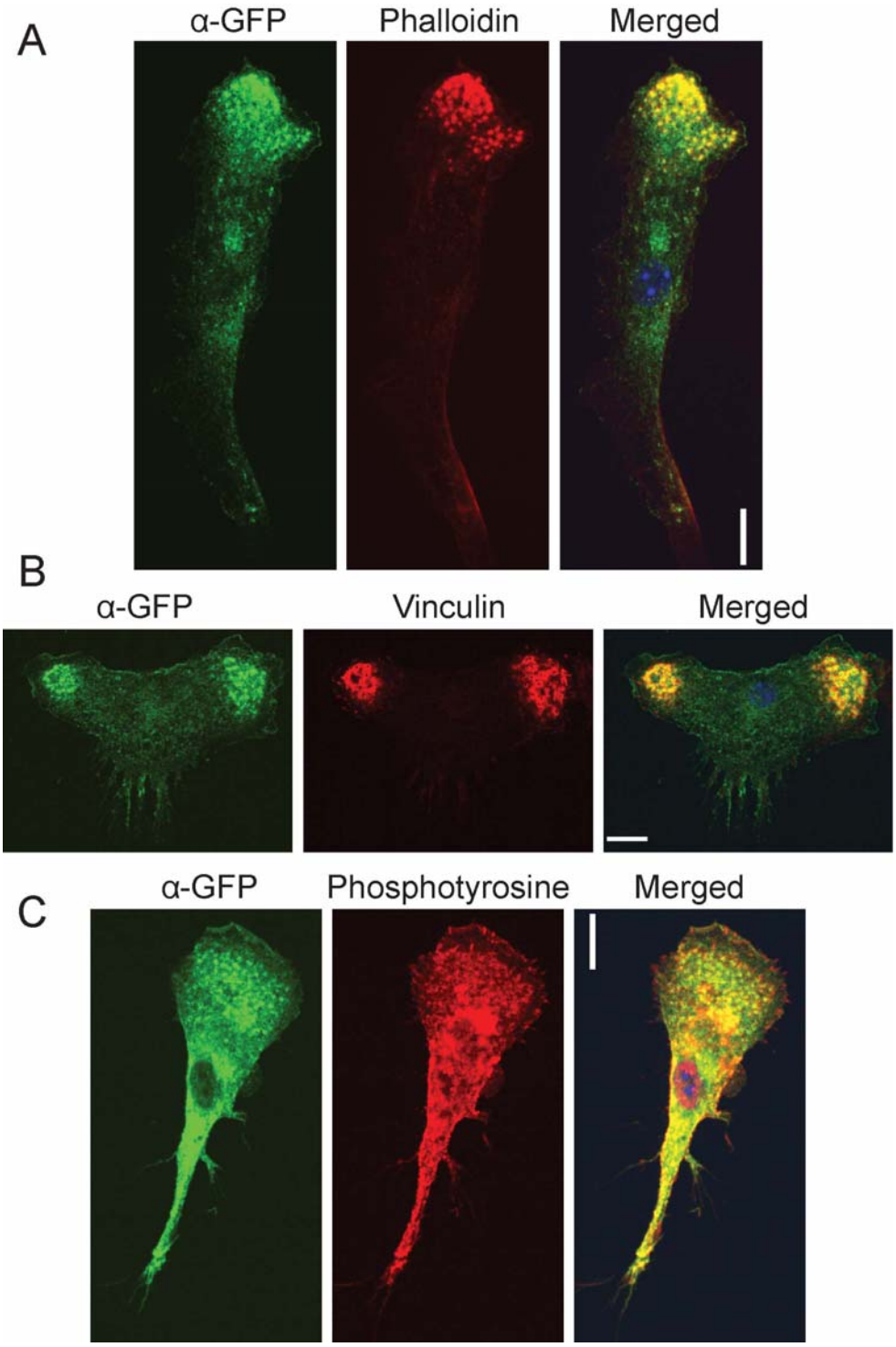

Figure 5.9. HS1 colocalizes with phosphotyrosine and is surrounded by vinculin in podosomes. Cells were prepared as in Figure 5.2. Cells were stained with anti-GFP (green) and anti-vinculin (red, A) or anti-phosphotyrosine (red, B). DAPI (blue) was used to identify nuclei. Scale bars equal 10 μm.

When transduced DCs were analyzed with respect to podosome packing, reciprocal results were obtained (Fig 5.7C). The abnormally loose packing observed in HS1$^{-/-}$ DCs and double knockout cells was rescued by ectopic expression of HS1 (gray bars). Expression of GFP-WASp (hatched bar) in double knockout DCs did not rescue this defect, supporting the idea that HS1, but not WASp, is needed to organize a closely packed podosome array. Interestingly, the HS1 SH3 domain mutant (open bar) was unable to rescue podosome organization in HS1$^{-/-}$ DCs, suggesting that HS1 must interact with WASp to carry out its function.

Recruitment of HS1 to podosomes is dependent on interactions with WASp

To complement our functional analysis of HS1 and WASp interactions, we asked if these proteins depend on one another for recruitment to podosomes and function in podosome formation/organization. As shown in Fig. 5.8A and C, Venus-HS1 localized efficiently to podosomes cores when expressed in HS1$^{-/-}$ DCs. Venus-HS1 colocalized with F-actin and phosphotyrosine within vinculin rings (Fig. 5.9). In double knockout DCs, however, Venus-HS1 localization to podosome cores was faint or nonexistent, and the protein instead exhibited a diffuse cytoplasmic distribution (Fig. 5.8A and C). Similar results were obtained when the SH3 domain mutant of HS1 was expressed in HS1$^{-/-}$ DCs. As shown in Fig. 5.8B and C, WASp localized efficiently to the podosome core when expressed in either WASp$^{-/y}$ or double knockout cells. Taken together, these results indicate that WASp localization to podosome cores is independent of HS1, but HS1

localization to podosome cores depends on SH3-domain mediated interactions with WASp.

HS1$^{-/-}$ DCs exhibit defects in directional migration

Podosomes are thought to promote cell migration in some settings, and WASp$^{-/y}$ DCs are defective in migration (11, 13, 53). We therefore asked if HS1 is also required for DC migration. Initial studies were performed using transwell assays. As reported previously (54), immature and mature BMDCs from WT mice preferentially migrated toward CXCL12 (SDF1α) and CCL21 (SLC), respectively (Fig. 5.10A and B). HS1$^{-/-}$ DCs migrated with the same efficiency as DCs from WT mice, and showed the same switch in chemokine sensitivity with maturation. Furthermore, WT and HS1$^{-/-}$ DCs exhibited similar sensitivity in chemokine dose response studies, and flow cytometry analysis showed that these two populations express similar surface levels of chemokine receptors (data not shown). We next used video microscopy to compare the ability of WT, HS1$^{-/-}$, WASp$^{-/y}$ and double knockout DCs to undergo chemotaxis in a gradient of CCL19. As shown in Fig 5.10C and D, HS1$^{-/-}$ DCs moved significantly faster than WT DCs, while WASp$^{-/y}$ DCs and double knockout cells moved significantly slower. Analysis of directionality revealed HS1$^{-/-}$ DCs exhibit diminished directional persistence (chemotactic index) (Fig 5.10C and E). The magnitude of this defect was greater in WASp$^{-/y}$ and double knockout DCs, but all three mutants were significantly less persistent that WT DCs. Taken together, these data show that while WASp is required for DC migration *per se*, HS1 is primarily important for persistent directional migration.

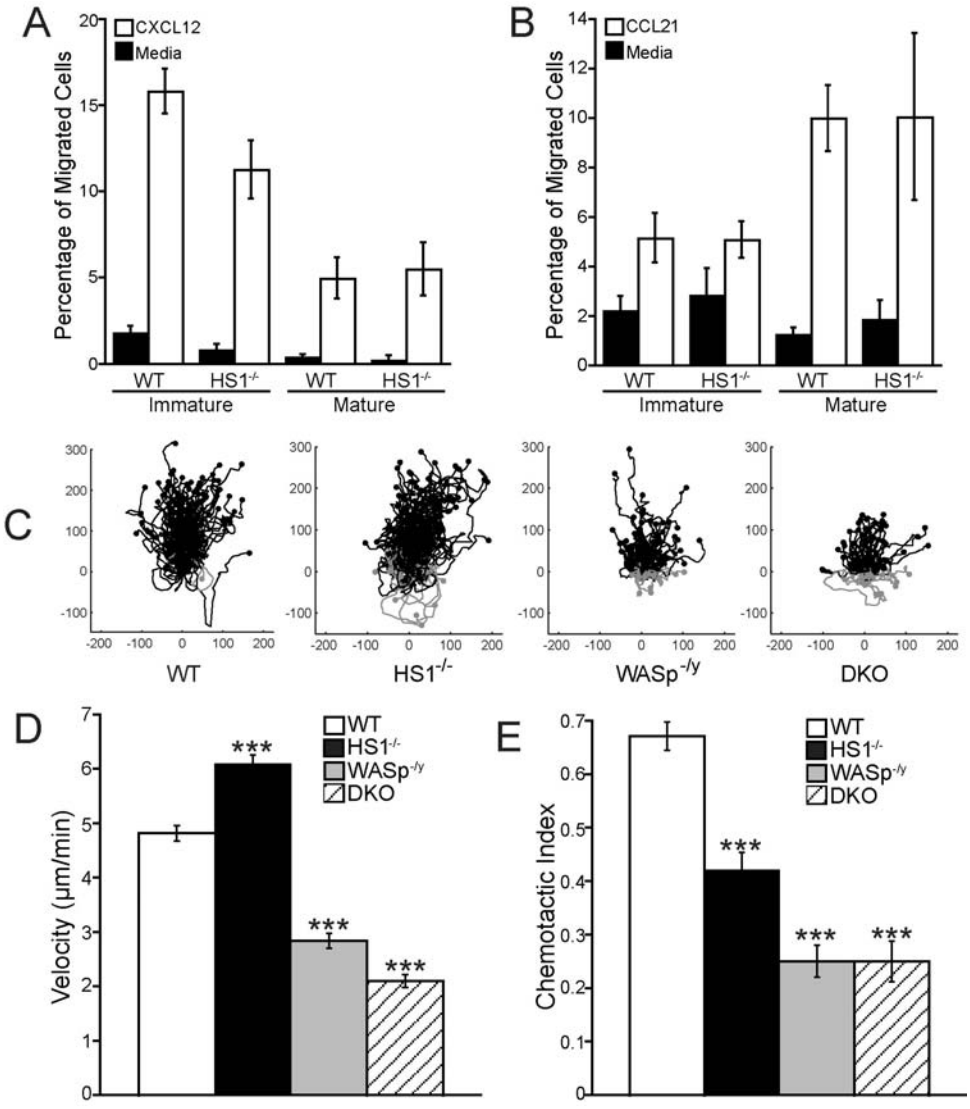

Figure 5.10. HS1$^{-/-}$ BMDCs show altered migration in a chemokine gradient. A and B. WT and HS1$^{-/-}$ BMDCs were treated with 100 ng/ml LPS (Mature) or left untreated (Immature). Migration toward media alone or media containing CXCL12 (SDF1α, C) or SLC (CCL21, D) was assessed by transwell assay. Data are averages of replicates from one representative experiment (of 4), +/- StDev. C, D and E. WT, HS1$^{-/-}$, WASp$^{-/y}$ or DKO BMDCs were injected into a fibronectin-coated microfluidic chamber with a gradient of CCL19 (0-20 nM) (C). The average velocity of motile cells in the direction of the gradient was determined (D). The chemotactic index, as defined by the distance migrated toward the chemokine source divided by the absolute distance traveled for each cell was calculated (E). Data represent averages of multiple cells from one representative experiment +/- SEM. (***p<0.00001)

Discussion

Our analysis of HS1-deficient DCs revealed two related defects, disorganization of the podosome array and diminished directional migration. WASp, which interacts with HS1, also affects podosomes and migration, but our analysis shows that the roles of these two proteins are distinct. It is well established that WASp and its obligate binding partner WIP are essential for formation of the actin-rich cores that nucleate podosome biogenesis (10, 14-16, 23, 55-59). (18, 60). Depending on the experimental system, WASp-deficient DC and macrophages ether lack podosomes altogether or show severe reductions in podosome numbers, and our data are consistent with this. In contrast, we find that HS1-deficient DCs and macrophages can form podosomes containing many, if not all, of the characteristic components. However, HS1-deficient cells show disordered podosome array packing and mislocalization of the arrays with respect to the leading edge of the cell.

The mechanisms through which HS1 controls podosome organization are unclear. Since HS1 stabilizes branched-actin filaments generated by WASp and other Arp2/3 complex activators, it seems likely that it stabilizes actin filaments within podosomes. While our FRAP data show that HS1 does not affect actin exchange in mature podosomes, it does accelerate podosome re-formation. Thus, HS1 may stabilize newly-formed actin cores, and the diminished numbers and loose packing of podosomes in HS1-deficient cells may result from stochastic disassembly of newly-formed podosome cores. Another appealing possibility is that HS1 aids in stabilizing the long actin filaments that form connections

between adjacent podosomes (61). Interestingly, these interconnecting filaments are frequently decorated with clathrin coated endocytic pits (61), and the HS1 homologue cortactin associates with coated vesicle components (26). Finally, it should be noted that in addition to directly regulating actin dynamics, HS1 functions as an adapter molecule, and can recruit other signaling molecules to sites of actin polymerization (35-36). We show here that HS1 is not needed for recruitment of WASp to podosomes, but HS1 could recruit Vav1 or PLCγ, proteins that are important regulators of podosome dynamics and directional persistence in dendritic cells (21, 62).

In addition to directly affecting F-actin dynamics in podosomes, HS1 may promote podosome organization indirectly, via effects on lamellipodial dynamics. HS1 localizes to lamellipodial edges in DCs, and it regulates lamellipodial protrusion in T cells (35-36). Moreover, cortactin regulates lamellipodial protrusion and retraction in non-hematopoietic cells (Bryce 2005, Krueger 2003). Since forward movement of the DC lamellipodium is closely linked to the cycle of podosome formation and dissolution (10, 14, 23, 56, 60), erratic leading edge dynamics in HS1-deficient DCs could result in disorganization of the podosome array. Indeed, this seems the likeliest mechanism to create the observed mislocalization of the array with respect to the leading edge of the cell.

The importance of HS1 function in podosomes and at the leading edge of the cell are demonstrated by the diminished ability of $HS1^{-/-}$ DCs to undergo directional chemotaxis. Here, too, the phenotypes of $HS1^{-/-}$ and $WASp^{-/y}$ DCs are related, but distinct. In keeping

with the literature (11, 13, 53), we found that WASp expression is essential for DC migration. $WASp^{-/y}$ DCs migrating in a chemokine gradient showed a large decrease in velocity, and those cells that did migrate exhibited diminished directional persistence. In contrast, HS1 deficient DCs actually migrated faster than wild type cells, but directional persistence was significantly reduced. The defects in directional persistence in $HS1^{-/-}$ cells may reflect defects in lamellipodial dynamics. Indeed, we observed an increase in cells showing multiple leading edges in the $HS1^{-/-}$ population, though this did not reach statistical significance. Alternatively, the defects in directional persistence may reflect the role of podosomes in stabilizing a dominant leading edge (14, 16, 52). In this scenario, HS1 would function to fine-tune the packing and localization of podosomes formed by WASp to aid the stabilization of the leading edge, promoting efficient directional cell migration. These two possibilities are not mutually exclusive, and in fact are likely to represent intertwined aspects of HS1 function.

All of our data point to a hierarchical relationship between WASp and HS1 in controlling DC actin dynamics. WASp localized to podosomes independently of HS1, but HS1 was not recruited efficiently to podosomes in the absence of WASp, or if its WASp-interacting SH3 domain was mutated. This indicates that HS1 is recruited to podosomes through SH3-domain-dependent interactions with WASp. Functional studies also support the view that WASp functions upstream of HS1 in this system. In cells lacking both proteins, the defects in both cell morphology and chemotaxis are indistinguishable from cells deficient for WASp alone. Interestingly, even though HS1 localization to podosomes is largely dependent on WASp, the cells that do form podosomes in the

absence of WASp show tightly packed arrays if HS1 is expressed. This may reflect WASp-independent HS1 function at the leading edge. Alternatively, it may reflect the ability of HS1 to interact weakly with podosomes by binding to F-actin. Evidence that such binding occurs is shown by the moderately enhanced podosome localization of the HS1 SH3 domain mutant in WASp-sufficient cells as compared with wildtype HS1 in $WASp^{-/y}$ DCs (Fig 5.8A).

The mild podosome phenotype we observe in $HS1^{-/-}$ DCs is somewhat surprising given that cortactin is essential for formation of invadopodia in metastatic tumor cells (63-64). While we cannot exclude the possibility that $HS1^{-/-}$ mice undergo compensatory developmental changes that blunt the DC phenotype, we deem this unlikely because we found no upregulation of WASp or cortactin, and because similar defects were observed with HS1 shRNA in a macrophage cell line. A more likely possibility is that HS1 and cortactin are functionally distinct, and that podosomes and invadopodia differ with respect to these two proteins. In keeping with this idea, cortactin has recently been found to be required for matrix metalloproteinase release at invadopodia (65), whereas we find that HS1 is not. Interestingly, cortactin is required for formation of podosomes in osteoclasts, which express both HS1 and cortactin (66). While this may represent an excepction to the podosome/invadopodium distinction, osteoclasts podosomes play an important role in matrix degradation, and in this sense may be more like invadopodia. Regardless of terminology, it seems that the HS1 may be important for adhesive contacts, and cortactin for contacts engaged in matrix degradation. It will be interesting to test this idea using 'rescuing' HS1-/- cells with cortactin, and *vice versa*.

The relationship between HS1 and WASp defined here is also somewhat different from the relationship between cortactin and N-WASp in other cell types. While we find that WASp recruits HS1 to podosomes, cortactin has been shown to recruit and N-WASp activity at sites of actin polymerization (67-68). Phosphorylation of cortactin has been shown to play an important role in its ability to regulate N-WASP (37-38, 63, 69). Phosphorylation of HS1 is important for its actin-regulatory function in T cells and NK cells (35, 40), but its role in DCs remains to be explored.

An important open question in this field is the extent to which podosomes are important for DC function *in vivo*. $WASP^{-/y}$ DCs have significant migration defects *in vivo*, but it is unclear to what extent this reflects a requirement for podosome formation. It has long been assumed that podosomes are sites for integrin-dependent adhesion to the extracellular matrix, but the importance of integrins in regulating DC migration is complex and highly dependent on environmental cues (4-5, 70-71). In this context, an appealing possibility is that these structures are important as mechanosensors, to allow DCs to adapt to movement along variable surfaces (9, 20, 72). Finally, since podosomes are most prominent in immature DCs, these structures may a play an important role in maintaining cell anchorage and/or dynamics of dendritic processes in peripheral tissues. By identifying and characterizing individual proteins that control distinct aspects of podosome function, we will have a better understanding of whether and how these structures contribute to the regulation of DC movements during an *in vivo* immune response.

References

1. Banchereau J, *et al.* (2000) Immunobiology of dendritic cells. *Annu Rev Immunol* 18:767-811.
2. Trombetta ES & Mellman I (2005) Cell biology of antigen processing in vitro and in vivo. *Annu Rev Immunol* 23:975-1028.
3. Alvarez D, Vollmann EH, & von Andrian UH (2008) Mechanisms and consequences of dendritic cell migration. (Translated from eng) *Immunity* 29(3):325-342 (in eng).
4. Lammermann T, *et al.* (2008) Rapid leukocyte migration by integrin-independent flowing and squeezing. (Translated from eng) *Nature* 453(7191):51-55 (in eng).
5. Renkawitz J, *et al.* (2009) Adaptive force transmission in amoeboid cell migration. (Translated from eng) *Nat Cell Biol* 11(12):1438-1443 (in eng).
6. Gimona M, Buccione R, Courtneidge SA, & Linder S (2008) Assembly and biological role of podosomes and invadopodia. *Curr Opin Cell Biol* 20(2):235-241.
7. Linder S & Kopp P (2005) Podosomes at a glance. *J Cell Sci* 118(Pt 10):2079-2082.
8. Linder S & Aepfelbacher M (2003) Podosomes: adhesion hot-spots of invasive cells. (Translated from eng) *Trends Cell Biol* 13(7):376-385 (in eng).
9. Albiges-Rizo C, Destaing O, Fourcade B, Planus E, & Block MR (2009) Actin machinery and mechanosensitivity in invadopodia, podosomes and focal adhesions. (Translated from eng) *J Cell Sci* 122(Pt 17):3037-3049 (in eng).
10. Burns S, Thrasher AJ, Blundell MP, Machesky L, & Jones GE (2001) Configuration of human dendritic cell cytoskeleton by Rho GTPases, the WAS protein, and differentiation. (Translated from eng) *Blood* 98(4):1142-1149 (in eng).
11. Snapper SB, *et al.* (2005) WASP deficiency leads to global defects of directed leukocyte migration in vitro and in vivo. *J Leukoc Biol* 77(6):993-998.
12. Curcio C, *et al.* (2007) WIP null mice display a progressive immunological disorder that resembles Wiskott-Aldrich syndrome. (Translated from eng) *J Pathol* 211(1):67-75 (in eng).
13. de Noronha S, *et al.* (2005) Impaired dendritic-cell homing in vivo in the absence of Wiskott-Aldrich syndrome protein. *Blood* 105(4):1590-1597.

14. Monypenny J, *et al.* (2010) Role of WASP in cell polarity and podosome dynamics of myeloid cells. (Translated from Eng) *Eur J Cell Biol* (in Eng).

15. Calle Y, Chou HC, Thrasher AJ, & Jones GE (2004) Wiskott-Aldrich syndrome protein and the cytoskeletal dynamics of dendritic cells. *J Pathol* 204(4):460-469.

16. Chou HC, *et al.* (2006) WIP regulates the stability and localization of WASP to podosomes in migrating dendritic cells. *Curr Biol* 16(23):2337-2344.

17. Linder S, Nelson D, Weiss M, & Aepfelbacher M (1999) Wiskott-Aldrich syndrome protein regulates podosomes in primary human macrophages. (Translated from eng) *Proc Natl Acad Sci U S A* 96(17):9648-9653 (in eng).

18. Dovas A, *et al.* (2009) Regulation of podosome dynamics by WASp phosphorylation: implication in matrix degradation and chemotaxis in macrophages. (Translated from eng) *J Cell Sci* 122(Pt 21):3873-3882 (in eng).

19. Goley ED & Welch MD (2006) The ARP2/3 complex: an actin nucleator comes of age. *Nat Rev Mol Cell Biol* 7(10):713-726.

20. Lammermann T, *et al.* (2009) Cdc42-dependent leading edge coordination is essential for interstitial dendritic cell migration. (Translated from eng) *Blood* 113(23):5703-5710 (in eng).

21. Spurrell DR, *et al.* (2009) Vav1 regulates the migration and adhesion of dendritic cells. (Translated from eng) *J Immunol* 183(1):310-318 (in eng).

22. Destaing O, Saltel F, Geminard JC, Jurdic P, & Bard F (2003) Podosomes display actin turnover and dynamic self-organization in osteoclasts expressing actin-green fluorescent protein. (Translated from eng) *Mol Biol Cell* 14(2):407-416 (in eng).

23. Calle Y, Carragher NO, Thrasher AJ, & Jones GE (2006) Inhibition of calpain stabilises podosomes and impairs dendritic cell motility. (Translated from eng) *J Cell Sci* 119(Pt 11):2375-2385 (in eng).

24. Takemoto Y, Furuta M, Li XK, Strong-Sparks WJ, & Hashimoto Y (1995) LckBP1, a proline-rich protein expressed in haematopoietic lineage cells, directly associates with the SH3 domain of protein tyrosine kinase p56lck. (Translated from eng) *EMBO J* 14(14):3403-3414 (in eng).

25. Bryce NS, *et al.* (2005) Cortactin promotes cell motility by enhancing lamellipodial persistence. *Curr Biol* 15(14):1276-1285.

26. Cao H, *et al.* (2003) Cortactin is a component of clathrin-coated pits and participates in receptor-mediated endocytosis. *Mol Cell Biol* 23(6):2162-2170.

27. van Rossum AG, Moolenaar WH, & Schuuring E (2006) Cortactin affects cell migration by regulating intercellular adhesion and cell spreading. (Translated from eng) *Exp Cell Res* 312(9):1658-1670 (in eng).

28. Lai FP, *et al.* (2009) Cortactin promotes migration and platelet-derived growth factor-induced actin reorganization by signaling to Rho-GTPases. (Translated from eng) *Mol Biol Cell* 20(14):3209-3223 (in eng).

29. Weaver AM (2008) Cortactin in tumor invasiveness. (Translated from eng) *Cancer Lett* 265(2):157-166 (in eng).

30. Buday L & Downward J (2007) Roles of cortactin in tumor pathogenesis. *Biochim Biophys Acta* 1775(2):263-273.

31. Artym VV, Matsumoto K, Mueller SC, & Yamada KM (2010) Dynamic membrane remodeling at invadopodia differentiates invadopodia from podosomes. (Translated from Eng) *Eur J Cell Biol* (in Eng).

32. Weed SA, *et al.* (2000) Cortactin localization to sites of actin assembly in lamellipodia requires interactions with F-actin and the Arp2/3 complex. (Translated from eng) *J Cell Biol* 151(1):29-40 (in eng).

33. Higgs H (2001) Branching out: cortactin stabilizes actin networks generated by the Arp2/3 complex. (Translated from eng) *Trends Biochem Sci* 26(4):219 (in eng).

34. Uruno T, Zhang P, Liu J, Hao JJ, & Zhan X (2003) Haematopoietic lineage cell-specific protein 1 (HS1) promotes actin-related protein (Arp) 2/3 complex-mediated actin polymerization. *Biochem J* 371(Pt 2):485-493.

35. Gomez TS, *et al.* (2006) HS1 functions as an essential actin-regulatory adaptor protein at the immune synapse. *Immunity* 24(6):741-752.

36. Carrizosa E*, et al.* (2009) Hematopoietic lineage cell-specific protein 1 is recruited to the immunological synapse by IL-2-inducible T cell kinase and regulates phospholipase Cgamma1 Microcluster dynamics during T cell spreading. (Translated from eng) *J Immunol* 183(11):7352-7361 (in eng).

37. Martinez-Quiles N, Ho HY, Kirschner MW, Ramesh N, & Geha RS (2004) Erk/Src phosphorylation of cortactin acts as a switch on-switch off mechanism that controls its ability to activate N-WASP. *Mol Cell Biol* 24(12):5269-5280.

38. Tehrani S, Tomasevic N, Weed S, Sakowicz R, & Cooper JA (2007) Src phosphorylation of cortactin enhances actin assembly. *Proc Natl Acad Sci U S A* 104(29):11933-11938.

39. Scielzo C*, et al.* (2010) HS1 has a central role in the trafficking and homing of leukemic B cells. (Translated from Eng) *Blood* (in Eng).

40. Butler B, Kastendieck DH, & Cooper JA (2008) Differently phosphorylated forms of the cortactin homolog HS1 mediate distinct functions in natural killer cells. (Translated from eng) *Nat Immunol* 9(8):887-897 (in eng).

41. Huang Y*, et al.* (2008) The c-Abl tyrosine kinase regulates actin remodeling at the immune synapse. *Blood* 112(1):111-119.

42. Taniuchi I*, et al.* (1995) Antigen-receptor induced clonal expansion and deletion of lymphocytes are impaired in mice lacking HS1 protein, a substrate of the antigen-receptor-coupled tyrosine kinases. (Translated from eng) *EMBO J* 14(15):3664-3678 (in eng).

43. Nagai T*, et al.* (2002) A variant of yellow fluorescent protein with fast and efficient maturation for cell-biological applications. (Translated from eng) *Nat Biotechnol* 20(1):87-90 (in eng).

44. Herzog M, Draeger A, Ehler E, & Small VJ (1994) Immunofluorescence microscopy of the cytoskeleton: double and triple immunofluorescence. *Cell Biology: a Laboratory Handbook*, ed Celis JE (Harcourt Brace and Company, San Diego, CA), Vol 2, pp 355-360.

45. Bowden ET, Coopman PJ, & Mueller SC (2001) Invadopodia: unique methods for measurement of extracellular matrix degradation in vitro. (Translated from eng) *Methods Cell Biol* 63:613-627 (in eng).

46. Jannat RA, Dembo M, & Hammer DA (2010) Neutrophil adhesion and chemotaxis depend on substrate mechanics. (Translated from Eng) *J Phys Condens Matter* 22(19):194117 (in Eng).

47. Matheu MP, Sen D, Cahalan MD, & Parker I (2008) Generation of bone marrow derived murine dendritic cells for use in 2-photon imaging. (Translated from eng) *J Vis Exp* (17) (in eng).

48. Quast T, *et al.* (2009) Cytohesin-1 controls the activation of RhoA and modulates integrin-dependent adhesion and migration of dendritic cells. (Translated from eng) *Blood* 113(23):5801-5810 (in eng).

49. Ammer AG & Weed SA (2008) Cortactin branches out: roles in regulating protrusive actin dynamics. (Translated from eng) *Cell Motil Cytoskeleton* 65(9):687-707 (in eng).

50. Linder S (2007) The matrix corroded: podosomes and invadopodia in extracellular matrix degradation. (Translated from eng) *Trends Cell Biol* 17(3):107-117 (in eng).

51. Isaac BM, *et al.* (2010) N-WASP has the ability to compensate for the loss of WASP in macrophage podosome formation and chemotaxis. (Translated from Eng) *Exp Cell Res* (in Eng).

52. Burns S, *et al.* (2004) Maturation of DC is associated with changes in motile characteristics and adherence. *Cell Motil Cytoskeleton* 57(2):118-132.

53. Bouma G, Burns S, & Thrasher AJ (2007) Impaired T-cell priming in vivo resulting from dysfunction of WASp-deficient dendritic cells. (Translated from eng) *Blood* 110(13):4278-4284 (in eng).

54. Vecchi A, *et al.* (1999) Differential responsiveness to constitutive vs. inducible chemokines of immature and mature mouse dendritic cells. (Translated from eng) *J Leukoc Biol* 66(3):489-494 (in eng).

55. Charrier S, *et al.* (2005) A lentiviral vector encoding the human Wiskott-Aldrich syndrome protein corrects immune and cytoskeletal defects in WASP knockout mice. (Translated from eng) *Gene Ther* 12(7):597-606 (in eng).

56. Jones GE, Zicha D, Dunn GA, Blundell M, & Thrasher A (2002) Restoration of podosomes and chemotaxis in Wiskott-Aldrich syndrome macrophages following induced expression of WASp. (Translated from eng) *Int J Biochem Cell Biol* 34(7):806-815 (in eng).

57. Tsuboi S (2007) Requirement for a complex of Wiskott-Aldrich syndrome protein (WASP) with WASP interacting protein in podosome formation in macrophages. (Translated from eng) *J Immunol* 178(5):2987-2995 (in eng).

58. Olivier A, *et al.* (2006) A partial down-regulation of WASP is sufficient to inhibit podosome formation in dendritic cells. (Translated from eng) *Mol Ther* 13(4):729-737 (in eng).

59. Calle Y, *et al.* (2004) WASp deficiency in mice results in failure to form osteoclast sealing zones and defects in bone resorption. (Translated from eng) *Blood* 103(9):3552-3561 (in eng).

60. Linder S, *et al.* (2000) The polarization defect of Wiskott-Aldrich syndrome macrophages is linked to dislocalization of the Arp2/3 complex. (Translated from eng) *J Immunol* 165(1):221-225 (in eng).

61. Akisaka T, Yoshida H, Suzuki R, & Takama K (2008) Adhesion structures and their cytoskeleton-membrane interactions at podosomes of osteoclasts in culture. (Translated from eng) *Cell Tissue Res* 331(3):625-641 (in eng).

62. Cremasco V, *et al.* (2010) Phospholipase C gamma 2 is critical for development of a murine model of inflammatory arthritis by affecting actin dynamics in dendritic cells. (Translated from eng) *PLoS One* 5(1):e8909 (in eng).

63. Oser M, *et al.* (2009) Cortactin regulates cofilin and N-WASp activities to control the stages of invadopodium assembly and maturation. (Translated from eng) *J Cell Biol* 186(4):571-587 (in eng).

64. Artym VV, Zhang Y, Seillier-Moiseiwitsch F, Yamada KM, & Mueller SC (2006) Dynamic interactions of cortactin and membrane type 1 matrix metalloproteinase at invadopodia: defining the stages of invadopodia formation and function. (Translated from eng) *Cancer Res* 66(6):3034-3043 (in eng).

65. Clark ES & Weaver AM (2008) A new role for cortactin in invadopodia: regulation of protease secretion. (Translated from eng) *Eur J Cell Biol* 87(8-9):581-590 (in eng).

66. Tehrani S, Faccio R, Chandrasekar I, Ross FP, & Cooper JA (2006) Cortactin has an essential and specific role in osteoclast actin assembly. (Translated from eng) *Mol Biol Cell* 17(7):2882-2895 (in eng).

67. Kowalski JR*, et al.* (2005) Cortactin regulates cell migration through activation of N-WASP. (Translated from eng) *J Cell Sci* 118(Pt 1):79-87 (in eng).

68. Kempiak SJ*, et al.* (2005) A neural Wiskott-Aldrich Syndrome protein-mediated pathway for localized activation of actin polymerization that is regulated by cortactin. (Translated from eng) *J Biol Chem* 280(7):5836-5842 (in eng).

69. Grassart A, Dujeancourt A, Lazarow PB, Dautry-Varsat A, & Sauvonnet N (2008) Clathrin-independent endocytosis used by the IL-2 receptor is regulated by Rac1, Pak1 and Pak2. (Translated from eng) *EMBO Rep* 9(4):356-362 (in eng).

70. Jain P, Coisne C, Enzmann G, Rottapel R, & Engelhardt B (2010) Alpha4beta1 integrin mediates the recruitment of immature dendritic cells across the blood-brain barrier during experimental autoimmune encephalomyelitis. (Translated from eng) *J Immunol* 184(12):7196-7206 (in eng).

71. Schumann K*, et al.* (2010) Immobilized chemokine fields and soluble chemokine gradients cooperatively shape migration patterns of dendritic cells. (Translated from eng) *Immunity* 32(5):703-713 (in eng).

72. Collin O*, et al.* (2008) Self-organized podosomes are dynamic mechanosensors. (Translated from eng) *Curr Biol* 18(17):1288-1294 (in eng).

Chapter 6: Measuring Dendritic Cell Traction Forces on Micropost Arrays

Adapted from: **Measuring Dendritic Cell Traction Forces on Micropost Arrays**

Brendon G. Ricart, Michael T. Yang, Christopher A. Hunter, Christopher S. Chen, and Daniel A. Hammer

In Preparation

Abstract

Dendritic cells (DCs) migrate from sites of inflammation to secondary lymphoid organs where they initiate the adaptive immune response. While motility is essential to DC function, the mode or mechanism of their migration is not fully understood. We used a combination of micropost array detectors and a microfluidic gradient generator to develop a novel method for probing traction force of murine DCs during directional migration. We find DCs migration is driven by short-lived traction stresses at the leading edge or filopodia. The magnitude (r.m.s. traction forces) of DCs are smaller in magnitude than found in neutrophils, and similar during chemotaxis and chemokinesis, at 18 +/- 1.4 and 16 +/- 1.3 nN/cell, respectively. Maximal stress in the cell occurs perpendicular to the axis of motion, forward of the centroid. We illustrate that spatiotemporal pattern of traction stresses can be used to predict changes in the direction of DC motion. Additionally, we determine the characteristic duration of local dendritic cell traction forces in the presence of inhibitors. Blocking chemokine signaling with pertussis toxin led to random motion in a chemokine gradient; traction forces were similar to that during chemokinesis even in a chemokine gradient. Overall, DCs show a mode of migration distinct from both mesenchymal cells and neutrophils, characterized by rapid turnover of traction forces in leading filopodia.

Introduction

Dendritic cells must navigate a series of varied microenvironments to move from sites of pathogen entry to lymph nodes where they orchestrate the adaptive immune response (1). Several recent studies have shed light on the mechanics of DC migration (2), though none have measured the traction forces of these cells. DCs were shown to be chemotactic toward soluble CCL19 and bound CCL21 (3), use actin polymerization and myosin contraction for locomotion (4), and readily adaptable to migration on adhesive and non-adhesive substrates (5).

Amoeboid cells are rapidly crawling cells thought to exert small forces. These cells are central to the functioning of the immune system, and elucidating the molecular mechanisms of directional control and force generation in these cells would be key to manipulating directional homing in the immune system. There is a diversity of modes of motility, even within the narrow family of amoeboid cell. Although the actin/myosin-based modules for cell migration are highly conserved within all cells, various cell types use different molecular signals to spatiotemporally organize this machinery. For example, PI3K is essential for neutophil polarization and migration (6), but dispensible for DC motility (7), where CDC-42 is important for regulating the leading edge (8). Myosin II is required for contractility in all cell types, but its upstream regulator Rho may be differentially regulated (9). Additionally, cells may place varying emphasis on contractility, protrusion and adhesion during migration (2, 10). Contractility and protrusion are purely intracellular processes mainly driven by actin/myosin interactions, while adhesion involves linkage to extracellular matrix.

Lammermann and coworkers have shown that DCs are capable of migrating in the absence of integrins (4). While this result is truly remarkable, subsequent studies have shown that there are substantial differences in migration when integrins are present (3, 11), and that TNF-α activated DCs employ a β_2 integrin-dependent mode of transmigration through lymphatic endothelium (12). Bone marrow DCs are able to adhere to fibronectin, but not collagen (Figure 3.7), possibly because they express the α_5, α_V and β_2 integrin subunits (4) for binding fibronectin (13), but not the α_1, α_2, or α_{11} subunits required for binding collagen.

Amoeboid cells are capable of transmitting force to substrates. In *Dictyostelium*, a well-studied model, forces are strongest at the contractile rear and weaker at the protrusive front (14-15). In fish keratocytes, another common amoeboid model, forces are similarly concentrated at the sides and rear of the moving cell, with negligible force detection at the leading edge (16-17). Smith *et al.* performed the first study with neutrophils, showing they also concentrate their forces in the rear on an ICAM-1 surface (18). A subsequent study by Shin *et al.* showed that for very short time scales on the order of 5 seconds, the traction forces can oscillate between the rear and front of the cell (19).

To study DC force generation, we placed cells on a micropost array detector (mPAD) (20-21). We chose the micropost force detector because of its greater sensitivity; forces exerted by dendritic cells ultimately prove to be much lower than that of neutrophils, and gel-based TFM proved inadequate to resolve forces in these cells. For chemotaxis

experiments, the mPADs were placed in a microfluidic gradient generator (7), and presented with a 0-20nM gradient of CCL19; cells crawled on fibronectin-coated posts of 1.5 kPa elasticity. Using this system, we found that dendritic cells concentrated their strongest forces at the leading edge. We find that the line of maximal stress can be used to predict the direction of motion. Additionally, the force on a micropost has a characteristic time scale which can be correlated to the force on that post. Finally, actomyosin inhibitors significantly depleted force generation, but not directional navigation. Conversely, pertussis toxin blocked navigation but did not affect traction forces.

Materials and Methods

Methods Overview

The experimental methods and protocols are described briefly; a detailed description is included below. The microfluidic gradient generator was fabricated as described previously (7). PDMS micropost array substrates were fabricated as in Tan *et al*. (20) The effective stiffness of the microposts (~1.5 kPa) was on the order of mammalian tissue. The tops of microposts were functionalized with fibronectin and the sides of the posts were blocked with an inert polymer. Murine dendritic cells were obtained by culturing stem cells from mouse femurs for 7 days in the presence of GM-CSF and matured by 24 h exposure to LPS. Local force on each post was calculated by a custom-written MATLAB (Natick, MA) script (22). Briefly, acquired images were imported, cell

area was defined, and mPAD post centroids were automatically determined. Forces were then computed via a known spring constant of the micropost, (1.9 nN/μm). Inhibitors were given 1 hour (blebbistatin and Latrunculin A) or 24 hours (Pertussis Toxin) prior to the experiment. The lines of maximal stress and front-rear distribution of forces were calculated using custom-made Matlab software. To determine the time scale of single-post deflections, half-max full-width (HMFW) analysis was performed on the raw post-displacement data. The duration of HMFW was then correlated to the maximum magnitude exerted on the micropost.

Cell Isolation and Culture Conditions

Dendritic cells were generated from murine bone marrow cells according to the procedure of Lutz *et al.* (23) with minor modifications. Briefly, bone marrow was flushed from the tibias and femurs of 8 to 10-week-old C57BL/6 mice and depleted of red blood cells using ammonium chloride lysis buffer. The cells were plated in 10-cm petri dishes (2×10^6 cells/ml; 10ml/plate) in RPMI-1640 supplemented with 10% heat-inactivated fetal bovine serum, 100 U/ml penicillin, 100 mg/ml streptomycin, 50 nM BME, and 20 ng/ml rmGM-CSF (Peprotech, Rocky Hill, NJ) at 37°C in 5% CO_2. On day 3 fresh media was added, and on day 6 half of the media was gently replaced. Immature DCs were used in experiments on day 7. For mature DCs, 1 μg/ml LPS (Sigma-Aldrich, St. Louis, MO) were added on day 6 and cells were used in experiments on day 7. On day 7, 80% or more of the non-adherent cells expressed the monocyte lineage marker CD11c as confirmed by flow cytometry. When inhibitors were used, they were added to

cell culture 1 hour prior to imaging, with the exception of pertussis toxin, which was added 24 hours prior. All inhibitors were supplied by Sigma-Alrich, St. Louis, MO. Inhibitors were Latrunculin A (150nM), blebbistatin (50 μM), and pertussis toxin (100 ng/ml).

Preparation of Micropost Substrates

Microposts masters were shaped using deep reactive ion etching (DRIE) as described previously (24). The silicon master is used to create a PDMS negative master, which is subsequently passivated with a fluorosilane. Elastomeric micropost array substrates were fabricated via polydimethylsiloxane (PDMS; Sylgard 184, Dow-Corning, Midland, MI) by casting against the negative master. Microposts were patterned with fibronectin by micro-contact printing as described previously (20). Subsequently, microposts were fluorescently labeled with 5 μg⁄ml Δ9-DiI (1,1′-dioleyl-3,3,3′,3′-tetramethylindocarbocyanine methanesulfonate; Invitrogen, Carlsbad, CA). Cell adhesion was restricted to the micropost tips by blocking the unprinted surface with 0.1% Pluronics F127 (BASF, Mount Olive, NJ). The micropost array was incorporated into the microfluidic device before plasma bonding, and posts were protected from oxidation by a physical barrier.

Fabrication of microfluidic device

A microfluidic gradient generator was fabricated in polydimethylsiloxane (PDMS) using soft lithography as described previously (7), with modifications. The microchannels were embossed in PDMS using soft lithography. First, the micropost array detectors were attached to an acrylic support using PDMS glue, then the microchannels were plasma bonded (600 mTorr O_2, 30 W, 20 s) onto this structure (see Figure 6.1). Assembled microfluidic devices containing microneedles were submerged in PBS and filled under vacuum. Chemoattractant solutions of CCL19, CCL21 or neither (Peprotech, Rocky Hill, NJ) in complete culture media were prepared for each of the three inlets. Fluorescein (Fluka) was added to one inlet at 10^{-5} M final concentration to aid visualization of the gradient and to confirm its persistence during the experiment. The total flowrate within the chamber was maintained at 9 μL/min using a syringe pump, resulting in a wall shear rate of 6 s^{-1}. After the gradient was visually established, the flow was stopped, and cells were injected via the side port and allowed to adhere for 10 min before resuming flow. Using custom built LabView (National Instruments, Austin, TX) software, 8-12 fields of view were imaged at 40X magnification by phase and red-channel fluorescence microscopy on a Nikon Eclipse TE300 (Nikon Inc., Melville, NY) in a custom enclosure maintained at 37°C and 5% CO_2. Images were captured every 3 minutes for standard experiments, and every 6 seconds for high time-resolution experiments. Cell trajectories were captured using the ImageJ ManualTracking plugin (http://rsbweb.nih.gov/ij), and chemotactic parameters were calculated using a custom-written MATLAB (Mathworks, Natick, MA) script.

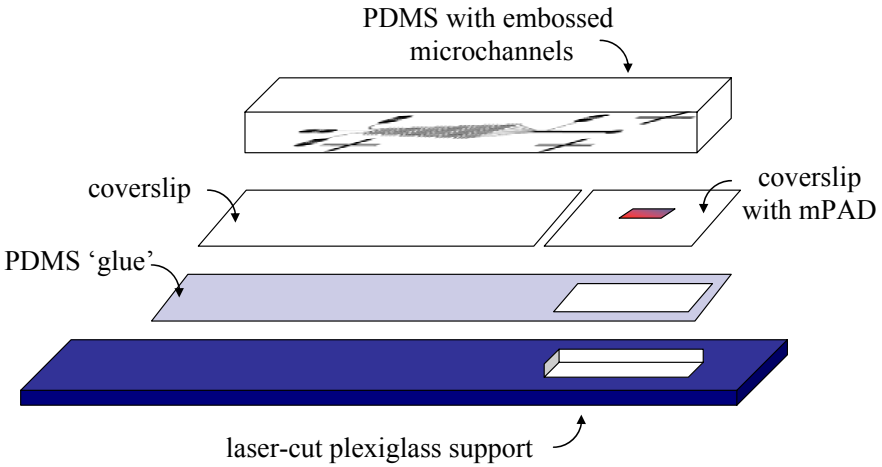

Figure 6.1. Microfluidic mPAD assembly.

Measurement of Traction Forces

To measure the bending of the microneedles, the tips and base of DiI-labeled microneedles were visualized by epifluorescence imaging using a 40X objective on a Nikon Eclipse TE300 inverted microscope (Nikon Inc., Melville, NY). The centroids of the microneedles at both the tip and base were determined by localized thresholding using an automated Matlab program (22) (Mathworks, Natick, MA), to yield the deflected and undeflected positions, respectively. After performing image registration on the tip and base centroids, the force on each needle is computed by multiplying the deflection by the spring constant of the microneedle, which is 1.92 nN⁄μm.

Results

DC Migration on Micropost Surfaces

We measured the motility of dendritic cells on microposts of 1.5kPa elasticity coated with fibronectin with chemokine fields imposed by a microfluidic gradient chamber. During chemokinesis in the absence of a chemokine gradient, DCs migrated randomly at an average velocity of 2.3 ± 0.5 μm/min, similar to their velocity on other substrates (2-3, 25). The random motility coefficient on the mPAD surface was 48 μm^2/min, slightly lower than on glass substrates (7). This difference may be due to the reduced perceived stiffness of the substrate, since substrate mechanics often affect migration parameters (26). During chemokinesis, we measured the average strain energy over the cell to be 2.3 +/- 0.3 fJ/cell. Overall, DC migration was not significantly altered by the micropost surface.

We use a microfluidic gradient generator in combination with the micropost array surface to present DCs with a chemokine gradient while monitoring their traction forces (Fig 6.2). We find that DCs concentrate integrin-based contractile forces at the leading edge, with almost no force at the trailing edge (Fig. 6.3 *A*). This pulling force is often characterized by a highly localized contraction of two to three microposts in which the net force is always pulling toward the nucleus. This force must be counterbalanced at the rear, and we observe these counterbalancing forces to be diffuse, weak adhesions under the cell body.

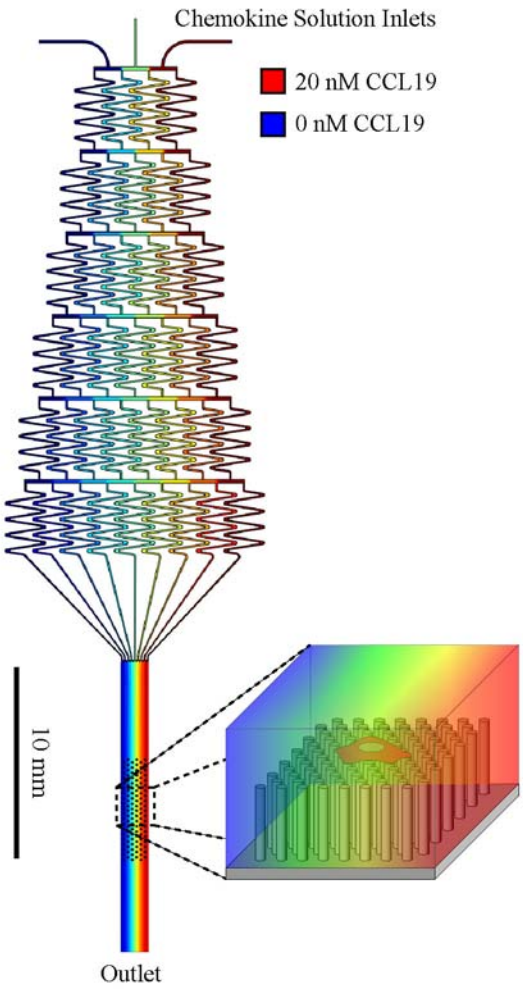

Figure 6.2. A microfluidic gradient generator coupled to a micropost array detector. Chemokine solutions containing 20, 10 or 0 nM CCL19 are perfused into inlets at the top of the chamber at 3 μL/min/inlet. Colors in the diagram correspond to chemokine concentration; red, green, and blue correspond to 20, 10 and 0 nM, respectively. The three inlets are mixed in a series of microchannels forming a smooth gradient in the cell viewing region. A micropost array detector of effective stiffness 1.5 kPa forms the migration surface within the viewing region. The tips of microposts are functionalized with fibronectin and the sides are passivated with an amphiphilic triblock copolymer. The gradient presented to cells (2 K_D/mm) has been optimized to induce maximal chemotactic index.

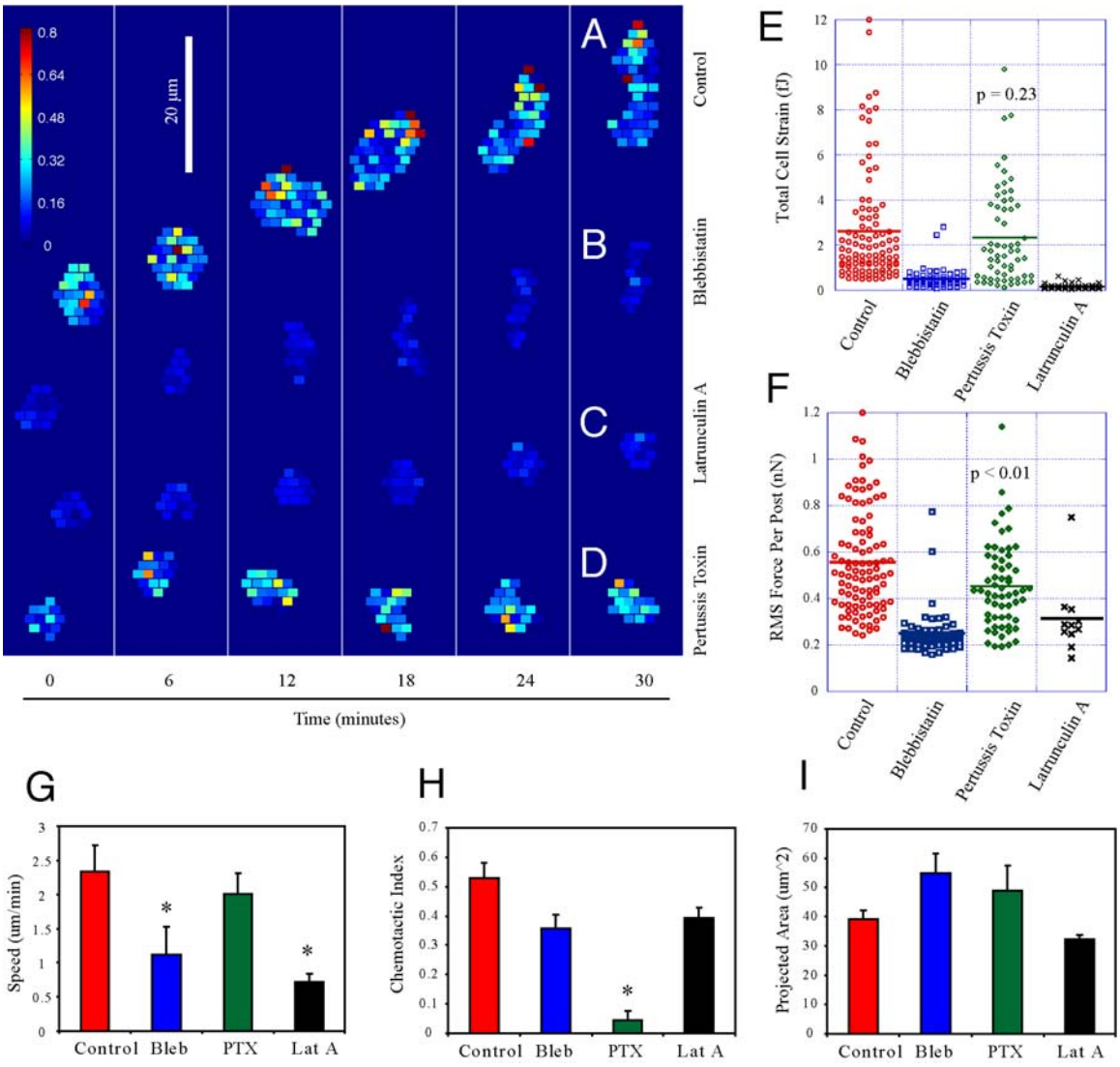

Figure 6.3. DCs migrating in a chemokine gradient concentrate traction forces at the leading edge. (*A*) A representative trace of a DC following an extracellular gradient of soluble CCL19 (highest at top). Each colored box underneath the cell represents a single micropost. (*B-D*) Representative traces of DCs treated with blebbistatin (*B*), Latrunculin A (*C*), or pertussis toxin (PTX) (*D*). (*E* and *F*) Total cellular strain energy and root-mean squared force per post generated by cells in a chemokine gradient (N = 10 per condition). (*G*) Average speed of cells on microposts in a chemokine gradient. Speed was significantly reduced with actomyosin inhibitors, but not PTX. (*H*) Chemotactic index, A modest decrease is observed with actomyosin inhibitors, but PTX greatly decreases directional migration. (*I*) The cell spread area is increased with blebbistatin and PTX treatment. Error bars represent standard error of the mean.

DC Forces Depend on Actomyosin, but not Gradient Sensing

The key components of cell motility are actin-based polymerization, myosin-based contraction, integrin-based adhesion, and GPCR-based signaling/polarity (2). To disrupt actin polymerization, we used the chemical inhibitor Latrunculin A. In the absence of actin polymerization, motility was completely abrogated (Fig. 6.3 *C* and *G*), and force transmission to the microposts was minimal (Fig. 6.3 *C, E, and F*) as cells failed to spread on the substrate (Fig. 6.3 *I*). After treatment with blebbistatin to disrupt myosin II-based contractility, cells displayed slower speeds (Fig. 6.3 *G*) and greater than 50% reduction in traction forces (Fig. 6.3 *B, E,* and *F*). We also used pertussis toxin (PTX) to disrupt chemokine signaling from the extracellular gradient (Fig. 6.3 *H*). This treatment gave only a slight reduction in force per post (Fig. 6.3 *F*), while the average cellular force was not affected (Fig. 6.3 *D* and *E*) because the treated cells had a greater spread area (Fig. 6.3 *I*). Taken together, this data shows that in DCs traction force and speed are correlated, but traction forces are somewhat independent of gradient sensing.

DC Tractions Stresses Predict Direction of Motion

While dendritic cells make use of polymerization, contraction and adhesion (2) for locomotion, we are able to directly measure the contractile stresses exerted through distinct adhesions. We find that traction forces are stronger at the leading edge than under the nucleus or at the rear of the cell. This was quantified by finding the point of maximal stress along the axis of motion (Fig. 6.4 *A, grey line*), which is typically in front of the cell centroid (Fig. 6.4 *F*). Even when gradient sensing was lost by PTX inhibition,

the point of maximal stress was still generally in front of the centroid (Fig. 6.4 *G*), meaning that forces are still concentrated at the leading edge in the absence of asymmetric GPCR signaling. Treatment with actomyosin inhibitors greatly reduced traction stresses, and the point of maximal stress was more likely to be at or near the cell centroid (Fig. 6.4 *H, I*), so directional information was lost.

Using a single traction map, the direction of motion can be calculated *a priori*. As a prediction, we search for the line of global maximum stress (Fig. 6.4 *A, black line*), and compare it to the line perpendicular to the empirical direction the cell moved over the following 5 minutes. The angle subtended by these lines (Θ) describes the agreement between our proposed prediction and experimental outcome. For mature dendritic cells migrating in a strong gradient of CCL19, we find that Θ is small (Fig. 6.4 *B*) indicating that the line of global maximal stress is close to perpendicular to the direction of motion. Combined with information about the cell centroid, this line gives accurate predictions for the direction of motion. Again, when PTX is used to disrupt gradient perception and induce random migration, the line of maximal stress still predicts the direction of motion, though with lesser accuracy, as Θ is not as tightly distributed around 0 and 180° (Fig. 6.4 *C*). The actomyosin inhibitors further widen the distribution of Θ, decreasing the sensitivity of the prediction, but the maximal stress may still be used to give a rough indication of directionality (Fig. 6.4 *D, E*). We propose that a global search of the traction stresses from a snapshot in time can be used to predict the direction of dendritic cell migration.

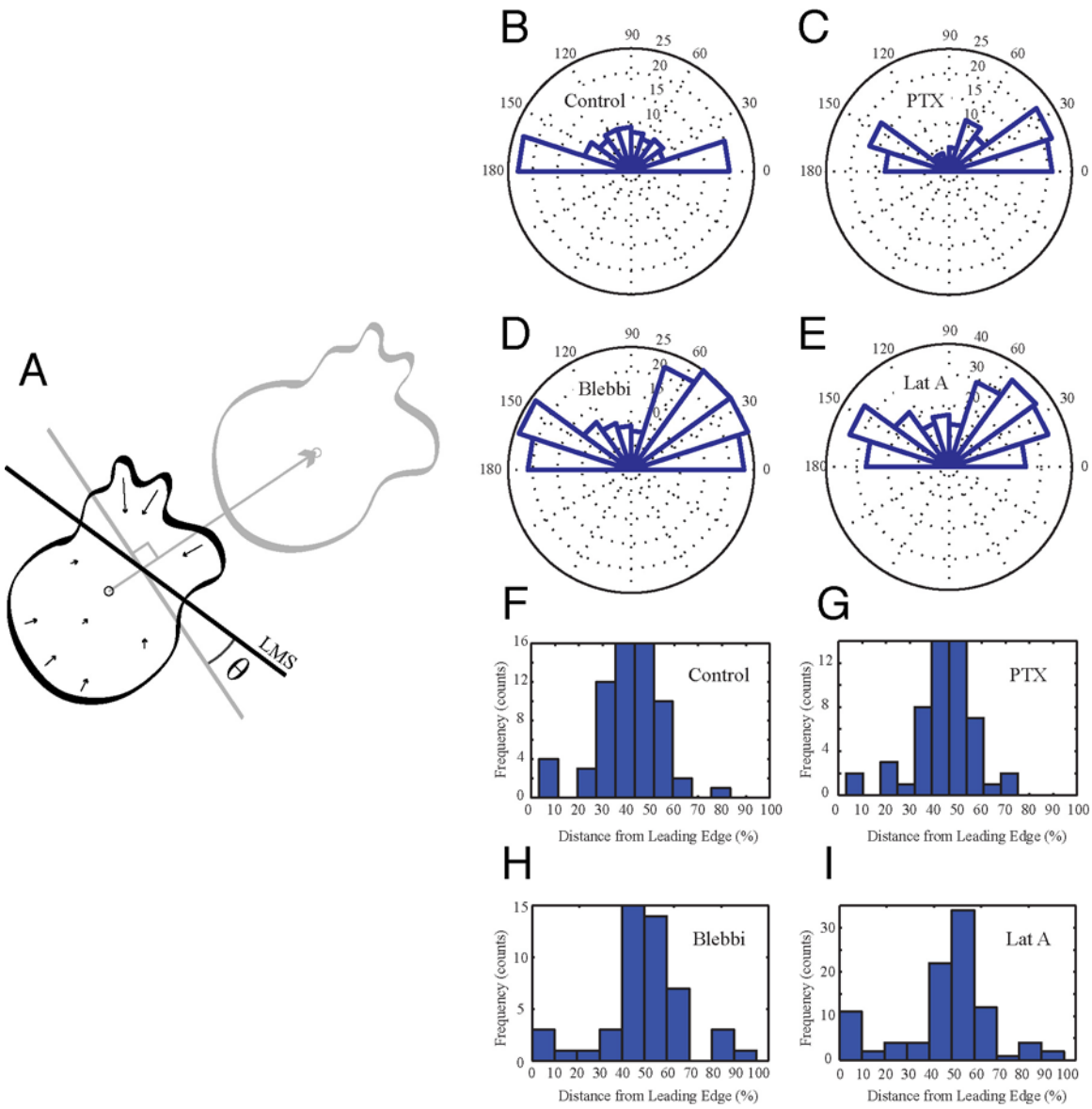

Figure 6.4. A single traction map can be used to predict the direction of migration. (*A*) Schematic. Traction forces are interrogated to find the line of maximal stress (LMS, black line). The angle θ is defined by the LMS and the vector normal to the direction of motion. (*B*) A histogram of θ for untreated cells. (*C*) Even in cells treated with PTX, the LMS can be used to approximate the direction of motion. (*D* and *E*) Blebbistatin or Latrunculin A treatment decreases the accuracy of predicting the direction of motion. (*F*) The LMS is generally found in front of the cell centroid. The intersections are measured from the leading edge and scaled to the cell length. (*G*) PTX treatment does not significantly change from results from the control. (*H* and *I*) Actomyosin inhibitors result in a random distribution of LMS – axis intersections.

Temporal Duration of Dendritic Cell Traction Stresses

DCs are highly motile amoeboid cells, moving on small timescales when compared to epithelial cells or fibroblasts. Consequently, the characteristic timescale of their traction forces are much smaller. DCs exert transient forces, releasing the substrate soon after the leading edge has passed. To measure the timescale of this interaction, we examined individual post deflections as the DC leading edge approached, bound, and released the post (Fig. 6.5 *A, B*). Since the post deflections resemble a pulse waveform, the characteristic time-scale (τ) was determined using a full-width, half-max analysis of the force profile over time (Fig. 6.5 *C*). By accumulating data from posts at the leading edge of many cells, we find a maximum in the frequency of τ around 2 minutes, but sometimes extending over 6 minutes in duration. The longer durations were associated with greater maximum forces exerted on the post. More generally, τ and F_{max} are correlated (Fig. 6.5 *E*), indicating a constant rate of energy input from the cell. In the relatively fast-moving DC, the greatest forces under the leading edge have a characteristic duration whose length is determined by the amount of time the cell supplies power to the substrate.

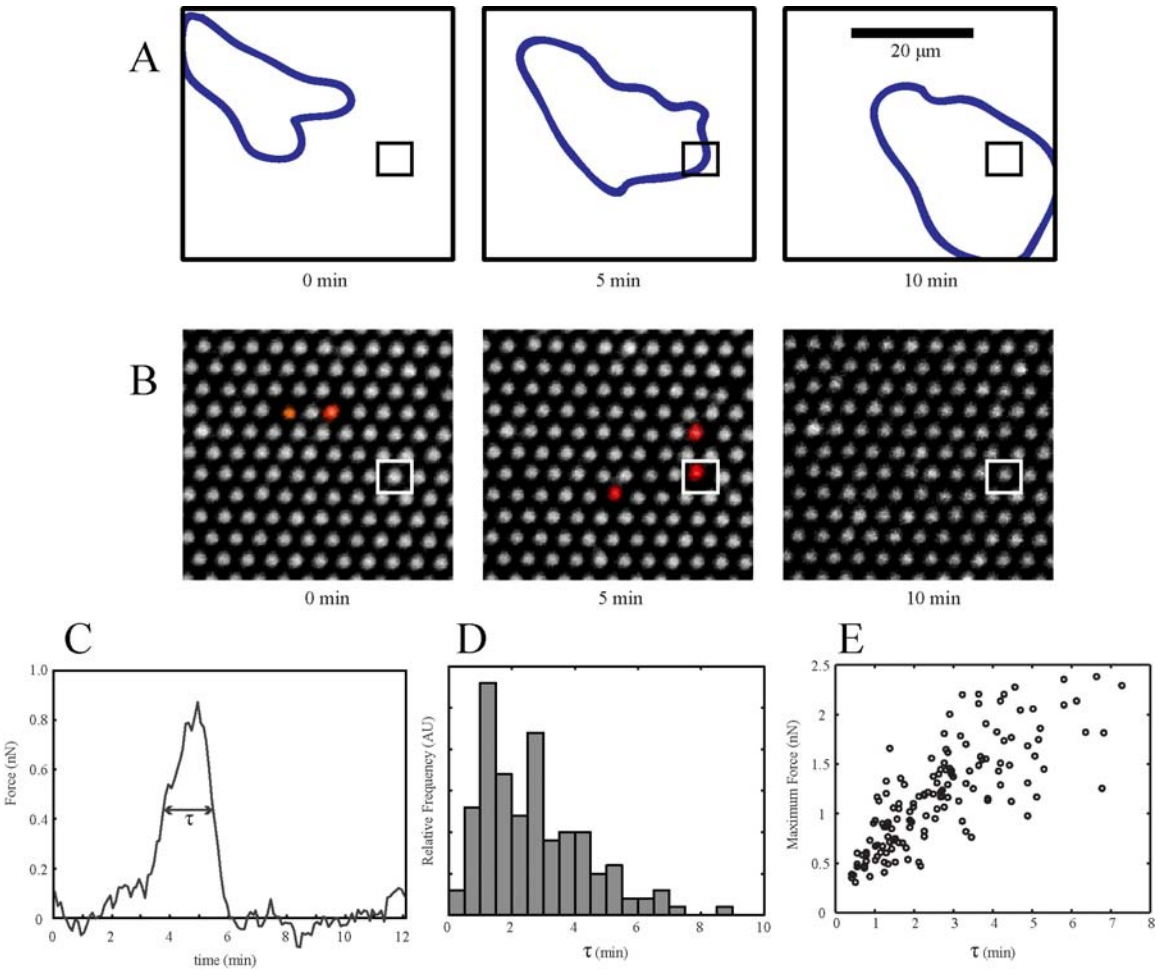

Figure 6.5. Temporal analysis of dendritic cell traction forces. (*A*) A dendritic cells deflect microposts under the leading edge. The cell outline was traced from a phase contrast image (blue line). The location of a representative micropost is identified by a black square as the cell approaches, binds and releases the post at 0, 5 and 10 minutes. Scale bar represents 20 microns. (*B*) Red-channel fluorescence images of microposts at time points corresponding to the traces in *A*. Deflected posts are pseudo-colored red for emphasis. The micropost of interest is tugged as the leading edge passes, then is released when underneath the cell. (*C*) A profile of the magnitude of force on the micropost boxed in *A* and *B*. A max-height full-width analysis is used to determine the characteristic duration (τ) of force application. (*D*) The frequency distribution of τ calculated over 144 microposts (N = 26). The maximum frequency is at approximately 2 minutes. (*E*) The duration of magnitude of force on a post are correlated. As the characteristic time τ increases, the maximum force reached also increases. This suggests a constant energy output from the cell.

Discussion

Microfluidic devices have become popular for delivering stable chemotactic gradients to cells (27-30). Other methods for inducing chemotaxis, such as transwell assays (31), Zigmond chambers (32), and under-agarose assays (33) rely on transient gradients which make them difficult to optimize. Similarly, micropost arrays have become popular for measuring traction forces due to their relatively simple fabrication and fidelity of results (22). In the present work, we combine these two technologies to measure DC-substrate stresses in an optimized chemotactic gradient. This type of multi-platform technology for accurately measuring the relationship between force and chemotactic signaling, will become increasingly important for elucidating cellular migration.

Although the molecular machinery for migration is shared across several subtypes of mammalian cells, traction force profiles vary among cell types (18-19, 34). The majority of research on cell-substrate forces has focused on strongly-adhesive cell types, such as fibroblasts (34-36), smooth muscle cells (20), epithelial cells (22, 37-38), endothelial cells (39-40), and stem cells (41). Amoeboid cells represent a distinct type of migration which does not use focal adhesions, but rather rapidly remodels the cell shape to achieve locomotion (5). It has even been shown that some leukocytes are capable of migrating in the absence of integrin-based adhesion (4). Although subsequent work has shown that integrins are used in DC motility (3, 8, 42), no description of traction stresses of denritic cells has ever been published. In contrast to neutrophils which concentrate a squeezing force in the uropod (18) and mesenchymal cells which generate stable pulling forces at

the leading edge and detachment forces at the uropod (43), we present the first traction force maps for DCs and show that their forces are concentrated at the leading edge or filopodia. This finding is in contrast to neutrophils, the other leukocyte subtype studied by traction force techniques which move primarily by squeezing at the rear (18-19, 44).

Since DCs have a characteristic force profile, we investigated whether migration direction could be predicted from a single force map. Since the greatest forces are generated at the leading edge, the line of maximal stress is generally found in front of the cell centroid. Additionally, by searching for the global axis of maximal stress, we were able to accurately predict the direction of migration on time scales shorter than the persistence time. Indeed, even when an external gradient could not be sensed due to pertussis toxin treatment, the direction of migration can still be predicted. When actomyosin inhibitors are used, the forces are greatly reduced and the axis of maximal stress is a less meaningful predictor.

Many migrating cells make use of focal adhesions to link actomyosin machinery to extracellular substrates. FAs form on the timescale of tens of minutes and last on the order of hours (45-47). Amoeboid cells will often displace a cell diameter or more within 10 minutes, so they must rely on much shorter-lived adhesions than seen in cells with focal adhesions. We find that DC adhesion forces are roughly bell-shaped and their characteristic timescale is approximately 2 minutes. Further, the duration and magnitude of the force are positively correlated, indicating that the work rate of the cell is constant

during post deflection. This may indicate that the myosin motors near the adhesion operate in an all-on or all-off mode.

To reach T cells in secondary lymphoid organs, mature dendritic cells must migrate through peripheral tissue, occasionally cross basement membranes, enter lymphatics, and navigate lymphoid tissue in an integrin-mediated fashion (11-12). Despite the requirement of integrins for parts of DC migration, no traction force maps have been produced until now. We show here that in addition to actin-based polymerization and myosin-based contraction (4), DCs are able to use short-lived integrin-based adhesions in leading filopodia to effect migration. Understanding these forces and the pathways that generate them leads us one step closer to being able to manipulate them for therapeutic value.

Acknowledgements

The authors thank Eric Johnston and Beena John for technical support. We acknowledge support from National Institutes of Health grant Nos. AI082292. B.G.R. received support from a Merck & Co. graduate fellowship.

References

1. Alvarez D, Vollmann EH, & von Andrian UH (2008) Mechanisms and Consequences of Dendritic Cell Migration. 29(3):325-342.

2. Lammermann T & Sixt M (2009) Mechanical modes of 'amoeboid' cell migration. (Translated from eng) *Curr Opin Cell Biol* 21(5):636-644 (in eng).

3. Schumann K, *et al.* (2010) Immobilized Chemokine Fields and Soluble Chemokine Gradients Cooperatively Shape Migration Patterns of Dendritic Cells. *Immunity* 32(5):703-713.

4. Lammermann T, *et al.* (2008) Rapid leukocyte migration by integrin-independent flowing and squeezing. *Nature* 453(7191):51-55.

5. Renkawitz J, *et al.* (2009) Adaptive force transmission in amoeboid cell migration. *Nat Cell Biol* 11(12):1438-1443.

6. Yoo SK, *et al.* (2010) Differential Regulation of Protrusion and Polarity by PI(3)K during Neutrophil Motility in Live Zebrafish. *Developmental Cell* 18(2):226-236.

7. Ricart BG, John B, Hunter CA, & Hammer DA (Dendritic Cell Chemotaxis in Engineered Chemokine Gradients. *Proc Natl Acad Sci U S A* In Preparation.

8. Lammermann T, *et al.* (2009) Cdc42-dependent leading edge coordination is essential for interstitial dendritic cell migration. *Blood* 113(23):5703-5710.

9. Van Keymeulen A, *et al.* (2006) To stabilize neutrophil polarity, PIP3 and Cdc42 augment RhoA activity at the back as well as signals at the front. *The Journal of Cell Biology* 174(3):437-445.

10. Gupton SL & Waterman-Storer CM (2006) Spatiotemporal Feedback between Actomyosin and Focal-Adhesion Systems Optimizes Rapid Cell Migration. *Cell* 125(7):1361-1374.

11. Quast T, *et al.* (2009) Cytohesin-1 controls the activation of RhoA and modulates integrin-dependent adhesion and migration of dendritic cells. *Blood* 113(23):5801-5810.

12. Johnson LA & Jackson DG (2010) Inflammation-induced secretion of CCL21 in lymphatic endothelium is a key regulator of integrin-mediated dendritic cell transmigration. *Int. Immunol.*:dxq435.

13. Humphries JD, Byron A, & Humphries MJ (2006) Integrin ligands at a glance. *J Cell Sci* 119(19):3901-3903.

14. Lombardi ML, Knecht DA, Dembo M, & Lee J (2007) Traction force microscopy in Dictyostelium reveals distinct roles for myosin II motor and actin-crosslinking activity in polarized cell movement. *J Cell Sci* 120(9):1624-1634.

15. Uchida KSK, Kitanishi-Yumura T, & Yumura S (2003) Myosin II contributes to the posterior contraction and the anterior extension during the retraction phase in migrating Dictyostelium cells. *J Cell Sci* 116(1):51-60.

16. Lee J, Leonard M, Oliver T, Ishihara A, & Jacobson K (1994) Traction forces generated by locomoting keratocytes. *The Journal of Cell Biology* 127(6):1957-1964.

17. Burton K, Park JH, & Taylor DL (1999) Keratocytes Generate Traction Forces in Two Phases. *Mol. Biol. Cell* 10(11):3745-3769.

18. Smith LA, Aranda-Espinoza H, Haun JB, Dembo M, & Hammer DA (2007) Neutrophil Traction Stresses are Concentrated in the Uropod during Migration. 92(7):L58-L60.

19. Shin ME*, et al.* (2010) Spatiotemporal organization, regulation and functions of tractions during neutrophil chemotaxis. *Blood*:blood-2009-2012-260851.

20. Tan JL*, et al.* (2003) Cells lying on a bed of microneedles: An approach to isolate mechanical force. *Proceedings of the National Academy of Sciences of the United States of America* 100(4):1484-1489.

21. Fu J*, et al.* (2010) Mechanical regulation of cell function with geometrically modulated elastomeric substrates. *Nat Meth* 7(9):733-736.

22. Lemmon CA*, et al.* (2005) Shear force at the cell-matrix interface: enhanced analysis for microfabricated post array detectors. (Translated from eng) *Mech Chem Biosyst* 2(1):1-16 (in eng).

23. Lutz MB*, et al.* (1999) An advanced culture method for generating large quantities of highly pure dendritic cells from mouse bone marrow. *Journal of Immunological Methods* 223(1):77-92.

24. Yang MT & Chen CS (2009) Mechanotransduction and the Study of Cellular Forces. *Methods in Bioengineering: Microdevices in Biology and Medicine*, eds Nahmias Y & Bhatia SN (Artech House, Norwood, MA).

25. Riol-Blanco L, *et al.* (2005) The Chemokine Receptor CCR7 Activates in Dendritic Cells Two Signaling Modules That Independently Regulate Chemotaxis and Migratory Speed. *J Immunol* 174(7):4070-4080.

26. Oakes PW, *et al.* (2009) Neutrophil morphology and migration are affected by substrate elasticity. *Blood* 114(7):1387-1395.

27. Li Jeon N, *et al.* (2002) Neutrophil chemotaxis in linear and complex gradients of interleukin-8 formed in a microfabricated device. *Nat Biotech* 20(8):826-830.

28. Jeon NL, *et al.* (2000) Generation of Solution and Surface Gradients Using Microfluidic Systems. *Langmuir* 16(22):8311-8316.

29. Lin F & Butcher EC (2006) T cell chemotaxis in a simple microfluidic device. *Lab on a Chip* 6(11):1462-1469.

30. Irimia D, *et al.* (2006) Microfluidic system for measuring neutrophil migratory responses to fast switches of chemical gradients. *Lab on a Chip* 6(2):191-198.

31. Boyden S (1962) THE CHEMOTACTIC EFFECT OF MIXTURES OF ANTIBODY AND ANTIGEN ON POLYMORPHONUCLEAR LEUCOCYTES. *The Journal of Experimental Medicine* 115(3):453-466.

32. Zigmond SH (1977) Ability of polymorphonuclear leukocytes to orient in gradients of chemotactic factors. *The Journal of Cell Biology* 75(2):606-616.

33. Nelson RD, Quie PG, & Simmons RL (1975) Chemotaxis Under Agarose: A New and Simple Method for Measuring Chemotaxis and Spontaneous Migration of Human Polymorphonuclear Leukocytes and Monocytes. *J Immunol* 115(6):1650-1656.

34. Beningo KA, Dembo M, Kaverina I, Small JV, & Wang Y-l (2001) Nascent Focal Adhesions Are Responsible for the Generation of Strong Propulsive Forces in Migrating Fibroblasts. *J. Cell Biol.* 153(4):881-888.

35. Yang M, Sniadecki N, & Chen C (2007) Geometric Considerations of Micro- to Nanoscale Elastomeric Post Arrays to Study Cellular Traction Forces. *Advanced Materials* 19(20):3119-3123.

36. Munevar S, Wang Y-l, & Dembo M (2001) Traction Force Microscopy of Migrating Normal and H-ras Transformed 3T3 Fibroblasts. *Biophysical journal* 80(4):1744-1757.

37. du Roure O, *et al.* (2005) Force mapping in epithelial cell migration. *Proceedings of the National Academy of Sciences of the United States of America* 102(7):2390-2395.

38. Trepat X, *et al.* (2009) Physical forces during collective cell migration. *Nat Phys* 5(6):426-430.

39. Reinhart-King CA, Dembo M, & Hammer DA (2002) Endothelial Cell Traction Forces on RGD-Derivatized Polyacrylamide Substrata†. *Langmuir* 19(5):1573-1579.

40. Nelson CM, *et al.* (2005) From the Cover: Emergent patterns of growth controlled by multicellular form and mechanics. *PNAS* 102(33):11594-11599.

41. Ruiz SA & Chen CS (2008) Emergence of Patterned Stem Cell Differentiation Within Multicellular Structures. *STEM CELLS* 26(11):2921-2927.

42. Eich C, *et al.* (2010) The lymphoid chemokine CCL21 triggers LFA-1 adhesive properties on human dendritic cells. *Immunol Cell Biol*.

43. Dembo M & Wang Y-L (1999) Stresses at the Cell-to-Substrate Interface during Locomotion of Fibroblasts. *Biophysical journal* 76(4):2307-2316.

44. Jannat RA, Robbins GP, Ricart BG, & Hammer DA (2010) Neutrophil adhesion and chemotaxis depend on substrate mechanics. *Journal of Physics: Condensed Matter* 22(19):194117.

45. Wang YL (1984) Reorganization of actin filament bundles in living fibroblasts. *The Journal of Cell Biology* 99(4):1478-1485.

46. Burridge K, Fath K, Kelly T, Nuckolls G, & Turner C (1988) Focal Adhesions: Transmembrane Junctions Between the Extracellular Matrix and the Cytoskeleton. *Annual Review of Cell Biology* 4(1):487-525.

47. Ridley AJ & Hall A (1992) The small GTP-binding protein rho regulates the assembly of focal adhesions and actin stress fibers in response to growth factors. 70(3):389-399.

Chapter 7: Conclusions and Future Work

Specific Aims

Research presented in this work shows that we were able to successfully characterize several aspects of dendritic cell migration. The specific aims of this work were as follows.

1. Characterize the effect of CCR7 ligands CCL19 and CCL21 on the random motility of dendritic cells and assess their adhesion to common extracellular matrix proteins.

2. Characterize the integration of chemotactic signals by dendritic cells in engineered gradients.

3. Make the first measurements of the forces exerted by DCs during chemokinesis and chemotaxis.

Specific Findings

Dendritic Cell Motility and Adhesion with Chemokine Stimulation

Migration parameters including cell speed, persistence time, and random motility coefficient have been measured for a variety of cells from bacterial to mammalian. Before this work, no such data existed for dendritic cells. In Chapter 3, we measured these metrics for dendritic cells, and showed them to be consistent with previous studies of similar cell types. We examined the differential adhesion of DCs to substrate ligands as a function of chemokine concentration, and we found that DCs are able to bind fibronectin, but not collagen. Adhesion was a relatively weak function of chemokine stimulation on both substrates. Additionally, we showed that DCs undergo haptokinesis on chemokine surfaces, increasing their random motility coefficient with higher chemokine concentrations. Additionally, CCL21 proved a superior ligand for inducing haptokinesis, which is consistent with new reports about how CCL19 and CCL21 signal DC motility (20). Finally, we showed that the cell speed, persistence time, and random motility coefficient are complex functions of CCL19 and CCL21 concentration on collagen surfaces, most likely due to CCR7 regulation. We found that the response is biphasic, with a maximum random motility coefficient at approximately 10 nM for both chemokines, indicating the K_D for CCR7 binding either ligand is ~10 nM. On fibronectin, we found the response to chemokine is minimal, indicating that integrin signaling has already saturated cell migration machinery. The inability of DCs to bind collagen is especially relevant for understanding DC literature, where several studies examine DC migration in 3D collagen matrices (1-3).

Integration of Single and Multiple Chemokine Gradients

Many studies have shown DCs migrate toward the chemokines CCL19 and CCL21 in transwell assays. These assays are limited in their ability to capture detailed information about the mechanisms by which cells polarize themselves and migrate in response to stimuli. In Chapter 4, we used a microfluidic device to quantitatively investigate immune cell migration in response to varying chemoattractant gradients (4). This tool allowed us to answer several fundamental questions about chemokine signal integration. We showed that DCs respond almost identically to CCL19, CCL21, and CXCL12 in a single, optimized gradient. Cells were better able to adapt to CCL19, however, which may be due to CCL19 binding by CRAM (5-6). In counter-gradients, we showed that CCL19 is preferred to CCL21 or CXCL12, indicating a hierarchy of preferred chemokines. Interestingly, in counter-gradient experiments, we showed that cells will seek a central position between matched counter-gradients. We believe this may play a role in how DCs find their ultimate position within secondary lymphoid organs.

Inhibitors of Dendritic Cell Chemotaxis

In Chapter 4, we went further to examine the role of specific molecular pathways in a migrating DC. By using small molecule inhibitors, we found that actomyosin components were required for maintaining optimal cell speed, but did not affect the cell's ability to navigate. Conversely, by using pertussis toxin, we showed that GPCR signaling is critical for directional sensing, but cells are fully motile in their absence. This ability to migrate on fibronectin substrates without chemokine cues supports our earlier findings from Chapter 3. Finally, we discovered the surprising result that the PI3K pathway is

dispensable for DC chemotaxis. After we made this observation, similar observations were made in a related cell type, monocytes (7).

Application of Microfluidic Techniques to HS1 Knockout DCs

Chapter 5 focuses on the role of HS1 in dendritic cells. This previously unstudied molecule is structurally related to cofilin, but its role in dendritic cells was unknown. We carefully characterized the HS1 knockout phenotype, especially its role in dendritic cell migration. This chapter places greater emphasis on immature dendritic cells, which coordinate podosomes arrays to facilitate migration. We found that the greatest impact of the HS1 KO phenotype was an inability to organize podosome arrays, which are typically found near the leading edge. After extensive analysis with transwell assays, only small differences in chemotaxis could be observed. By the application of our microfluidic gradient generator and direct observation of migration, however, we were able to observe subtle nuances of HS1 deficiency. Specifically, we found that loss of HS1 lead to increased migration speed and random motility coefficient, but decreased chemotactic index (8). Thus we were able to conclude that HS1 helps stabilize filopodia extended in the correct direction of migration.

Measurement of Dendritic Cell Traction Forces

In Chapter 6, we extended the use of microfluidic gradient technology to the study of DC migration on substrates suitable for traction force microscopy to enable simultaneous measurements of migration and force in individual cells. DCs have been shown here to be "front wheel drive" cells, in contrast to their leukocyte cousins, neutrophils. In

Chapter 6, we used a combination of micropost array detectors and a microfluidic gradient generator to develop a novel method for probing traction forces of murine DCs during directional migration. We found that DCs migration was primarily driven by short-lived traction stresses near the leading edge. The magnitude of DC traction forces was smaller in magnitude than found in neutrophils, and similar during chemotaxis and chemokinesis. Interestingly, we found that maximal stress in the cell occurs perpendicular to the axis of motion, ahead of the cell centroid. We further illustrated how the spatiotemporal pattern of traction stresses could be used to predict changes in the direction of DC motion. Additionally, we determined the characteristic duration of local dendritic cell traction forces, and found that DCs produce a constant energy output as they deflect posts. When we blocked chemokine signaling with pertussis toxin, we observed traction forces similar to that during chemokinesis, even in a chemokine gradient. Overall, we showed that DCs possess a mode of migration distinct from both mesenchymal cells and neutrophils, characterized by rapid turnover of traction forces in leading filopodia. This represents the first measurement of traction forces in dendritic cells (9).

Future Recommendations

This work demonstrated the modulation of dendritic cell motility in a variety of *in vitro* environments. In this section, recommendations will be made for direct extension of the aims that have described throughout this dissertation and preliminary data will be presented.

Extending Knowledge of CCR7 Signaling in DCs

Our studies focus on observing phenomena at the cellular level. However, it is often useful to extend observations to larger scales, such as animal models, or smaller scales, employing molecular biology. Such is the case with CCR7 signaling. We cite seminal work with CCL19 and CCL21 to show that their K_Ds are similar (10), and we observe a maxima in chemokinesis at the same value (see Chapter 3). However, in the same paper, when Yoshida *et al* used primary T cells for the same type of experiment they came to the following conclusion: "Notably, however, SLC was somehow less efficient in cross-desensitization against ELC in calcium mobilization and in cross-competition with ELC for binding when assessed using cultured normal T cells" (10). Later, Britschgi *et al* made a related observation (11). They stained T cells with a CCC19-Fc construct and observed that CCL19-Fc could be displaced by untagged CCL19 as expected. However it was not possible to outcompete CCL19-Fc binding with CCL21. This may suggest different affinities or K_{on}/K_{off} rates. Hence it would be useful to perform radiological studies of CCL19-I^{125} and CCL21-I^{125} binding to our DCs to more accurately measure the specific K_D in our experimental system.

In Chapter 4, we showed that cells are better able to adapt to CCL19 gradients than CCL21 or CXCL12. One way to further analyze this phenomenon would be to globally increase one attractant and expose the cells to gradients of the other. Such measurements could be extremely interesting as many groups have shown internalization differences between CCL19 and CCL21. Initially the Sallusto group demonstrated this (12) and the finding was followed up in numerous studies (13) and the molecular basis of the

signaling differences have been investigated (14-15). MAPK signaling appears to be stronger in response to CCL19 and it is firmly established that CCL19 triggers CCR7 serine phosphorylations, arrestin recruitment and thereby endocytosis while CCL21 does not (15). If the signaling is different between the chemokines the effects in the competing gradients could be nicely investigated and the situation might be similar to previous findings (16) where it is described on a molecular level how cells can prioritize one chemotactic signal over another. Following up the results of Byers *et al*, one could try to knock down arrestins and investigate the response in competing gradients.

Combining Microfluidic Gradients with Cell Staining

Another technique used to gather information about subcellular organization is immunocytochemistry (ICC). ICC is a common laboratory technique that uses antibodies that target proteins within a cell via specific epitopes. These bound antibodies can later be detected using several methods, most commonly secondary labeling with an antibody conjugated to a fluorophore. This could give valuable information about where specific proteins, such as myosin IIb, Rac, Rho, Cdc42, etc. are distributed in a chemotaxing cell. However, this technique is not possible with our current microfluidic system because the PDMS microfluidic gradient generator is covalently attached to the glass substrate. An adapted gradient generator has been developed (Figure 7.1) that would allow the PDMS channels to be removed from the substrate. The new gradient generator is sealed to the glass surface via vacuum suction and proof of concept experiments have already been completed. This device should be used to induce chemotaxis, then removed and ICC used to probe proteins of interest.

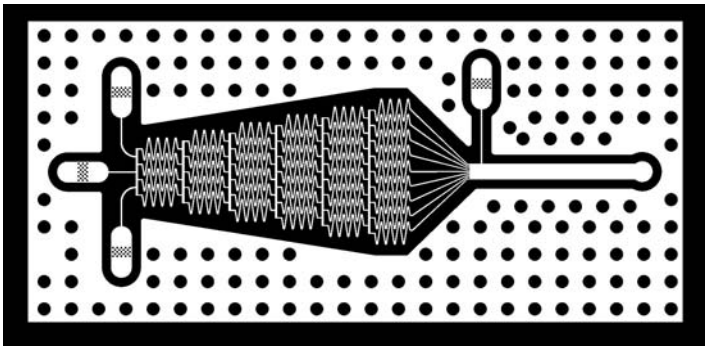

Figure 7.1. Schematic for the photomask of a microfluidic gradient generator. This gradient generator can be vacuum sealed to the migration surface and removed after the experiment allowing facile ICC staining of cells undergoing chemotaxis.

Mathematical Model of DC Navigation

Chapter 4 provides valuable experimental data for mature dendritic cells migrating in overlapping gradients. We showed experimentally how cells respond to gradients of CCL19, CCL21 and CXCL12. This is a rich data set, which could be applied to a model of dendritic cell—or more generally, leukocyte—migration. Some modeling framework for chemokine integration of multiple signals already exists (17). Indeed, we have applied this model to our dataset, and successfully modeled migration in single chemokine gradients. In overlapping gradients, this model fails to predict the cells' preference for CCL19 over CCL21 or CXCL12. We hypothesized earlier that an explanation for this preference is the presence of the CRAM receptor on DCs (5). The CRAM receptor binds CCL19, effectively lowering its local concentration. This would explain how DCs are better able to adapt to large concentrations of CCL19. It also provides a qualitative explanation for the behavior we observe in counter-gradients.

Mathematical modeling of this behavior would be an elegant addition to our experimental data.

Extension of Overlapping Gradients to Other Cell Types

This thesis deals exclusively with dendritic cells, which hold a special place in this researcher's heart. However, the techniques developed in this thesis are readily adaptable to studying other cell types. Specifically, endothelial cell chemotaxis in controlled gradients has only recently been attempted, and several questions remain unanswered. Additionally, the mPAD system is well suited to studying small forces, below the force resolution of polyacrylamide gels, so other 'weak' cells such as T and B lymphocytes, macrophages, and NK cells could be examined. We hope the platform developed here is extended to several motile cells, allowing commonalities to be identified and comparisons to be made.

Comparison of Traction Force Techniques

As described in Chapter 2, several techniques have been developed for studying the forces cells transmit to their surroundings. The two most prominent platforms at present are polyacrylamide gels and micropost arrays. Since these platforms are both designed to measure the same forces, yet have distinct characteristics—most notably a continuous versus discontinuous binding surface—it would be interesting to compare their results. Dendritic cells may not be optimally suited for this side-by-side experiment, since their forces are so small that they are difficult to resolve using polyacrylamide gels. Neutrophils would be an excellent choice because they are motile under a variety of

conditions (18), they exert reasonably strong traction forces (19), and they are well studied in literature. A side-by-side comparison could highlight the relative strengths and weaknesses of these two traction force techniques.

Final Thoughts

This thesis attempts to address the question of how cells migrate to perform their function. Although the work contained in this thesis is substantial, it is but a small step forward in a journey of many miles. The problem of cell migration is so vast that it has spawned new journals, inspired a handful of annual conferences, and attracted incredible sums of research dollars. Cell migration is absolutely essential for physiological processes such as wound healing, cancer metastasis, innate and adaptive immune responses, neurological development, and maintaining homeostasis. This thesis answers fundamental questions about dendritic cell migration, but it is my hope that it will help form the foundation for future work that will ultimately improve the quality of human life.

References

1. Gunzer M, *et al.* (2000) Migration of dendritic cells within 3-D collagen lattices is dependent on tissue origin, state of maturation, and matrix structure and is maintained by proinflammatory cytokines. *J Leukoc Biol* 67(5):622-629.
2. Lammermann T, *et al.* (2008) Rapid leukocyte migration by integrin-independent flowing and squeezing. *Nature* 453(7191):51-55.
3. Lammermann T, *et al.* (2009) Cdc42-dependent leading edge coordination is essential for interstitial dendritic cell migration. *Blood* 113(23):5703-5710.
4. Ricart BG, John B, Hunter CA, & Hammer DA (Dendritic Cell Chemotaxis in Engineered Chemokine Gradients. *Proc Natl Acad Sci U S A* In Preparation.
5. Leick M, *et al.* (2010) CCL19 is a specific ligand of the constitutively recycling atypical human chemokine receptor CRAM-B. *Immunology* 129(4):536-546.
6. Hartmann TN, *et al.* (2008) Human B cells express the orphan chemokine receptor CRAM-A/B in a maturation-stage-dependent and CCL5-modulated manner. *Immunology* 125(2):252-262.
7. Volpe S, Thelen S, Pertel T, Lohse MJ, & Thelen M (2010) Polarization of migrating monocytic cells is independent of PI 3-kinase activity. (Translated from eng) *PLoS ONE* 5(4):e10159 (in eng).
8. Dehring DAK, *et al.* (2010) HS1 functions in concert with WASp to promote podosome organization and chemotaxis in dendritic cells. *Journal of Immunology* submitted.
9. Ricart BG, Yang MT, Hunter CA, Chen CS, & Hammer DA (2010) Measuring Dendritic Cell Traction Forces on Micropost Arrays. *Journal of Immunology* Under Revision.
10. Yoshida R, *et al.* (1998) Secondary Lymphoid-tissue Chemokine Is a Functional Ligand for the CC Chemokine Receptor CCR7. *Journal of Biological Chemistry* 273(12):7118-7122.
11. Britschgi MR, Link A, Lissandrin TKA, & Luther SA (2008) Dynamic Modulation of CCR7 Expression and Function on Naive T Lymphocytes In Vivo. *J Immunol* 181(11):7681-7688.

12. Sallusto F, *et al.* (1999) Distinct patterns and kinetics of chemokine production regulate dendritic cell function. (Translated from eng) *Eur J Immunol* 29(5):1617-1625 (in eng).

13. Otero C, Groettrup M, & Legler DF (2006) Opposite Fate of Endocytosed CCR7 and Its Ligands: Recycling versus Degradation. *J Immunol* 177(4):2314-2323.

14. Kohout TA, *et al.* (2004) Differential Desensitization, Receptor Phosphorylation, β-Arrestin Recruitment, and ERK1/2 Activation by the Two Endogenous Ligands for the CC Chemokine Receptor 7. *Journal of Biological Chemistry* 279(22):23214-23222.

15. Byers MA, *et al.* (2008) Arrestin 3 Mediates Endocytosis of CCR7 following Ligation of CCL19 but Not CCL21. *J Immunol* 181(7):4723-4732.

16. Heit B, *et al.* (2008) PTEN functions to 'prioritize' chemotactic cues and prevent 'distraction' in migrating neutrophils. *Nat Immunol* 9(7):743-752.

17. Lin F & Butcher EC (2008) Modeling the Role of Homologous Receptor Desensitization in Cell Gradient Sensing. *J Immunol* 181(12):8335-8343.

18. Jannat RA, Robbins GP, Ricart BG, & Hammer DA (2010) Neutrophil adhesion and chemotaxis depend on substrate mechanics. *Journal of Physics: Condensed Matter* 22(19):194117.

19. Smith LA, Aranda-Espinoza H, Haun JB, Dembo M, & Hammer DA (2007) Neutrophil Traction Stresses are Concentrated in the Uropod during Migration. 92(7):L58-L60.

20. Schumann K, et al. (2010) Immobilized Chemokine Fields and Soluble Chemokine Gradients Cooperatively Shape Migration Patterns of Dendritic Cells. Immunity 32(5):703-713.